공학박사 학위논문

Design and Synthesis of Fluorinated Conjugated Polymers Based on 3,3'-Difluoro-2,2'-bithiophene for High Performance Polymer Solar Cells

고성능 고분자 태양전지를 위한 3,3'-difluoro-2,2'-bithiophene에 기반한 불소화 전도성 고분자의 설계 및 합성

2015년 2월

서울대학교 대학원

재료공학부

조 제 웅

Abstract

Design and Synthesis of Fluorinated Conjugated Polymers Based on 3,3'-Difluoro-2,2'-bithiophene for High Performance Polymer Solar Cells

Jea Woong Jo

Department of Materials Science and Engineering

The Graduate School

Seoul National University

Electronic energy level engineering of conjugated polymers including low-bandgap for harvesting a wide range of solar spectrum, deep highest occupied molecular orbital (HOMO) energy level for high open circuit voltage (V_{OC}) and sufficient offset of lowest unoccupied molecular orbital (LUMO) energy levels between polymer donor and fullerene acceptor is a key strategy to achieve high performance polymer solar cells (PSCs) and several modification methods of chemical structure have been proposed to control energy levels of conjugated polymers.

Among these methods, introduction of fluorine atom has attracted much attention for the past few years because high power conversion efficiencies (PCEs) over 7% have been reported with fluorine substituted polymer-based solar cells. However, the effects of fluorination on optoelectrical and photovoltaic properties of polymers have not been revealed clearly and have been studied in only few polymer systems. For further investigation, more fluorinated monomers and polymers for PSCs should be designed and

synthesized.

In this work, we synthesized difluoro-bithiophene as a new fluorinated building block in conjugated polymers for PSCs and various fluorinated copolymers based on difluoro-bithiophene are successfully designed and synthesized in order to clarify the effect of fluorination on the properties of polymers and its device performance of PSCs.

First, fluorinated poly(3,4-dialkylterthiophenes) (PDATs) composed of difluoro-bithiophene and 3,4-dialkylterthiophene are synthesized. Fluorination on polymer backbone changes its electronic structure, leading to deeper HOMO energy level and enhances molecular packing of the polymers as evidenced by strong vibronic shoulder in UV−Vis absorption spectrum and π−π stacking pattern in GIWAXS. When bulky side chain (ethylhexyl) are introduced as a solubilizing group, fluorinated polythiophenes develop finer fibril structure and exhibit a high PCE of 5.12% with a V_{OC} of 0.87 V and a short circuit current density (J_{SC}) of 9.82 mA/cm^2.

Fluorinated D−A type polymer, copolymerized by diketopyrrolo[3,4-c]-pyrrole (DPP) as an A unit and difluoro-bithiophene as a D unit, is also synthesized for investigating the fluorination effect on D−A type polymer. After introduction of fluorine atoms on DPP-based polymer, deeper HOMO energy level of polymer is observed without significant change of optical properties. Although fluorination increases fibril size and lowers J_{SC} of DPP-based polymer, fluorinated DPP-based polymer exhibits higher PCE of 6.39% than non-fluorinated DPP-based polymer (PCE = 5.47%) due to large improvement of V_{OC}.

Furthermore, for investigating the effect of fluorination position on the properties of D−A type polymer, two types of fluorinated polymers are synthesized, HF with fluorination on D unit and FH with fluorination on A unit. Compared to non-fluorinated polymer, fluorinated polymers exhibit

deeper HOMO energy levels without change of bandgap and stronger vibronic shoulder in UV−Vis absorption spectra, indicating that fluorination enhances intermolecular interaction. HF exhibits a high PCE of 7.10%, which is higher than the PCE (6.41%) of FH, with well-developed fibril network, low bimolecular recombination and high hole mobility.

Finally, D−A polymers with different degree of fluorination are synthesized by using 2,1,3-benzothiadiazole (BT) unit substituted by different number of fluorine atoms. 3F with mono-fluorinated BT and 4F with di-fluorinated BT have deeper HOMO energy levels, stronger vibronic shoulder in UV-Vis absorption spectra, and narrower size of fibril in blend film with PCBM than 2F with non-fluorinated BT. Among fluorinated polymers, 3F exhibits the highest PCE of 7.92% with low bimolecular recombination, high hole mobility and well-developed interconnected network with nanoscale fibril.

From these results, it can be concluded that the optoelectrical and photovoltaic properties of conjugated polymer are significantly influenced by introduction of fluorine atoms and fluorinated conjugated polymers are promising materials for achieving high performance PSCs.

Keywords: polymer solar cells, bulk-heterojunction, conjugated polymer, low-bandgap, fluorination, organic electronics

Student Number: 2009-20640

Contents

List of Tables

List of Schemes

List of Figures

Chapter 1. Introduction

1.1 Polymer solar cells

1.1.1 Background

As fossil fuels are depleted, the development of inexpensive renewable energy has been stimulated to satisfy the global energy demand. Solar energy has attracted much attention as the most promising alternative due to clean and abundant energy source. The total amount of solar energy that reaches the earth is over 100,000 TW and although almost energy is reflected and absorbed by earth's atmosphere and clouds, enormous energy highly exceeds the global energy needs (~17 TW).[1-4]

The technology of converting light source to electrical energy using semiconductors is photovoltaics (PV). Recently, the most widely used material for PV is silicon (Si) and the power conversion efficiencies (PCEs) of PV cells based on crystalline Si have reached up to 25%.[5-8] However, in spite of many efforts to develop Si-based PVs, manufacturing cost is still too expensive to alternate the conventional electricity such as thermal, hydroelectric or nuclear power generation. Hence, recently, other inorganic and organic materials have been proposed for collecting energy from sunlight, and among several candidates, organic PVs based on conjugated polymer have been considered as a promising alternative for renewable energy because

of low cost, light weight, solution processability and flexibility.[9-17]

1.1.2 Operating principles and device structure

Since exciton in conjugated polymer has large binding energy and limited diffusion length (10−15 nm) due to low dielectric constant of polymer (ε ~ 3), large interface area between *p*-type and *n*-type materials in active layer of polymer solar cells (PSCs) is necessary for effectively dissociating exciton into charge carriers.[18,19] As one of the breakthrough, bulk heterojunction (BHJ) solar cells are have been proposed to develop *p*-*n* junction in PSCs, and an interpenetrating network structure with nanoscale domain size can be obtained in active layer of solar cells by simple mixing of *p*-type conjugated polymer as an electron donor and *n*-type fullerene derivative as an electron acceptor. Over the decades, BHJ PSCs have been significantly improved with the device optimization and development of new materials, and PCEs over 7% have been achieved under AM 1.5G (AM = air mass) illumination.[20-30]

The fundamental operation mechanism of *p*-*n* junction in PSCs is briefly represented in Scheme 1.1. The energy conversion process has multiple steps in the commonly accepted mechanism; Step 1—Light absorption: The incident light are absorbed in the active layer of PSCs. The absorption spectra of the conjugated polymers should be well matched to the solar irradiation for maximizing light absorption.[31] Step 2—Exciton formation and diffusion: After light are absorbed by the polymers, excitons (electron-hole pairs bound by electrostatic Coulomb force) are generated and diffuse in the polymer domain

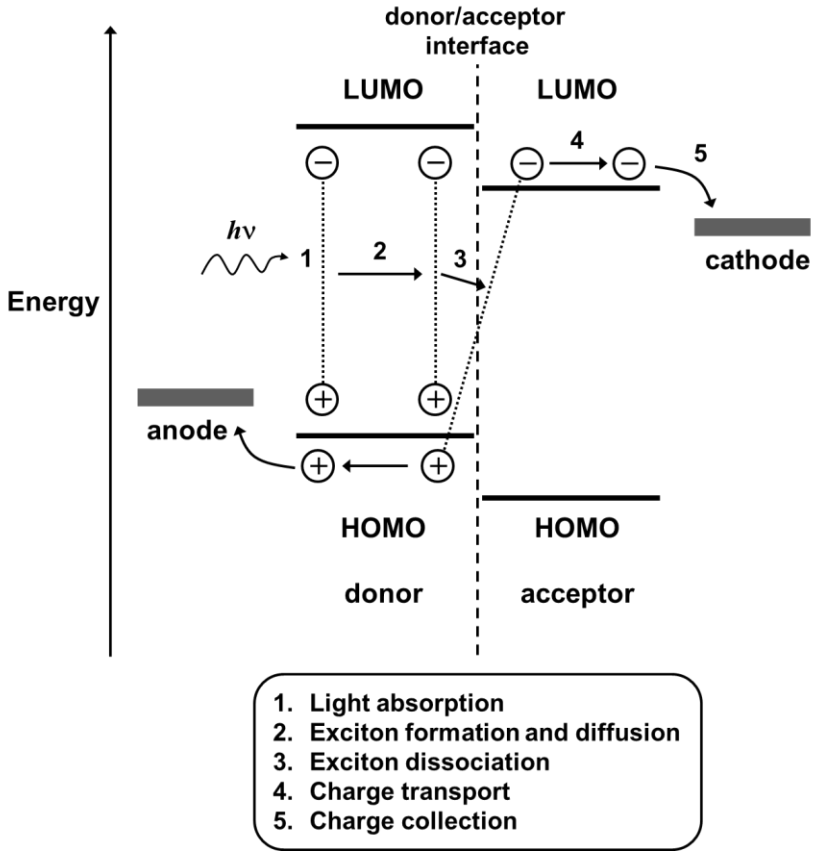

Scheme 1.1. Operation mechanism of *p-n* junction in PSCs.

with a characteristic diffusion length typically of the order of 10–15 nm.[18,19] Step 3—Exciton dissociation or charge separation: During the diffusion, excitons reaching interface between *p*-type and *n*-type materials can be dissociated to form charge carrier before recombination through several decay mechanism.[32] In this process, *p*-*n* junction with nanoscale domain size and large interface area are essential for efficient exciton dissociation. Step 4—Charge transport: Because the dissociated hole and electrons should move through materials of active layer toward their corresponding electrodes, the charge carrier mobilities for both electron and hole play an important role in determining efficiency of solar cells. In PSCs, thickness of active layer is controlled below l μm due to low charge carrier mobilities of polymers.[33,34] Step 5—Charge collection: Finally, at the electrode interfaces, the charge carriers are collected and passed through the circuit to generate photocurrent.

A schematic device structure of a general BHJ PSCs is illustrated in Figure 1.1 and the configuration of conventional PSC device is indium tin oxide (ITO)/poly(3,4-ethylenedioxythiophene):poly(styrenesulfonate) (PEDOT:PSS)/polymer:PCBM/Ca/Al. As a transparent anode, ITO is used due to high optical transparency and electrical conductivity.[35,36] On the ITO-coated glass substrate, PEDOT:PSS is coated as a hole transport layer for lowering the contact resistance between anode and active layer, smoothing the ITO surface and promoting the efficient hole transport.[37-40] And then, the polymer:PCBM blend film is coated from solution on top of the PEDOT:PSS layer. Finally, as a cathode, metal electrode was evaporated on the active layer of PSC. Generally, buffer layer such as Ca and LiF is also coated under Al layer to

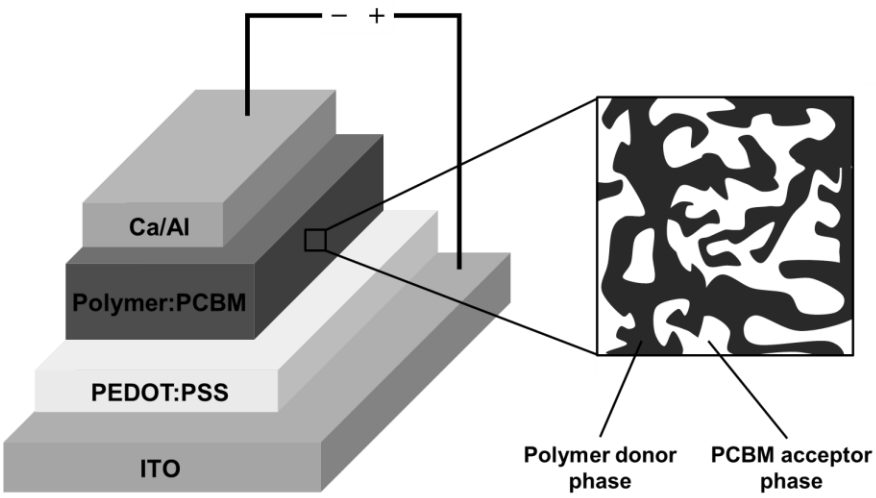

Figure 1.1. Device structure of a general BHJ PSCs.

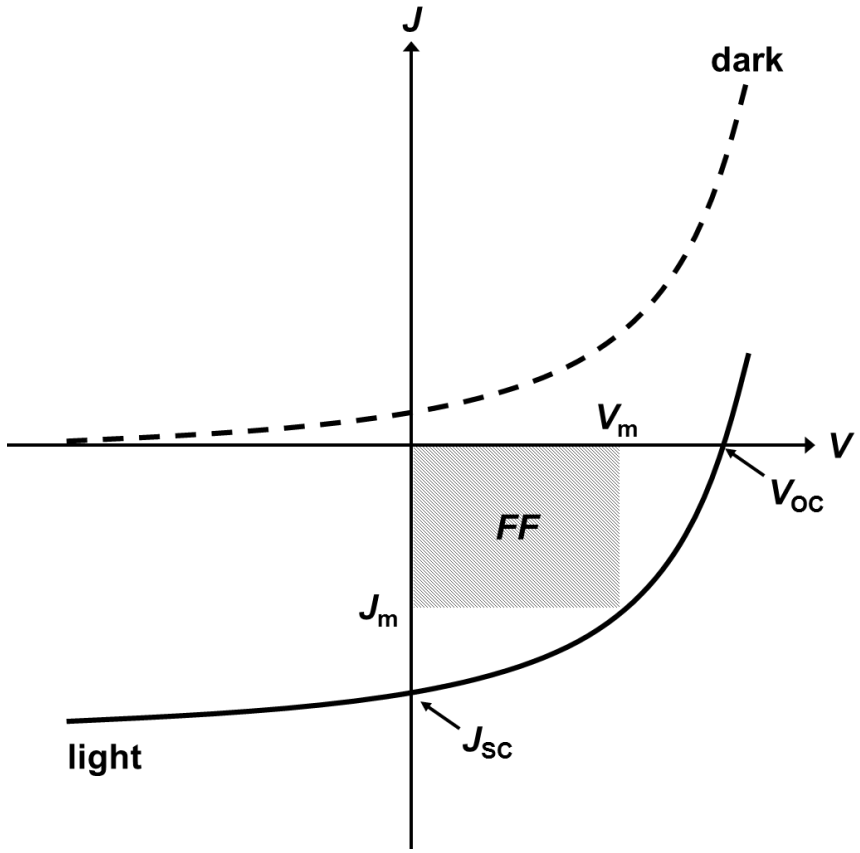

Figure 1.2. Current–voltage curves of solar cell under illumination with the parameters.

lower work function of cathode, which improves electron injection/collecting ability of cathode by forming Ohmic contact with active layer.[41-45]

The current-voltage curves of solar cell under illumination with the parameters are illustrated in Figure 1.2. The PCE of a solar cell is determined by the following formula:

$$PCE = FF \times \frac{V_{OC} \cdot J_{SC}}{P_{in}}, \quad (1.1)$$

$$FF = \frac{J_m \cdot V_m}{J_{SC} \cdot V_{OC}}, \quad (1.2)$$

where V_{OC} is the open circuit voltage, J_{SC} is the short circuit current density, FF is the fill factor, and P_{in} is the incident light power density. This light intensity is standardized at 100 mW/cm^2 with a spectral intensity distribution matching the AM 1.5G condition. J_m and V_m are the current density and voltage at the maximum power point.[46]

1.1.3 Active layer materials for polymer solar cells

Semiconducting polymers in active layers of PSCs must have solubilizing group for low-cost solution process and π–conjugated backbone for electrical charge transport and optical absorption.[47] After the photoinduced electron transfer from conjugated polymers onto electron acceptor was reported,[48] several conjugated polymers have been designed and synthesized for PSCs. The important polymers are described in Figure 1.3.

In early studies about PSCs, the conjugated polymers for active layers mainly come from the materials of the organic light-emitting diodes such as

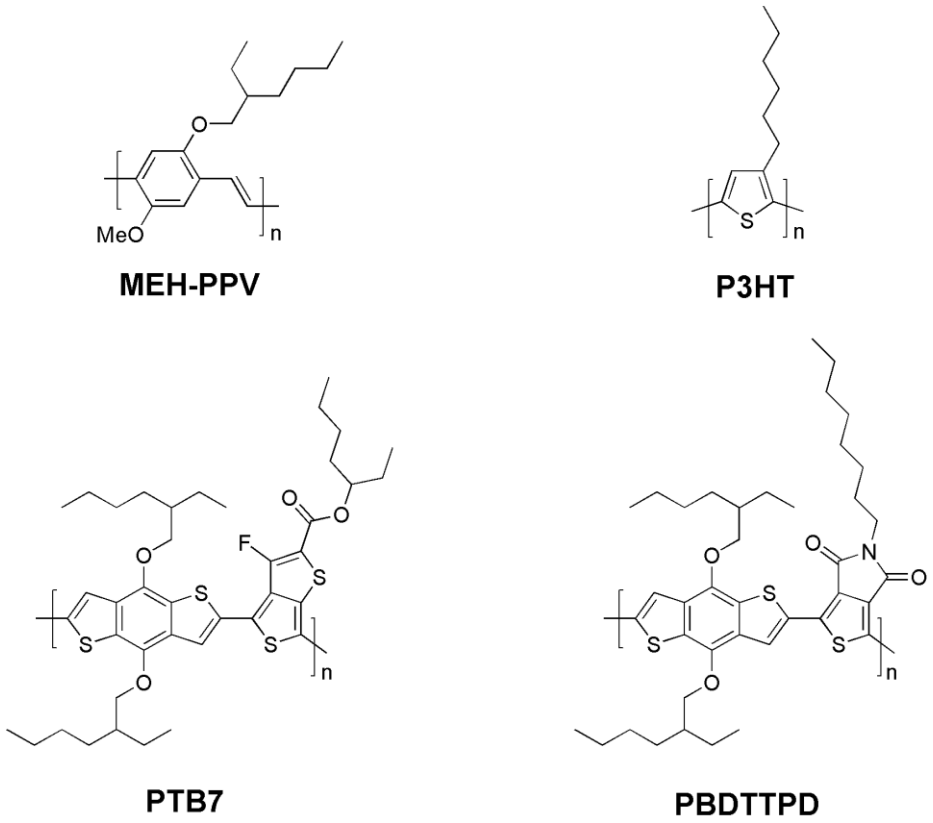

Figure 1.3. Chemical structures of *p*-type polymers used as electron donors in active layers of PSCs.

poly(2-methoxy-5-(-2-ethylhexyloxy)-*p*-phenylenevinylene) (MEH-PPV) and poly(2-methyl-5-(3,7-dimethyloctyl-oxy)-1,4-phenylenevinylene) (MDMO-PPV). However, the solar cell devices fabricated with PPV derivatives have shown low PCEs of 2–3 % because of wide bandgap and low hole mobility with amorphous nature.[49-52] After then, researches of PSCs have focused on the regioregular poly(3-hexylthiophene) (P3HT), which has high crystallinity and excellent charge transport properties. When blended with PCBM, P3HT-based PSCs have achieved promising PCEs of 4–5% after morphology optimization.[53-58] Currently, alternating copolymers, such as PTB7 and PBDTTPD, synthesized with electron-donating (D) and electron-accepting (A) units have been proposed for developing low-bandgap, and the devices with D–A type polymers have reached PCEs over 7%.[20-30]

The chemical structures of *n*–type electron acceptors in active layers of PSCs are described in Figure 1.4. Generally, the buckminsterfullerene (C_{60}), a symmetric fullerene stabilized by resonance structure, and its derivatives are used as a *n*-type electron acceptor in active layer of PSCs. C_{60} has been known to be highly resistant to oxidation and up to six electrons can be accommodated in the lowest unoccupied molecular orbital (LUMO).[59-60] However, since C_{60} has limited solubility in common organic solvents, electron acceptor for PSCs is replaced to [6,6]-phenyl-C_{61}-butyric acid methyl ester ($PC_{61}BM$) having high solubility in chlorobenzene and o-dichlorobenzene with solubilizing substituent.[61] Currently, in order to increase LUMO energy levels of electron acceptors for high V_{OC}, C_{60}-bisadducts such as bis-PCBM and ICBA have also been proposed.[62-65]

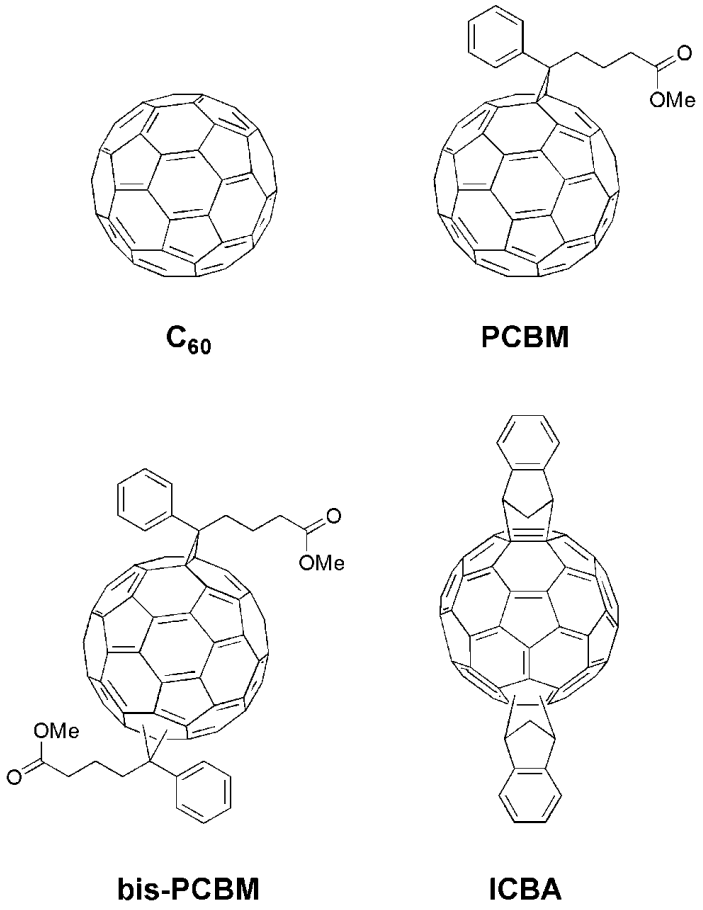

Figure 1.4. Chemical structures of *n*-type materials used as electron acceptors in active layers of PSCs.

1.2 Energy level control of conjugated polymer in active layer of PSC

1.2.1 Energy levels of conjugated polymers

In PSCs, energy levels influence optoelectrical properties of materials including charge extraction, light absorption, charge transport and exciton dissociation, and thus energy levels of each component in solar cells should be controlled cautiously for achieving high performance. Especially, energy levels of conjugated polymer donor in active layer of PSC have been known to be closely related to the parameters used to determine performances of solar cells such as J_{SC}, V_{OC} and *FF*. Over the years, many efforts to find relationships between energy levels of polymer and solar cell performance have been reported and there are some requirements of polymers for highly efficient PSCs.[66-68]

First, polymers should have low-bandgap to harvest a wide range of solar spectrum for attaining high J_{SC}.[13,69-74] The maximum peak of photon flux reaching the earth from the sun is at approximately 1.8 eV. However, representative conjugated polymers such as MEH-PPV (E_g = 2.2 eV) or P3HT (E_g = 2.0 eV) cannot effectively harvest photons due to the mismatch between absorption range of polymers and solar spectrum. Concretely, the P3HT is capable of absorbing only 22.4% of the available photons giving a maximum theoretical J_{SC} of 14.3 mA/cm^2, but polymer with low-bandgap of 1.24 eV can harvest up to 53% of all the solar photons giving a maximum J_{SC} of 33.9

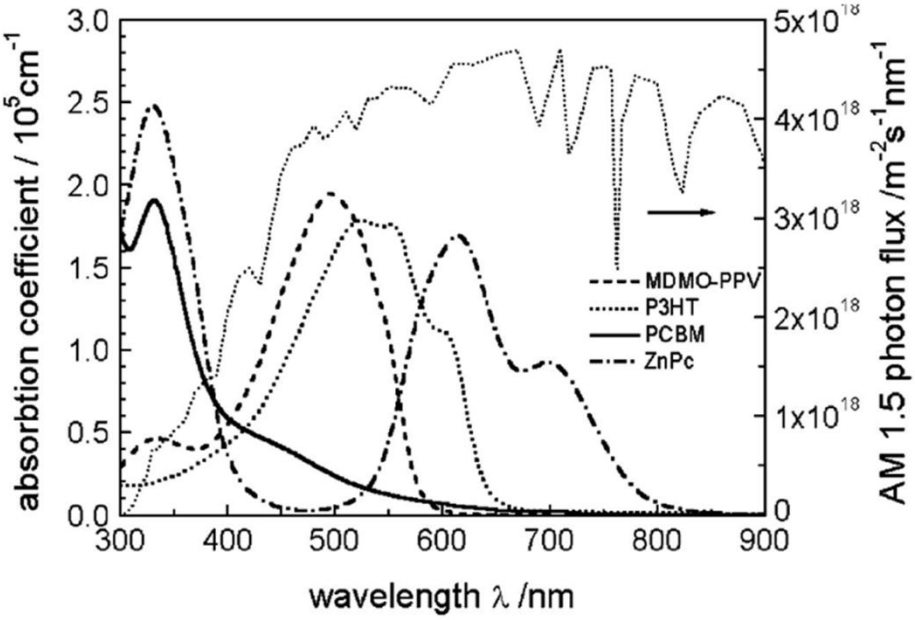

Figure 1.5. Optical absorption spectra of electron donors for organic solar cells and AM 1.5G solar spectrum. (ref. 70)

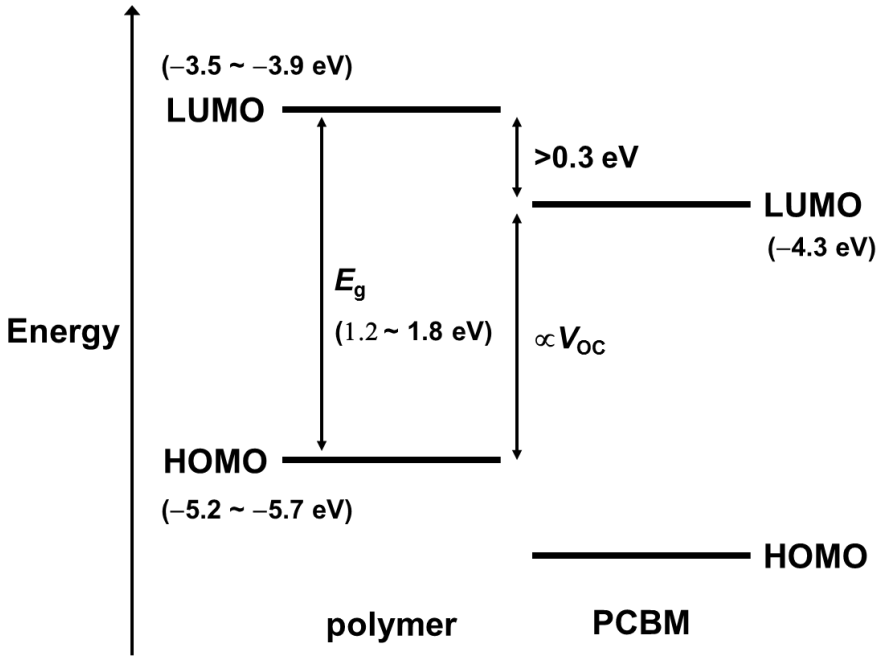

Scheme 1.2. The optimum energy levels of polymer donor for high performance PSCs.

mA/cm^2.[69] Therefore, low-bandgap conjugated polymer which can absorb photons at longer wavelengths where much of the photon flux emitted from the sun is strongly required.

Second, V_{OC} of PSCs is proportional to the difference between the HOMO energy level of donor polymer and the LUMO energy level of acceptor and can be expressed as $V_{OC} = (|E_{HOMO}^{donor}| - |E_{LUMO}^{acceptor}| - 0.3\ eV)/e$, where e is the elementary charge, E_{HOMO}^{donor} is the HOMO energy level of donor polymer, $E_{LUMO}^{acceptor}$ is the LUMO energy level of acceptor and 0.3 eV is an empirical value for efficient charge separation.[75-79] Thus, deep HOMO energy level of polymer is needed for achieving high V_{OC} in PSCs.

Third, the offset of LUMO energy levels between donor and acceptor materials in active layer of PSCs should be at least higher than 0.3 eV for effective exciton dissociation.[80-82]

The optimum energy levels of polymer donor are illustrated in Scheme 1.2 and, when PCBM (LUMO energy level = –4.3 eV) is used as electron acceptor in PSCs, the energy levels of conjugated polymers should have HOMO energy levels between –5.2 and –5.7 eV and LUMO energy levels between –3.5 and –3.9 eV for obtaining the optimum values of both V_{OC} and light harvesting.[83,84]

1.2.2 Factors influencing energy levels of conjugated polymers.

Until now, several polymers for active layers of PSCs have been designed

and synthesized for satisfying optimum energy levels. From many researches about molecular engineering, energy levels of conjugated polymers can be influenced by multiple factors including conjugation length, side chain, stabilization of quinoidal structure, internal charge transfer and substituents on polymer backbone.[69]

Conjugation length is one of the critical factors determining the optoelectrical properties of conjugated polymers, and as the conjugation length increases, the bandgap of polymer is reduced due to extended delocalization of π–electrons in conjugated backbone. In general, for large π–orbital overlap and long conjugation length, the backbone of polymer should have planar structure and the planarity of backbone can be modified by the ways of reducing steric hindrance between two adjacent aromatic rings, such as insertion of vinylene group between rings[85] and backbone rigidification by fusing aromatic rings.[86-88]

The energy levels of polymers can be also changed by side chains owing to mesomeric and inductive effects. For examples, the HOMO energy levels of polythiophene were raised from –5.1 to –4.5 eV by changing the side chain from alkyl to alkoxy group,[89] while polythiophene polymer with two ester side chains exhibits deeper HOMO energy level of –5.26 eV.[90]

The stabilization of the quinoid form in the backbone is another factor influencing energy levels of conjugated polymers. Stabilization of the quinoid structure can be achieved by fusing an aromatic ring with another aromatic system having high resonance energy, and this quinoid form of polymer stabilized by delocalization of π–electrons in fused ring contributes to lower-

lying LUMO energy level and low-bandgap of polymer.[71]

1.2.3 Alternating polymer copolymerized with electron-donating and electron-accepting units

Over the years, alternating copolymer polymerized with electron-donating (D) and electron-accepting (A) units have been considered to be the most promising way for developing low-bandgap polymers. These D–A type polymers are based on internal charge transfer from D unit to A unit and the orbital hybridization of the D–A structure leads to reduction of bandgap by raising the HOMO level and lowering the LUMO level of conjugated polymer, as shown in Scheme 1.3. One of the important advantages in D–A strategy is that photophysical and optoelectronics properties of conjugated polymers can be tuned by a proper combination of D and A units. Especially, because the HOMO and LUMO levels of D–A alternating copolymers are mainly governed by D and A units, respectively, the suitable energy levels of D–A polymers for high performance PSCs can be achieved by modifying each of D and A building blocks separately.[71,91]

The widely used D units in D–A alternating copolymers include thiophene,[92] thieno[3,2-b]thiophene,[93] dithieno[3,2-b:2',3'-d]thiophene,[94] benzene,[95] naphthalene,[96] cyclopenta[2,1-*b*:3,4-*b*']dithiophene,[97,98] anthracene,[99] benzo[1,2-*b*:4,5-*b*']dithiophene,[100-102] fluorene,[103-105] carbazole[106,107] and thiophene-phenylene-thiophene fused ring,[108,109] described in Figure 1.6. Recently, D units with fused ring structure have been attracted

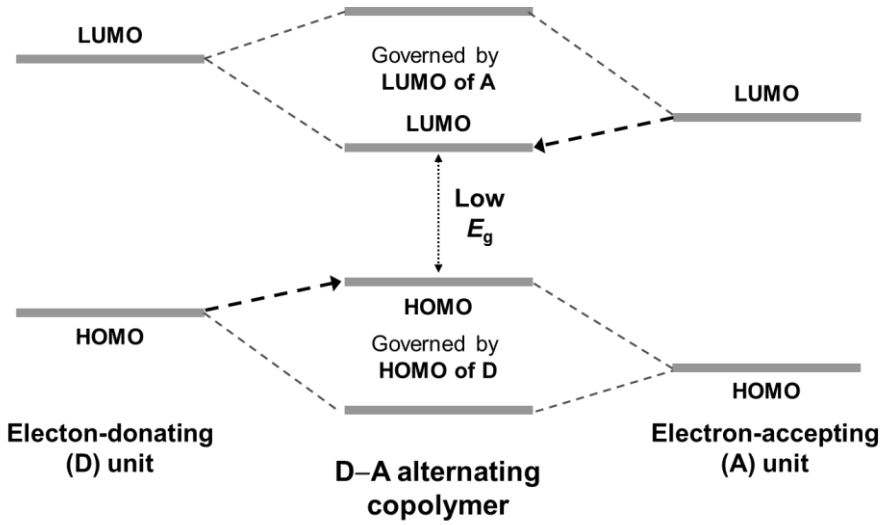

Scheme 1.3. Energy level diagram of the orbital hybridized HOMO and LUMO in D–A alternating copolymers.

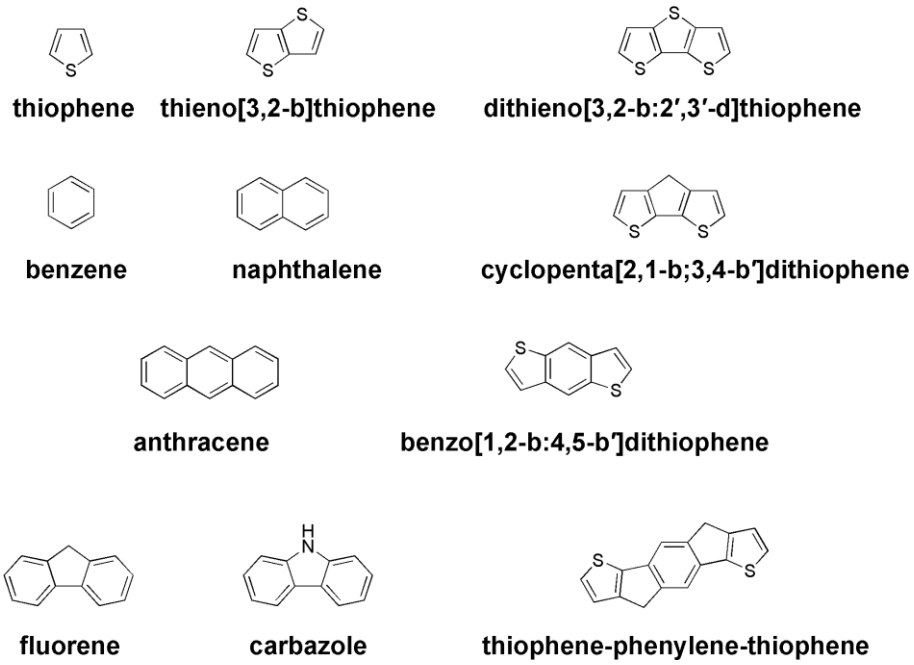

Figure 1.6. Chemical structures of D units widely used in D–A alternating copolymers.

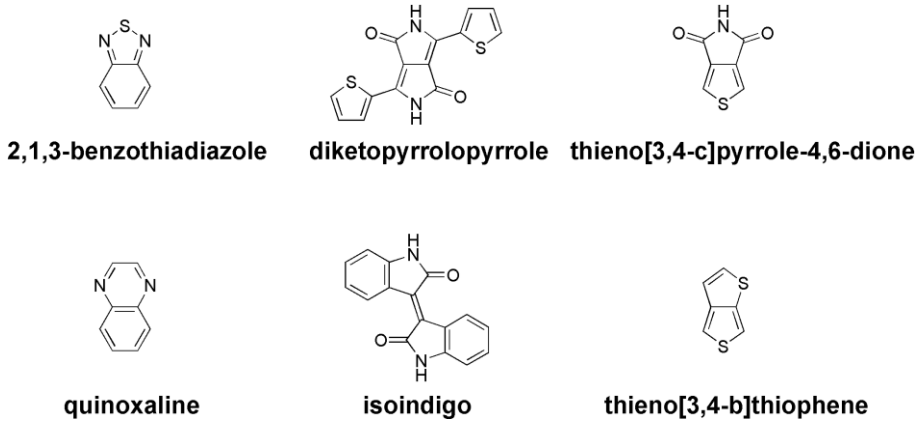

Figure 1.7. Chemical structures of A units widely used in D–A alternating copolymers.

due to strong intermolecular interaction and high hole mobility.

The widely used A units in alternating D–A copolymers include 2,1,3-benzothiadiazole (BT),[106,107,110-112] diketopyrrolo[3,4-*c*]-pyrrole (DPP),[113-116] quinoxaline,[117] thieno[3,4-*c*]pyrrole-4,6-dione (TPD),[118-120] isoindigo (Ii),[121-123] and thieno[3,4-b]thiophene,[124-126] described in Figure 1.7. These A units have different electron-withdrawing properties, determined by electron deficient group and stabilization of quinoidal structure, and should be controlled cautiously for low-bandgap and sufficient offset of LUMO energy levels between polymer and PCBM.

1.2.4 Introduction of heteroatom in backbone

Introduction of heteroatoms on backbone is another powerful method to modify conjugated polymers for PSCs and the optoelectrical properties of conjugated polymers can be varied depending on the kind of heteroatom. These variations in properties of heteroatoms substituted polymers are based on unique characteristics of carbon–heteroatom bonds, which are closely related to different electronegativity of heteroatoms, as shown in Figure 1.8. For example, when the bridging atom in cyclopenta[2,1-*b*:3,4-*b*']dithiophene is replaced to Si or Ge atom, π–π stacking interactions and charge carrier mobilities of polymers are improved due to reduced steric hindrance with long length of carbon–heteroatom bonds.[127-129] And, since Se atom is more easily polarized than S atom, polymers with Se have exhibit stronger intermolecular interaction than polymers with thiophene.[130-132]

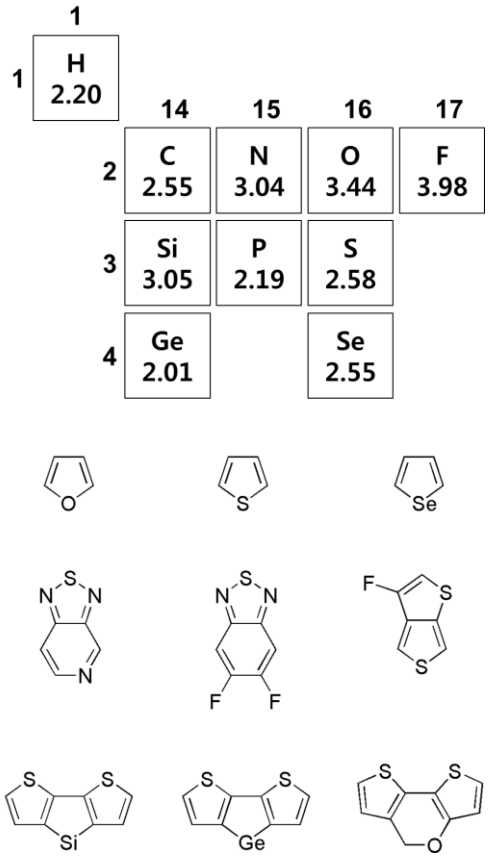

Figure 1.8. Electronegativity of heteroatoms and chemical structures of moieties modified by heteroatoms for conjugated polymers of PSCs.

For optimization energy levels of polymers for PSCs, introduction of heteroatoms with high electronegativity such as N, O, F have been used to develop low-bandgaps and deep HOMO energy levels of polymers. For instance, one of BT derivatives, [1,2,5]thiadiazolo[3,4-*c*]pyridine (PT), has lower LUMO energy level than BT due to π–electron deficient pyridine moiety and the bandgaps of PT-based copolymers are narrower than BT-based polymers, which contribute to efficient light harvesting.[133,134]

1.2.5 Fluorinated organic compounds

Fluorinated organic compounds are a new class of materials and their special features are closely related to the highest electronegativity of fluorine atom (electronegativity of F atoms ≈ 4). When C–F bond is introduced instead of C–H bond in organic compound, fluorinated compounds exhibit interesting properties including high thermal and oxidative stability, enhanced hydrophobicity and lipophobicity, inverted charge distribution and strong interaction involving C–F bond. These positive effects of fluorination have contributed to the development of conjugated organic materials and fluorinated compounds have shown high performances in organic electronics such as organic light-emitting diodes, organic thin film transistors, organic photovoltaic and sensors.[135]

Currently, PSCs with fluorinated polymers have been reported by several research groups. Because fluorine atom is the smallest electron-withdrawing group (van der Waals radius, r = 1.35 Å), fluorinated polymers exhibit lower

energy levels than non-fluorinated analogues without imposing steric hindrance between adjacent monomeric units.[136-138] And, since fluorine atom has strong electron-withdrawing nature with the highest electronegativity, fluorinated conjugated polymers exhibit deeper HOMO energy levels without change of bandgap, and thus afford higher V_{OC}s than non-fluorinated ones without sacrifice of J_{SC}s.[21,137] Furthermore, enhanced inter/intramolecular interaction of polymers due to strongly induced dipole in C−F bond leads to high charge carrier mobility and well-developed fibril structure in the active layer of PSCs, which contribute to both enhancement of J_{SC} and FF.[136]

1.3 Objectives of this study

For developing high efficiency PSCs, understanding of the relation between chemical structure and photovoltaic property of semiconducting conjugated polymer is essential. It has been reported that the electronic properties of conjugated polymers can be tuned by modification of molecular structure such as atomic substitution,[106,133,127,139] optimization of length and position of alkyl chain,[140-142] introduction of bridge unit,[143-145] and type of chain end-group.[146,147]

Among these methods, the atomic substitution, especially, the substitution of fluorine atom has attracted much attention for the past few years.[148] It has recently been reported that fluorine substituted polymer-based solar cells exhibit high PCEs over 7%.[21,136-138] However, improvement of photovoltaic performances by fluorination on conjugated polymers have been studied in

only few polymers owing to lack of fluorinated monomers and, for further investigation about effect of fluorination, more fluorinated monomers and polymers should be designed and synthesized.

In this work, we synthesized difluoro-bithiophene as a new fluorinated building block in conjugated polymers for PSCs and various fluorinated copolymers based on difluoro-bithiophene are successfully designed and synthesized. First of all, fluorinated poly(3,4-dialkylterthiophenes) (PDATs) composed of difluoro-bithiophene and 3,4-dialkylterthiophene were synthesized in order to clarify the effect of fluorination on the properties of polymers and its device performance of PSCs. Bao group previously reported that non-fluorinated PDATs exhibited a high hole mobility up to 0.12 $cm^2 \cdot V^{-1} \cdot s^{-1}$ in organic field-effect transistors and a promising PCE of 4.2% in PSCs.[149,150]

And then, for investigating the effect of fluorine atom substitution on the optoelectrical and photovoltaic properties of D–A type polymer, we prepared a fluorinated D–A type polymer copolymerized by DPP as an A unit and difluoro-bithiophene as a D unit. D–A type polymers have been considered the most promising molecular structure for high performance PSCs, because energy levels of the copolymers can be effectively tuned with a proper combination of D and A units.[71,91]

In addition, two kinds of D–A polymers with each being fluorinated on A and D unit, where quaterthiophene and BT are used as D and A unit, respectively, are synthesized. Until now, the effect of fluorination on D unit in D−A polymer on photovoltaic properties has scarcely been studied, while

most of studies have focused on the fluorination on A unit in the copolymers. By comparison between two D–A polymers substituted by fluorine at different positions, it is investigated that D–A polymer fluorinated on D unit can be applied for high performance PSCs.

Finally, D–A polymers with different degree of fluorination are synthesized. Although fluorination on conjugated polymers has many benefits, high fluorine content can also lead to harmful effects such as low solubility of polymers in organic solvent, unsuitable energy levels for charge transfer and large aggregation of polymers in active layer.[151-153] For highly efficient PSC with fluorinated conjugated polymer, the degree of fluorination should be controlled cautiously to optimize morphology of active layer and energy levels of polymer, and the degree of fluorination of D–A polymer in this work is controlled by using BT unit substituted by different number of fluorine atoms.

Chapter 2. Experimental Section

2.1 Synthesis and characterization

2.1.1 Materials

Tetrahydrofuran (THF) (Daejung Chemicals & Metals) was dried over sodium/benzophenone under nitrogen and freshly distilled before use. All reagents were purchased from Sigma-Aldrich, Alfa-Aesar, TCI chemicals, and Acros Organics unless specified and used as received.

2.1.2 Synthesis of monomers and conjugated polymers

2.1.2.1 Synthesis of 3,3'-difluoro-2,2'-bithiophene and poly(3,4-dialkylterthiophene) polymers

5,5'-Bis(trimethylstannyl)-2,2'-bithiophene (1): To 5,5'-dibromo-2,2'-bithiophene **2** (1 g, 3.09 mmol) in anhydrous THF (15 mL), 2.5 M of *n*-BuLi in hexane (2.8 mL, 7.0 mmol) was added dropwise at −78 ℃. After stirring for 30 min, the solution was further stirred for 30 min at room temperature. The solution was then cooled to −78 ℃ again before 1 M of trimethyltin chloride in hexane (7.7 mL, 7.7 mmol) was added. After warming up to room temperature and stirring overnight, the resulting mixture was poured

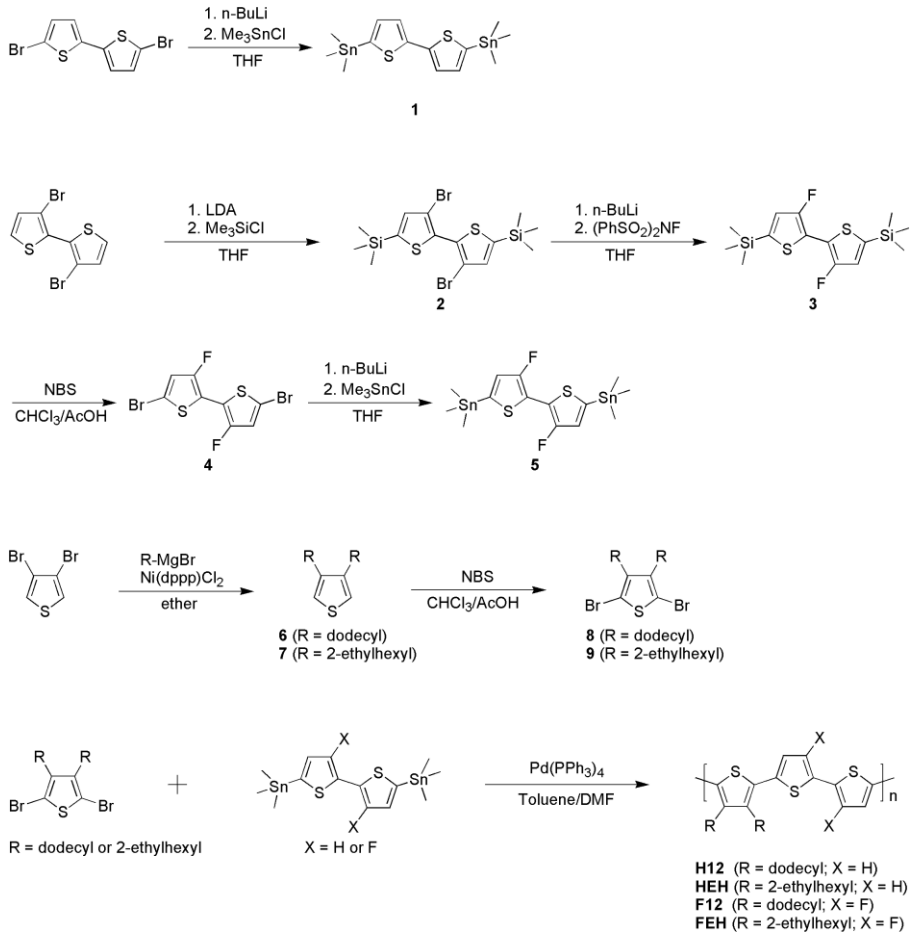

Scheme 2.1. Synthetic scheme of 3,3'-difluoro-2,2'-bithiophene monomer and poly(3,4-dialkylterthiophene) polymers.

into water and extracted with diethyl ether. The organic phase was collected and dried over $MgSO_4$. Recrystallization from methanol yielded the compound **1** (0.97 g, 64%). ^{1}H NMR (300 MHz, $CDCl_3$): δ(ppm) 7.28 (d, 2H), 7.09 (d, 2H), 0.38 (m, 18H).

5,5'-Bis(trimethylsilyl)-3,3'-dibromo-2,2'-bithiophene (2): To diisopropylamine (2.5 mL) in anhydrous THF (30 mL), 2.5 M of *n*-BuLi in hexane (7.68 mL, 19.2 mmol) was added at −78 ℃, and the resulting solution was stirred at 0 ℃ for 30 min. 3,3'-dibromo-2,2'-bithiophene (2.5 g, 7.71 mmol) in anhydrous THF (20 mL) was added dropwise at −78 ℃. After stirring for 30 min, the solution was further stirred for 30 min at room temperature. The solution was then cooled to −78 ℃ again before trimethylsilyl chloride (2.9 mL, 23.1 mmol) was added. After warming up to room temperature and stirring overnight, the resulting mixture was poured into water and extracted with diethyl ether. The organic phase was collected and dried over $MgSO_4$. The product was purified by column chromatography on silica gel (hexane as eluent) and recrystallization from ethanol yielded the compound **2** as a white solid (2.5 g, 69%). ^{1}H NMR (300 MHz, $CDCl_3$): (ppm) 7.15 (s, 2H), 0.34 (s, 18H).

5,5'-Bis(trimethylsilyl)-3,3'-difluoro-2,2'-bithiophene (3): To compound **2** (2.5 g, 5.34 mmol) solution in anhydrous THF (25 mL), 2.5 M of *n*-BuLi in hexane (4.7 mL, 11.8 mmol) was added dropwise at −78 ℃.

After stirring for 30 min, the solution was further stirred for 30 min at room temperature. The solution was then cooled to −78 ℃ again before *N*-fluorobenzenesulfonimide ($(PhSO_2)_2NF$) (4 g, 12.7 mmol) in THF (10 mL) was added. After warming up to room temperature and stirring overnight, the resulting mixture was poured into water and extracted with diethyl ether. The organic phase was collected and dried over $MgSO_4$. The product was purified by column chromatography on silica gel (hexane as eluent) to yield the compound **3** as a white solid (1.65 g, 89%). ^{1}H NMR (300 MHz, $CDCl_3$): δ (ppm) 6.95 (s, 2H), 0.32 (s, 18H). ^{13}C NMR (300 MHz, $CDCl_3$): δ (ppm) 155.47 (d), 136.23 (d), 124.49 (d), 127.28 (dd), –8.14. *m*/*z* (MS-EI) calcd: 347, found: 346.

5,5'-Dibromo-3,3'-difluoro-2,2'-bithiophene (4): To a solution of compound **3** (2 g, 5.77 mmol) in chloroform/acetic acid (1/1, 20 mL), *N*-bromosuccinimide (NBS) (2.36 g, 13.3 mmol) was added in the dark. After stirring overnight at 60 ℃, the reaction mixture was poured into water, extracted with chloroform, and dried over $MgSO_4$. Then the residue was purified by column chromatography on silica gel (hexane as eluent). Recrystallization from acetonitrile afforded the compound **4** (1.62 g, 78%). ^{1}H NMR (300 MHz, $CDCl_3$): δ (ppm) 6.87 (s, 2H). ^{13}C NMR (300 MHz, $CDCl_3$): δ (ppm) 152.01 (d), 120.12 (d), 112.37 (dd), 111.59 (d). *m*/*z* (MS-EI) calcd: 360, found: 360.

5,5'-Bis(trimethylstannyl)-3,3'-difluoro-2,2'-bithiophene (5): To the compound **4** (1.2 g, 3.33 mmol) in anhydrous THF (15 mL), 2.5 M of *n*-BuLi in hexane (3 mL, 7.5 mmol) was added dropwise at −78 ℃. After stirring for 30 min, the solution was further stirred for 30 min at room temperature. The solution was then cooled to −78 ℃ again before 1 M of trimethyltin chloride in hexane (8.3 mL, 8.3 mmol) was added. After warming up to room temperature and stirring overnight, the resulting mixture was poured into water and extracted with diethyl ether. The organic phase was collected and dried over $MgSO_4$. Recrystallization from methanol yielded the compound **5** (1 g, 57%). ^{1}H NMR (300 MHz, $CDCl_3$): δ (ppm) 6.89 (t, 2H), 0.39 (m, 18H). ^{13}C NMR (300 MHz, $CDCl_3$): δ (ppm) 155.20 (d), 138.19 (d), 123.31 (d), 116.75 (dd), −0.38. *m*/*z* (MS-EI) calcd: 528, found: 528.

3,4-Didodecylthiophene (6): 3,4-Dibromo-thiophene (1 g, 4.13 mmol) was added to a mixture of 1 M of dodecyl magnesium bromide in diethyl ether (20 mL, 20 mmol) and catalytic amount of Ni(dppp)Cl_2. After stirring at room temperature for 2 days, the solution was cooled to 0 ℃ and 30 mL of 1 M HCl was added. Then, the organic phase was extracted with hexane and dried over $MgSO_4$. The product was purified by column chromatography on silica gel (hexane as eluent) to yield the compound **6** (0.63 g, 36%). ^{1}H NMR (300 MHz, $CDCl_3$): δ (ppm) 6.89 (s, 2H), 2.50 (t, 4H), 1.35-0.82 (m, 46H).

3,4-Bis-(2-ethylhexyl)-thiophene (7): 3,4-Dibromo-thiophene (1 g, 4.13 mmol) was added to a mixture of 1 M of (2-ethylhexyl)magnesium bromide in diethyl ether (20 mL, 20 mmol) and catalytic amount of Ni(dppp)Cl_2. After stirring at room temperature for 2 days, the solution was cooled to 0 ℃ and 30 mL of 1 M HCl was added. Then, the organic phase was extracted with hexane and dried over $MgSO_4$. The product was purified by column chromatography on silica gel (hexane as eluent) to yield the compound **7** (0.55 g, 43%). ^{1}H NMR (300 MHz, $CDCl_3$): δ (ppm) 6.85 (s, 2H), 2.43 (d, 4H), 1.65-0.82 (m, 30H). ^{13}C NMR (300 MHz, $CDCl_3$): δ (ppm) 141.21, 120.74, 39.42, 33.28, 32.68, 28.93, 25.75, 23.11, 14.17, 10.85. *m*/*z* (MS-EI) calcd: 309, found: 308.

2,5-Dibromo-3,4-didodecylthiophene (8): To a solution of compound **6** (0.5 g, 1.19 mmol) in chloroform/acetic acid (1/1, 10 mL), NBS (0.53 g, 2.98 mmol) was added in the dark and stirred overnight at 60 ℃. After pouring into water, the product was extracted with chloroform, washed with saturated $NaHCO_3$, and dried over $MgSO_4$. The product was purified by column chromatography on silica gel (hexane as eluent) to yield the compound **8** (0.56 g, 82%). ^{1}H NMR (300 MHz, $CDCl_3$): δ (ppm) 2.51 (t, 4H), 1.35-0.82 (m, 46H).

2,5-Dibromo-3,4-bis-(2-ethylhexyl)-thiophene (9): To a solution of compound **7** (0.5 g, 1.62 mmol) in chloroform/acetic acid (1/1, 10 mL), NBS

(0.72 g, 4.04 mmol) was added in the dark and stirred overnight at 60 ℃. After pouring into water, the product was extracted with chloroform, washed with saturated $NaHCO_3$, and dried over $MgSO_4$. The product was purified by column chromatography on silica gel (hexane as eluent) to yield the compound **9** (0.65 g, 86%). ^{1}H NMR (300 MHz, $CDCl_3$): δ (ppm) 2.47 (d, 4H), 1.65-0.82 (m, 30H). ^{13}C NMR (300 MHz, $CDCl_3$): δ (ppm) 141.02, 108.58, 39.64, 33.42, 32.53, 28.89, 25.75, 23.12, 14.15, 11.11. *m*/*z* (MS-EI) calcd: 466, found: 466.

Polymer H12: The compound **1** (150 mg, 0.30 mmol) and **8** (174 mg, 0.30 mmol) were dissolved in a mixture of toluene (10 mL) and DMF (1 mL) solution. After the solution was flushed with N_2 for 20 min, 20 mg of $Pd(PPh_3)_4$ was added. The reaction mixture was stirred for 4 h at 150℃ in a microwave reactor, followed by end-capping using 2-bromothiophene and 2-tributyltinthiophene. After being cooled to room temperature, the mixture was poured into methanol. The crude product was filtered through a Soxhlet thimble, and then subjected to Soxhlet extraction with methanol, ethyl acetate, hexane and chloroform. The polymer was recovered from chloroform fraction, and the fraction was precipitated into methanol to afford the product as a dark red solid (54 mg, 31%).

Polymer HEH: HEH was synthesized by following the same procedure as used in the synthesis of H12. The compound **1** (157 mg, 0.32 mmol) and **9** (150 mg, 0.32 mmol) were used as monomers, and a dark purple solid was

obtained as a product (41 mg, 28%).

Polymer F12: The compound **5** (288 mg, 0.55 mmol) and **8** (316 mg, 0.55 mmol) were dissolved in a mixture of toluene (15 mL) and DMF (1 mL) solution. After the solution was flushed with N_2 for 20 min, 20 mg of $Pd(PPh_3)_4$ was added. The reaction mixture was refluxed for 3 days, followed by end-capping using 2-bromothiophene and 2-tributyltinthiophene. After being cooled to room temperature, the mixture was poured into methanol. The crude product was filtered through a Soxhlet thimble, and then subjected to Soxhlet extraction with methanol, ethyl acetate, hexane and chloroform. The polymer was recovered from chloroform fraction, and the fraction was precipitated into methanol to afford the product as a dark purple solid (93 mg, 27%).

Polymer FEH: FEH was synthesized by following the same procedure as used in the synthesis of F12. The compound **5** (310 mg, 0.59 mmol) and **9** (280 mg, 0.59 mmol) were used as monomers, and a dark purple solid was obtained as a product (110 mg, 37%).

2.1.2.2 Synthesis of polymer composed of 3,3'-difluoro-2,2'-bithiophene and diketopyrrolopyrrole

3,6-Di(thien-2-yl)pyrrolo[3,4-*c*]pyrrole-1,4(2H,5H)-dione (10): To t-amyl alcohol (250 mL), sodium metal pieces (2.56 g, 108 mmol) were slowly

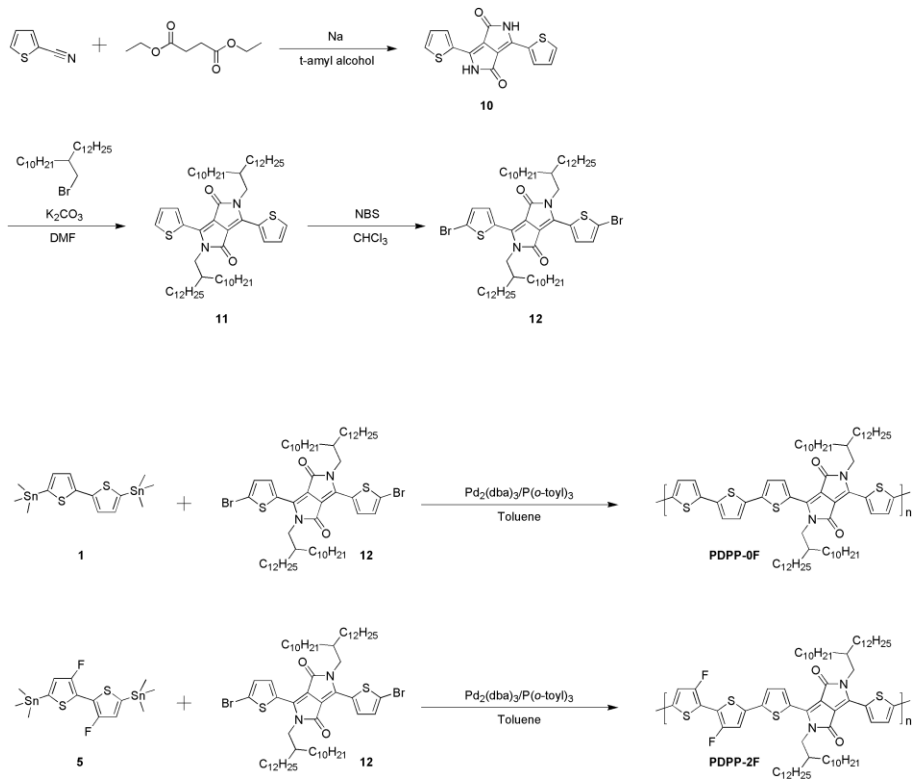

Scheme 2.2. Synthetic scheme of alternating copolymer composed of 3,3'-difluoro-2,2'-bithiophene and diketopyrrolopyrrole.

added to the reaction mixture over a 1.5 h and the temperature of solution was increased to 120 ℃. After all the sodium metal pieces were dissolved, thiophene-2-carbonitrile (11.9 g, 108 mmol) and dimethyl succinate (5.29 g, 36.2 mmol) was added to the solution. The reaction mixture was stirred overnight at 120 ℃ and then poured into acidic MeOH (400 mL MeOH and 20 mL conc. HCl). Filtration of the suspension yielded the product as a dark red solid. This product was used in next reactions without further purification (6 g, 47%).

3,6-Bis-(thiophen-2-yl)-*N,N'*-bis(2-decyltetradecyl)-1,4-dioxo-pyrrolo [3,4-*c*]pyrrole (11): To the compound **10** (5.0 g, 16.6 mmol) in DMF (150 mL), anhydrous K_2CO_3 (6.43 g, 49.9 mmol) were added and stirred at 120 ℃ for 1 h. And then the 2-decyltetradecyl bromide (20.1 g, 49.9 mmol) was added dropwise, and the reaction mixture was further stirred overnight at 130 ℃. After being cooled to room temperature, the solution was poured into water, and stirred for 30 min. The product was extracted with chloroform, then washed with water, and dried over $MgSO_4$. The product was purified by column chromatography on silica gel (hexane/methylene chloride as eluent) to yield the compound **11** (1.7 g, 11%). ^{1}H NMR (300 MHz, $CDCl_3$): δ (ppm) 8.88 (d, 2H), 7.62 (d, 2H), 7.27 (d, 2H), 4.03 (d, 4H), 1.85-0.87 (m, 94H).

3,6-Bis-(5-bromo-thiophen-2-yl)-*N,N'*-bis(2-decyltetradecyl)-1,4-dioxo-pyrrolo[3,4-*c*]pyrrole (12): To the compound **11** (1 g, 1.03 mmol) in $CHCl_3$ (30 mL), NBS (0.38 g, 2.11 mmol) was added slowly in the dark and stirred

overnight at room temperature. After pouring into water, the product was extracted with $CHCl_3$ and dried over $MgSO_4$. The solvent was evaporated under reduced pressure and the product was purified by column chromatography on silica gel (hexane/ methylene chloride as eluent) and recrystallization from acetone yield the compound **12** (0.94 g, 81%). ^{1}H NMR (300 MHz, $CDCl_3$): δ (ppm) 8.63 (d, 2H), 7.22 (d, 2H), 7.52 (d, 2H), 3.98 (d, 4H), 1.85-0.87 (m, 94H).

Polymer PDPP-0F: The compound **1** (65 mg, 0.13 mmol) and **12** (150 mg, 0.13 mmol) were dissolved in toluene (10 mL). After the solution was flushed with N_2 for 20 min, 4 mg of $Pd_2(dba)_3$ and 8mg of $P(o\text{-}toyl)_3$ was added. The reaction mixture was stirred for 4 h at 150℃ in a microwave reactor. After being cooled to room temperature, the mixture was poured into methanol. The crude product was filtered through a Soxhlet thimble, and then subjected to Soxhlet extraction with methanol, ethyl acetate, hexane and chloroform. The polymer was recovered from chloroform fraction, and the fraction was precipitated into methanol to afford the product as a dark green solid (120 mg, 81%).

Polymer PDPP-2F: PDPP-2F was synthesized by following the same procedure as used in the synthesis of PDPP-0F. The compound **5** (70 mg, 0.13 mmol) and **12** (150 mg, 0.13 mmol) were used as monomers, and a dark green solid was obtained as a product (118 mg, 78%).

2.1.2.3 Synthesis of fluorinated or non-fluorinated alternating copolymers composed of 2,2'-bithiophene and 2,1,3-benzothiadiazole

3-(2-Octyldodecyl)-thiophene (13): To a solution of magnesium (0.9 g) in THF (50 mL), a catalytic amount of 1,2-dibromoethane and 2-octyldodecyl bromide (9 mL) was slowly added. After being refluxed for 1.5 h, the solution was added to a mixture of catalytic amount of $Ni(dppp)Cl_2$ and 3-bromothiophene (3 g, 18.4 mmol) in THF (10 mL). The reaction mixture was stirred at 50 ℃ for 1 day and then poured into 30 mL of 1 M HCl. The organic phase was extracted with hexane and dried over $MgSO_4$. The solvent was evaporated under reduced pressure and the product was purified by column chromatography on silica gel (hexane as eluent) to yield the compound **13** (2.1 g, 32%). ^{1}H NMR (300 MHz, $CDCl_3$): δ (ppm) 7.23 (dd, 1H), 6.90 (d, 1H), 6.88 (d, 1H), 2.55 (d, 2H), 1.59-0.82 (m, 38H).

5-Trimethylstannyl-3-(2-octyldodecyl)-thiophene (14): To diisopropyl-amine (1.3 mL) in anhydrous THF (30 mL), 2.5 M of *n*-BuLi in hexane (4.0 mL, 9.88 mmol) was added at −78 ℃, and the resulting solution was stirred at 0 ℃ for 30 min. 3-(2-Octyldodecyl)-thiophene (3 g, 8.23 mmol) in anhydrous THF (10 mL) was added dropwise at −78 ℃. After stirring for 30 min, the solution was further stirred for 30 min at room temperature. The solution was then cooled to −78 ℃ again before 1 M of trimethylstannyl chloride in hexane (10.7 mL, 10.7 mmol) was added. After stirring overnight,

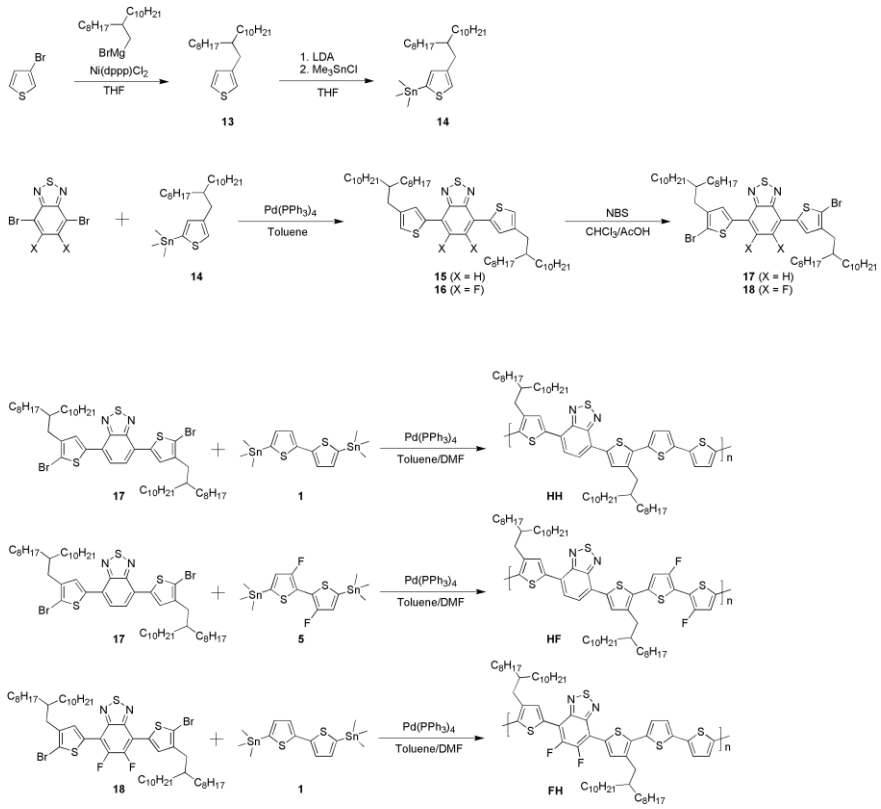

Scheme 2.3. Synthetic scheme of fluorinated or non-fluorinated alternating copolymers composed of 2,2’-bithiophene and 2,1,3-benzothiadiazole.

the resulting mixture was poured into water and extracted with diethyl ether. The organic phase was collected and dried over $MgSO_4$. The solvent was evaporated under reduced pressure and the resultant liquid product was directly used in the next step without further purification (3.7 g, 85%).

4,7-Bis(4-(2-octyldodecyl)-thiophen-2-yl)benzo[c]-[1,2,5]thiadiazole (15): The 4,7-dibromobenzo[c][1,2,5]thiadiazole (0.5 g, 1.7 mmol) and **14** (2.7 g, 5.1 mmol) were dissolved in toluene (10 mL). After the solution was flushed with N_2 for 20 min, 40 mg of $Pd(PPh_3)_4$ was added. The reaction mixture was stirred for 5 h at 150℃ in a microwave reactor. After being cooled to room temperature, the resulting mixture was poured into water, extracted with $CHCl_3$ and dried over $MgSO_4$. The solvent was evaporated under reduced pressure and the product was purified by column chromatography on silica gel (hexane/$CHCl_3$ as eluent) to yield the compound **15** (0.92 g, 63%). ^{1}H NMR (300 MHz, $CDCl_3$): δ (ppm) 7.95 (d, 2H), 7.83 (s, 2H), 7.01 (s, 2H), 2.64 (d, 4H), 1.65-0.82 (m, 78H).

5,6-Difluoro-4,7-bis(4-(2-octyldodecyl)-thiophen-2-yl)benzo[c]-[1,2,5] thiadiazole (16): Compound **16** was synthesized by following the same procedure as used in the synthesis of compound **15**. The 5,6-difluoro-4,7-dibromobenzo[c][1,2,5]thiadiazole (0.5 g, 1.52 mmol) and **14** (2.41g, 4.56 mmol) were used, and an orange solid was obtained as a product (0.58 g, 43%). ^{1}H NMR (300 MHz, $CDCl_3$): δ (ppm) 8.07 (s, 2H), 7.83 (s, 2H), 2.64 (d, 4H), 1.65-0.82 (m, 78H).

4,7-Bis(5-bromo-4-(2-octyldodecyl)-thiophen-2-yl)benzo[c]-[1,2,5] thiadiazole (17): To a solution of compound **15** (0.5 g, 0.58 mmol) in chloroform/acetic acid (1/1, 10 mL), NBS (0.22 g, 1.25 mmol) was added in the dark and stirred overnight at room temperature. After pouring into water, the product was extracted with chloroform, washed with saturated $NaHCO_3$, and dried over $MgSO_4$. The product was purified by column chromatography on silica gel (hexane/$CHCl_3$ as eluent) and recrystallization from methanol yield the compound **17** (0.54 g, 92%). ^{1}H NMR (300 MHz, $CDCl_3$): δ (ppm) 7.75 (s, 2H), 7.74 (s, 2H), 2.58 (d, 4H) 1.65-0.82 (m, 78H).

5,6-Difluoro-4,7-bis(5-bromo-4-(2-octyldodecyl)-thiophen-2-yl)benzo [c]-[1,2,5] thiadiazole (18): Compound **18** was synthesized by following the same procedure as used in the synthesis of compound **17**. The compound **16** (0.5 g, 0.56 mmol) and NBS (0.21 g, 1.2 mmol) were used, and an orange solid was obtained as a product (0.56 g, 95%). ^{1}H NMR (300 MHz, $CDCl_3$): δ (ppm) 7.93 (s, 2H), 2.58 (d, 4H), 1.65-0.82 (m, 78H).

Polymer HH: The compounds **17** (120 mg, 0.12 mmol) and **1** (60 mg, 0.12 mmol) were dissolved in a mixture of toluene (10 mL) and DMF (1 mL). After the solution was flushed with N_2 for 20 min, 20 mg of Pd(PPh3)4 was added. The reaction mixture was then refluxed for 3 days. After being cooled to room temperature, the mixture was poured into methanol. The crude product was filtered through a Soxhlet thimble and then subjected to Soxhlet extraction successively with methanol, ethyl acetate, hexane and chloroform.

The chloroform fraction was precipitated into methanol to afford the product as a dark green solid (39 mg, 32%).

Polymer HF: HF was synthesized by following the same procedure as used in the synthesis of HH. The compound **17** (120 mg, 0.12 mmol) and **5** (64 mg, 0.12 mmol) were used as monomers, and a dark green solid was obtained as a product (85 mg, 67%).

Polymer FH: FH was synthesized by following the same procedure as used in the synthesis of HH. The compound **18** (139 mg, 0.13 mmol) and **1** (65 mg, 0.13 mmol) were used as monomers, and a dark green solid was obtained as a product (100 mg, 72%).

2.1.2.4 Synthesis of alternating copolymers composed of 3,3'-difluoro-2,2'-bithiophene and fluorinated 2,1,3-benzothiadiazole

3-(2-decyltetradecyl)-thiophene (19): To a solution of magnesium (0.3 g) in THF (50 mL), a catalytic amount of 1,2-dibromoethane and 2-decyltetradecyl bromide (3 mL) was slowly added. After being refluxed for 1.5 h, the solution was added to a mixture of catalytic amount of $Ni(dppp)Cl_2$ and 3-bromothiophene (1 g, 6.13 mmol) in THF (10 mL). The reaction mixture was stirred at 50 ℃ for 1 day and then poured into 30 mL of 1 M HCl. The organic phase was extracted with hexane and dried over $MgSO_4$. The solvent was evaporated under reduced pressure and the product

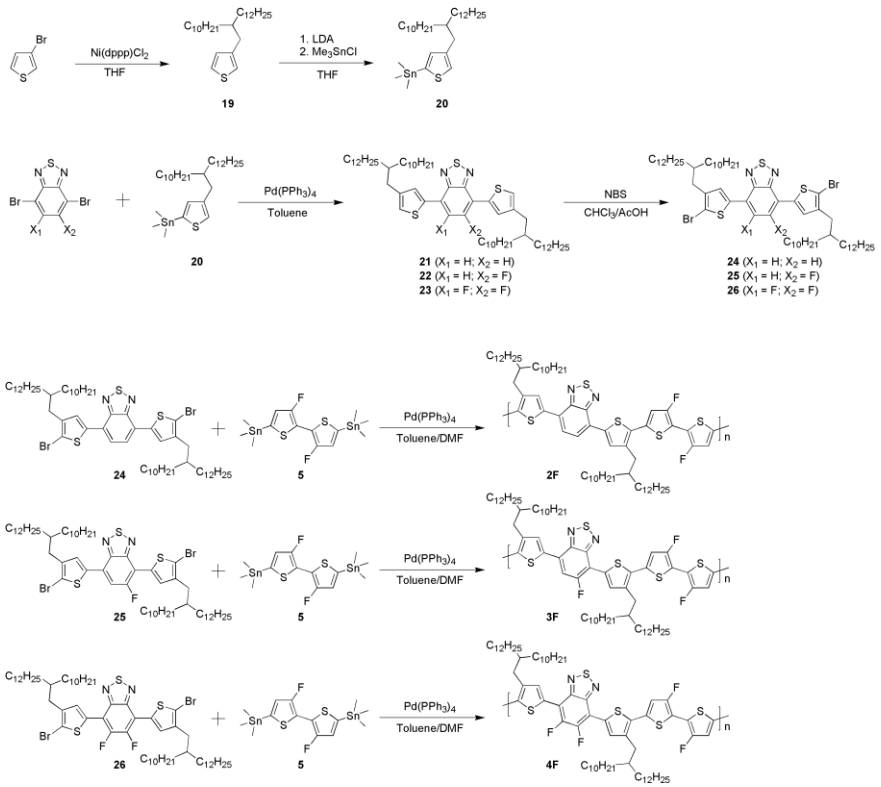

Scheme 2.4. Synthetic scheme of alternating copolymers composed of 3,3'-difluoro-2,2'-bithiophene and fluorinated 2,1,3-benzothiadiazole.

was purified by column chromatography on silica gel (hexane as eluent) to yield the compound **19** (0.3 g, 12%). ^{1}H NMR (300 MHz, $CDCl_3$): δ (ppm) 7.23 (dd, 1H), 6.90 (d, 1H), 6.88 (d, 1H), 2.56 (d, 2H), 1.59-0.82 (m, 47H).

5-Trimethylstannyl-3-(2-decyltetradecyl)-thiophene (20): To diisopropylamine (0.8 mL) in anhydrous THF (20 mL), 2.5 M of *n*-BuLi in hexane (2.28 mL, 5.7 mmol) was added at −78 ℃, and the resulting solution was stirred at 0 ℃ for 30 min. compound **19** (2 g, 4.75 mmol) in anhydrous THF (10 mL) was added dropwise at −78 ℃. After stirring for 30 min, the solution was further stirred for 30 min at room temperature. The solution was then cooled to −78 ℃ again before 1 M of trimethylstannyl chloride in hexane (6.2 mL, 6.18 mmol) was added. After stirring overnight, the resulting mixture was poured into water and extracted with diethyl ether. The organic phase was collected and dried over $MgSO_4$. The solvent was evaporated under reduced pressure and the resultant liquid product was directly used in the next step without further purification (2.3 g, 82%).

4,7-Bis(4-(2-decyltetradecyl)-thiophen-2-yl)benzo[c]-[1,2,5]thiadiazole (21): The 4,7-dibromobenzo[c][1,2,5]thiadiazole (250 mg, 0.85 mmol) and **20** (1.49 g, 2.55 mmol) were dissolved in toluene (10 mL). After the solution was flushed with N_2 for 20 min, 40 mg of $Pd(PPh_3)_4$ was added. The reaction mixture was stirred for 5 h at 150℃ in a microwave reactor. After being cooled to room temperature, the resulting mixture was poured into water,

extracted with $CHCl_3$ and dried over $MgSO_4$. The product was purified by column chromatography on silica gel (hexane/$CHCl_3$ as eluent) to yield the compound **21** (310 mg, 37%). ^{1}H NMR (300 MHz, $CDCl_3$): δ (ppm) 7.95 (d, 2H), 7.83 (s, 2H), 7.01 (s, 2H), 2.64 (d, 4H), 1.65-0.82 (m, 94H).

5-fluoro-4,7-bis(4-(2-decyltetradecyl)-thiophen-2-yl)benzo[c]-[1,2,5] thiadiazole (22): Compound **22** was synthesized by following the same procedure as used in the synthesis of compound **21**. The 5-difluoro-4,7-dibromobenzo[c][1,2,5]thiadiazole (250 mg, 0.8 mmol) and **20** (1.4 g, 2.4 mmol) were used, and an orange solid was obtained as a product (220 mg, 28%). ^{1}H NMR (300 MHz, $CDCl_3$): δ (ppm) 8.07 (s, 1H), 7.95 (d, 1H), 7.73 (d, 1H), 7.12 (s, 1H), 7.06 (1, 1H) 2.64 (d, 4H), 1.65-0.82 (m, 94H).

5,6-Difluoro-4,7-bis(4-(2-decyltetradecyl)-thiophen-2-yl)benzo[c]-[1,2, 5]thiadiazole (23): Compound **23** was synthesized by following the same procedure as used in the synthesis of compound **21**. The 5,6-difluoro-4,7-dibromobenzo[c][1,2,5]thiadiazole (250 mg, 0.76 mmol) and **20** (1.33 g, 2.28 mmol) were used, and an orange solid was obtained as a product (210 mg, 27%). ^{1}H NMR (300 MHz, $CDCl_3$): δ (ppm) 8.07 (s, 2H), 7.83 (s, 2H), 2.64 (d, 4H), 1.65-0.82 (m, 94H).

4,7-bis(5-bromo-4-(2-decyltetradecyl)-thiophen-2-yl)benzo[c]-[1,2,5] thiadiazole (24): To a solution of compound **21** (310 mg, 0.31 mmol) in chloroform/acetic acid (1/1, 10 mL), NBS (119 mg, 0.67 mmol) was added

in the dark and stirred overnight at room temperature. After pouring into water, the product was extracted with chloroform, washed with saturated $NaHCO_3$, and dried over $MgSO_4$. The product was purified by column chromatography on silica gel (hexane/$CHCl_3$ as eluent) and recrystallization from methanol yield the compound **24** (294 mg, 84%). ^{1}H NMR (300 MHz, $CDCl_3$): δ (ppm) 7.75 (s, 4H), 2.57 (d, 4H) 1.65-0.82 (m, 94H).

5-Difluoro-4,7-bis(5-bromo-4-(2-decyltetradecyl)-thiophen-2-yl)benzo [c]-[1,2,5]thiadiazole (25): Compound **25** was synthesized by following the same procedure as used in the synthesis of compound **24**. The compound **22** (220 mg, 0.22 mmol) and NBS (86 mg, 0.48 mmol) were used, and an orange solid was obtained as a product (206 mg, 80%). ^{1}H NMR (300 MHz, $CDCl_3$): δ (ppm) 7.93 (s, 1H), 7.73 (s, 1H), 7.65 (d, 1H), 2.58 (d, 4H), 1.65-0.82 (m, 94H).

5,6-Difluoro-4,7-bis(5-bromo-4-(2-decyltetradecyl)-thiophen-2-yl)benzo [c]-[1,2,5]thiadiazole (26): Compound **26** was synthesized by following the same procedure as used in the synthesis of compound **24**. The compound **23** (210 mg, 0.21 mmol) and NBS (80 mg, 0.45 mmol) were used, and an orange solid was obtained as a product (211 mg, 86%). ^{1}H NMR (300 MHz, $CDCl_3$): δ (ppm) 7.94 (s, 2H), 2.59 (d, 4H), 1.65-0.82 (m, 94H).

Polymer 2F: The compounds **24** (150 mg, 0.13 mmol) and **5** (70 mg, 0.13 mmol) were dissolved in a mixture of toluene (10 mL) and DMF (1 mL).

After the solution was flushed with N_2 for 20 min, 10 mg of Pd(PPh3)4 was added. The reaction mixture was stirred for 5 h at 150℃ in a microwave reactor. After being cooled to room temperature, the mixture was poured into methanol. The crude product was filtered through a Soxhlet thimble and then subjected to Soxhlet extraction successively with methanol, ethyl acetate, hexane and chloroform. The chloroform fraction was precipitated into methanol to afford the product as a dark green solid (82 mg, 54%).

Polymer 3F: 3F was synthesized by following the same procedure as used in the synthesis of 2F. The compound **25** (150 mg, 0.13 mmol) and **5** (69 mg, 0.13 mmol) were used as monomers, and a dark green solid was obtained as a product (112 mg, 72%).

Polymer 4F: 4F was synthesized by following the same procedure as used in the synthesis of 2F. The compound **26** (150 mg, 0.13 mmol) and **5** (68 mg, 0.13 mmol) were used as monomers, and a dark green solid was obtained as a product (120 mg, 76%).

2.1.3 Characterization methods

The chemical structures of compounds were identified by ^{1}H NMR and ^{13}C NMR (Avance DPX-300). Molar masses of compounds were measured on a mass spectrometer (HP 5890) in electron-impact mode. Molecular weight and its distribution of polymers were measured by GPC (Polymer Labs GPC 220

and Waters) with a refractive index detector. 1,2,4-Trichlorobenzene (high temperature GPC at 135 ℃) and chloroform (room temperature GPC) was used as an eluent, and the molecular weight of polymers were calibrated by polystyrene standards.

The optical absorption spectra were obtained by a UV–Vis spectrophotometer (Shimadzu UV-3600 and Lambda 25, Perkin Elmer). Cyclic voltammetry was conducted on a potentiostat/galvanostat (VMP 3, Biologic) in an electrolyte solution of 0.1 M tetrabutylammonium hexafluorophosphate acetonitrile. Pt wires (Bioanalytical System Inc.) were used as both counter and working electrodes, and silver/silver ion (Ag in 0.1 M $AgNO_3$ solution, Bioanalytical System Inc.) was used as a reference electrode. The HOMO energy levels of polymers were calculated by using the flowing relation: HOMO (eV) = $-[E_{ox} - E_{1/2}(\text{ferrocene}) + 4.8]$, where E_{ox} is the onset oxidation potential of the polymer and $E_{1/2}$(ferrocene) is the onset oxidation potential of ferrocene vs. Ag/Ag^+. Density functional theory (DFT) calculations were carried out at the B3LYP/6-31G(d,p) level on Gaussian 03 and 09. Dipole moments in ground and excited states were calculated with time-dependent DFT. Thermogravimetric analysis (TGA) was carried out at a heating rate of 10 ℃ min^{-1} under nitrogen atmosphere using a thermogravimetric analyzer (TA 2050, TA Instruments). Melting and crystallization temperatures were measured by heating and cooling the sample from 20 to 350 ℃ at a scan rate of 10 ℃ min^{-1} using a differential scanning calorimeter (DSC) (TA Instruments, 2920 Modulated DSC).

2.2 Device fabrication and measurements

2.2.1 Materials

ITO-patterned glass was used as an anode in PSC device. The sheet resistance of the ITO was less than 20 Ω/square. Poly(3,4-ethylenedioxy-thiophene):poly(styrenesulfonate) (PEDOT:PSS) (CleviosP VP AI 4083) was purchased from H. C. Stark and passed through a 0.45 μm PVDF syringe filter before spin-coating. [6,6]-Phenyl-C71-butyric acid methyl ester ($PC_{71}BM$) was obtained from American Dye Source or Nano-C. All reagents were purchased from Sigma-Aldrich unless specified and used as received.

2.2.2 Solar cell device fabrication

The polymer solar cells were fabricated with a standard device configuration of ITO/PEDOT:PSS/polymer:$PC_{71}BM$/Ca/Al. PEDOT:PSS was spin-coated with 40 nm thickness on the ITO-coated glass and annealed at 150 ℃ for 30 min. The blend solution in o-dichlorobenzene was spin-coated on the top of the PEDOT:PSS layer at 800–1000 rpm for 40–60 s. The film thickness of the active layer was measured by atomic force microscopy (Nano Xpert II, EM4SYS). Calcium (20 nm) and aluminum (100 nm) was thermally evaporated on the top of the active layer under vacuum ($<10^{-6}$ Torr). The effective area of the cell was 0.1 cm^2.

2.2.3 Solar cell performance measurements

The *J*–*V* characteristics were measured with a Keithley 4200 source-meter under AM 1.5G (100 mW/cm^2) simulated by a Newport-Oriel solar simulator. The light intensity was calibrated using a NREL-certified photodiode prior to each measurement. The external quantum efficiencie (EQE) was measured using a lock-in amplifier with a current preamplifier (K3100, Mac Science Co.) under short circuit current state with illumination of monochromatic light. The morphologies of polymer/$PC_{71}BM$ blend films were observed by transmission electron microscopy (TEM) (JEM-1010, JEOL). The space charge limited current (SCLC) *J*–*V* curves were obtained in the dark using hole-only devices (ITO/PEDOT:PSS/polymer:$PC_{71}BM$/Au), and hole mobilities were calculated using the Mott-Gurney square law, $J = (9/8)\varepsilon_0\varepsilon_r\mu(V^2/L^3)$, where ε_0 is vacuum permittivity, ε_r is the dielectric constant of polymer, μ is the charge carrier mobility, V is the effective applied voltage, and L is the thickness of the film. Grazing incidence wide angle X–ray scattering (GIWAXS) scans were obtained at the Advanced Light Source at the Lawrence Berkeley National Laboratory. The wavelength of X-ray used was 1.240 Å, and the scattered intensity was detected by PILATUS 1M detector. Transmission resonant soft X-ray scattering (R-SoXS) spectra were obtained using the transmission geometry with a beam energy of 284.2 eV.

Chapter 3. Results and Discussion

3.1 Fluorination of polythiophene derivatives for high performance organic photovoltaics

3.1.1 Synthesis and characterization

Although fluorination has been known to cause multiple effects on photophysical properties of conjugated polymers, the relationship between improved photovoltaic performance and modified properties by introducing fluorine on polymer has not been revealed clearly. In this work, we synthesized, difluoro-bithiophene, was prepared as a new building block for conjugated polymers and polymerized with 3,4-dialkylterthiophene to afford fluorinated PDAT in order to clarify the effect of fluorine atom substitution on the properties of polymers and its device performance of PSCs.

The synthetic routes for monomers and polymers are illustrated in Scheme 2.1. Dodecyl or 2-ethylhexyl side chains were introduced to enhance the solubility of synthesized polymer in organic solvents. When shorter linear alkyl chains (hexyl or octyl) were introduced, fluorinated polymers exhibited poor solubility in organic solvents. Fluorinated bithiophene **3** was synthesized from 3,3′-dibromo-2,2′-bithiophene, electrophilic fluorination agent $(PhSO_2)_2NF$, and trimethylsilane protecting group. Trimethylsilane groups in **3** were replaced by bromine to afford the

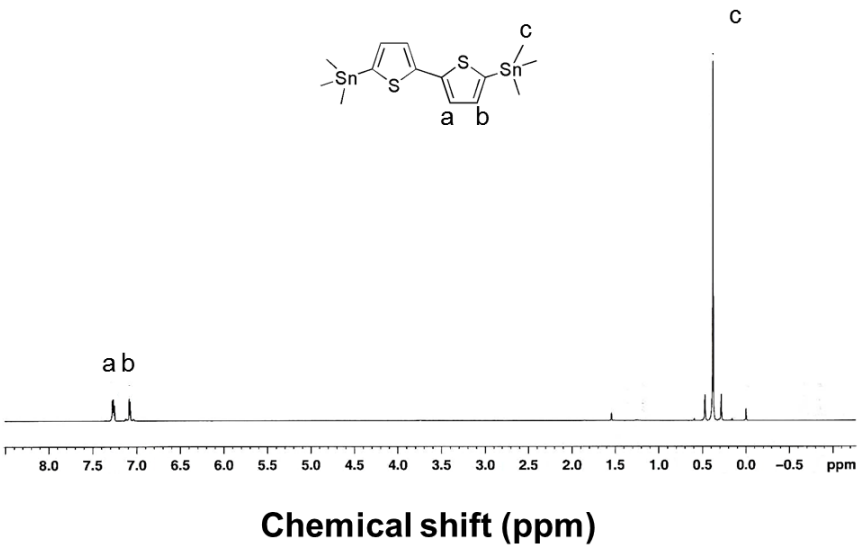

Figure 3.1. ^{1}H NMR spectrum of compound **1** in Scheme 2.1.

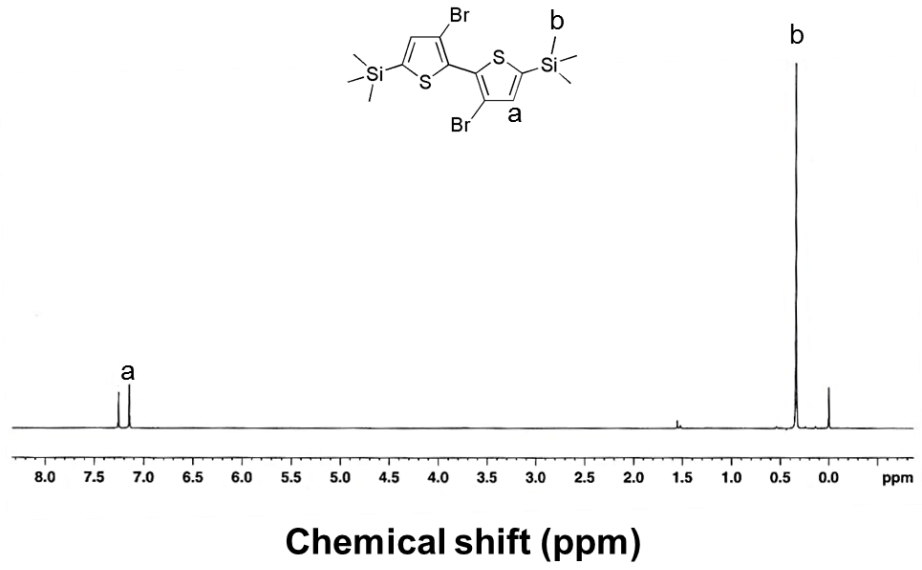

Figure 3.2. ^{1}H NMR spectrum of compound **2** in Scheme 2.1.

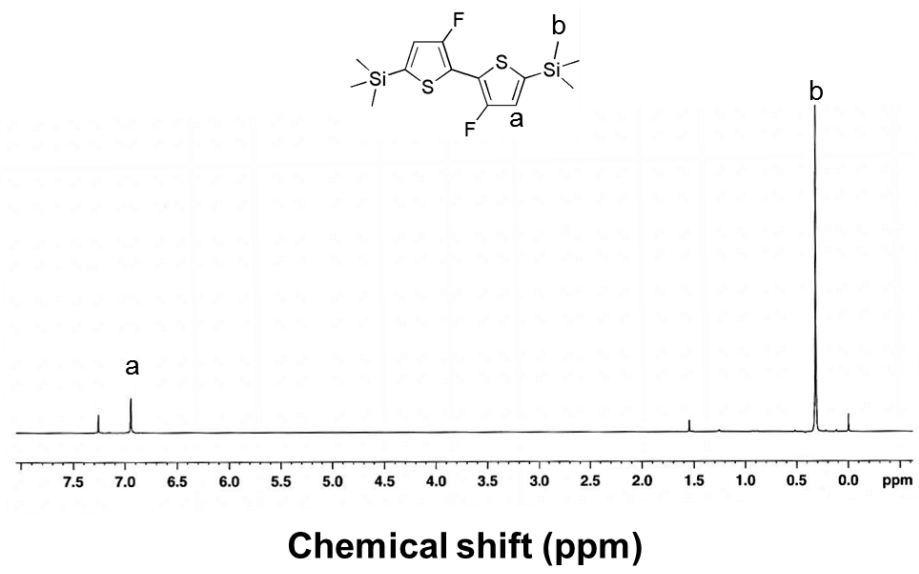

Figure 3.3. ^{1}H NMR spectrum of compound **3** in Scheme 2.1.

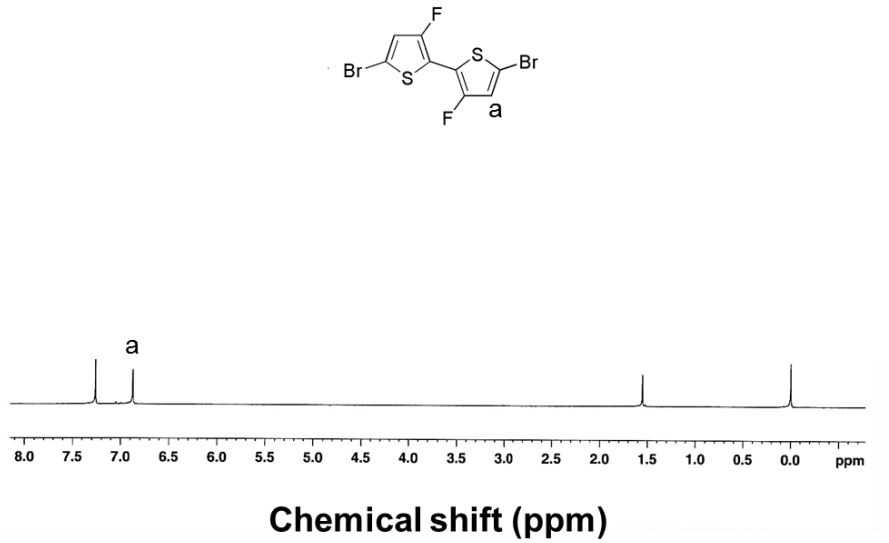

Figure 3.4. ^{1}H NMR spectrum of compound **4** in Scheme 2.1.

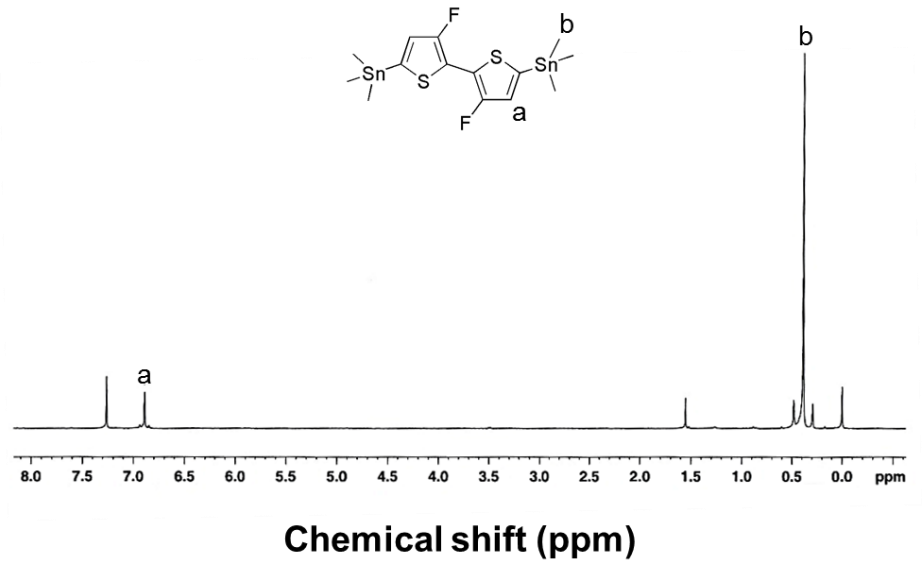

Figure 3.5. ^{1}H NMR spectrum of compound **5** in Scheme 2.1.

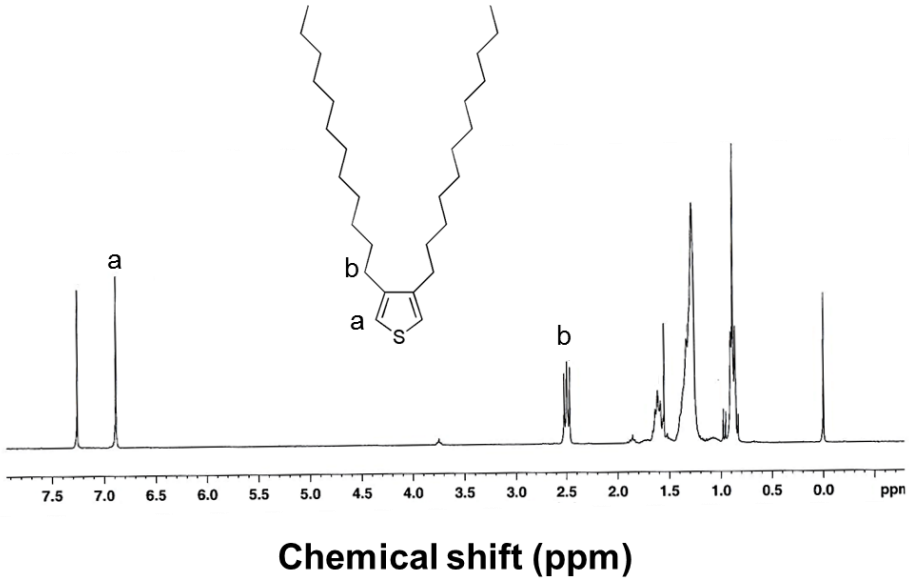

Figure 3.6. ^{1}H NMR spectrum of compound **6** in Scheme 2.1.

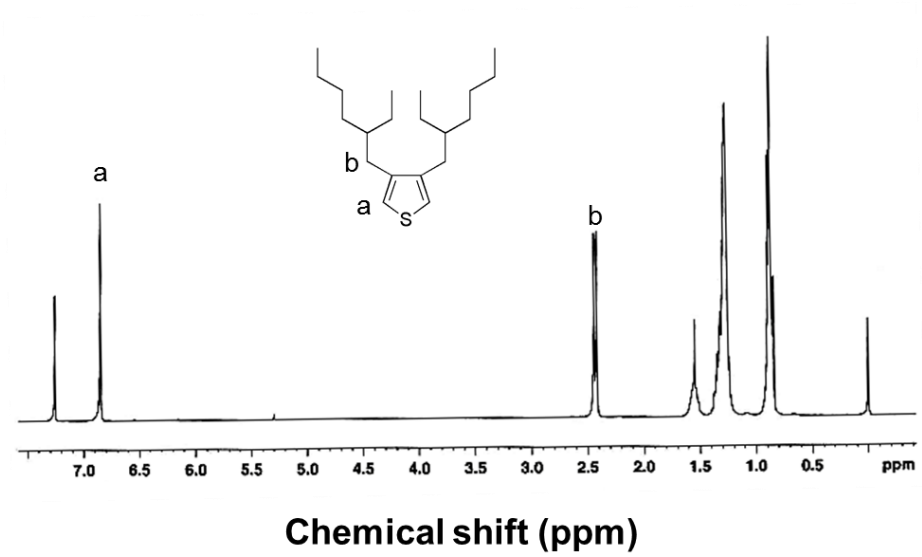

Figure 3.7. ^{1}H NMR spectrum of compound **7** in Scheme 2.1.

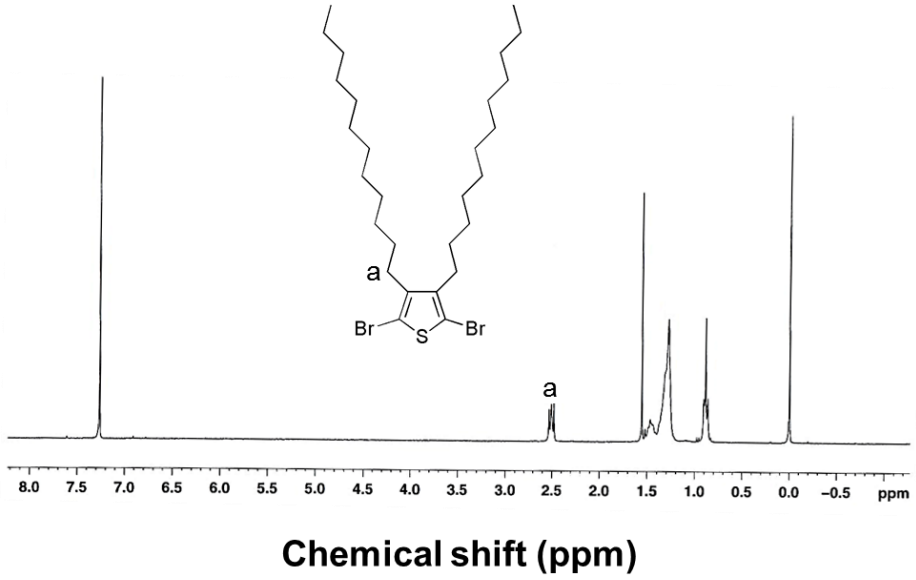

Figure 3.8. ^{1}H NMR spectrum of compound **8** in Scheme 2.1.

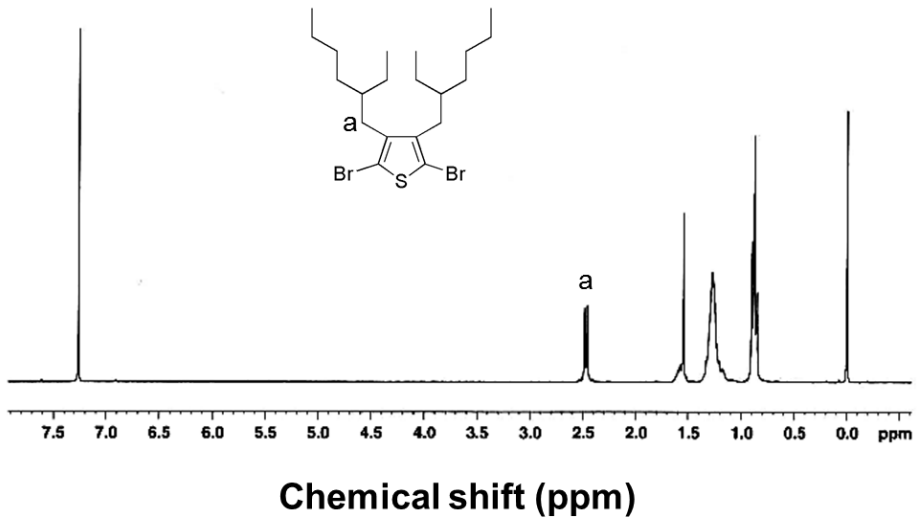

Figure 3.9. ^{1}H NMR spectrum of compound **9** in Scheme 2.1.

compound **4** and then the monomer **5** was synthesized through lithiation of the compound **4** with n-BuLi and subsequent quenching with trimethyltin chloride. Polymerization was carried out via the Stille coupling reaction in toluene/DMF with $Pd(PPh_3)_4$ as a catalyst. The molecular weights and polydispersity indexes (PDI) of polymers were measured by high temperature GPC and listed in Table 3.1.

3.1.2 Optical and electrochemical properties

The UV–Vis absorption spectra of four polymers in chloroform solution and film state are shown in Figure 3.10. In film state, fluorinated polymers (F12 and FEH) show stronger vibronic shoulder at 598 nm than non-fluorinated polymers (H12 and HEH), indicating that the fluorine substitution enhances interchain interaction between polymers. Another interesting feature to note is that F12 exhibits a strong vibronic shoulder at 598 nm in solution while FEH does not show the vibronic absorption, indicating that FEH is soluble in chloroform while F12 is not completely dissolved in the solvent. Therefore, bulky side chain (ethylhexyl) is more effective to dissolve the fluorinated polymers. The optical bandgaps of all PDATs are nearly identical (~1.95 eV) except FEH with slightly lower bandgap.

When electrochemical properties are measured by cyclic voltammetry, as shown in Figure 3.11, the HOMO energy levels of fluorinated polymers (F12 and FEH) were around −5.41 eV while those of non-fluorinated polymers (H12 and HEH) are around −5.28 eV, as listed in Table 3.1. Hence, higher

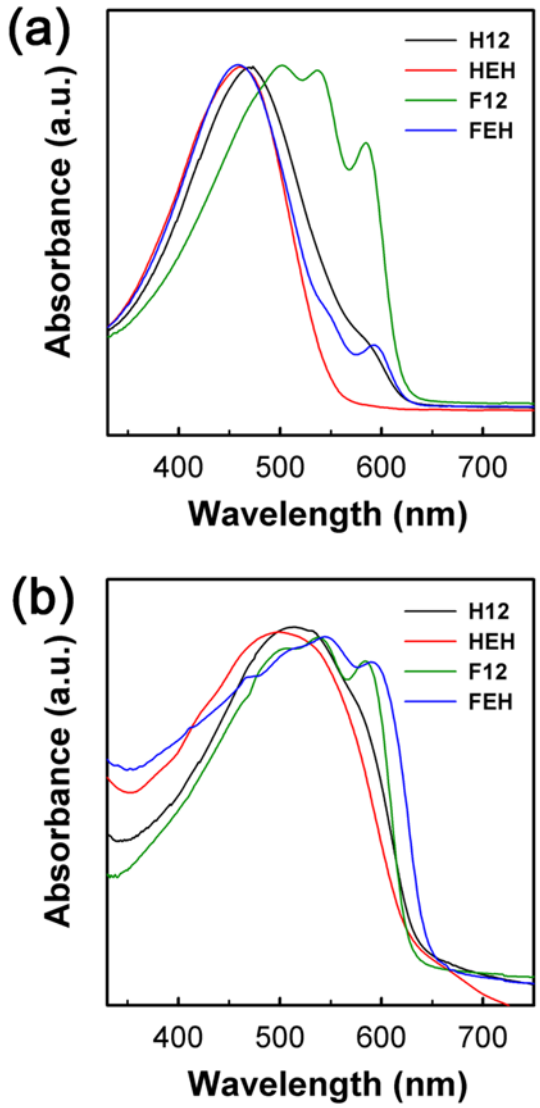

Figure 3.10. UV−Vis absorption spectra of PDATs in (a) $CHCl_3$ solution and (b) film state.

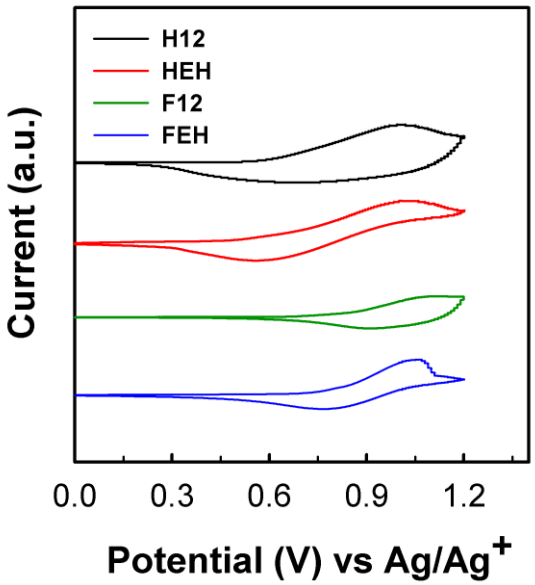

Figure 3.11. Cyclic voltammograms of PDATs.

Table 3.1. Characteristics of PDATs.

PDAT	M_n[a] (kg/mol)	PDI	$E_{g,opt}$[b] (eV)	HOMO (eV)	LUMO[c] (eV)
H12	14	1.38	1.95	−5.28	−3.33
HEH	12	1.73	1.96	−5.27	−3.31
F12	16	1.45	1.95	−5.40	−3.45
FEH	14	2.34	1.91	−5.42	−3.51

[a] Measured from 1,2,4-trichlorobenzene GPC at 135 ℃.

[b] Determined from the onset of UV−Vis absorption spectra.

[c] $E_{g,opt}$ + HOMO.

V_{OC} are expected in the devices fabricated from F12 and FEH. When the LUMO energy levels of polymers were estimated by adding the optical bandgap to the HOMO energy level, the LUMO energy levels of four polymers are in the range of −3.31 to −3.51 eV, which provides sufficient LUMO level offset between polymers and PCBM (−4.3 eV) for effective exciton dissociation at the interface between donor and acceptor.[154]

3.1.3 Computational simulation

To further understand the effect of fluorination on polymer properties, torsional angles, dipole moments, orbital distribution of terthiophenes as model compounds were calculated using the DFT (Figure 3.12, 3.13 and 3.14). Fluorinated terthiophene exhibits more planar structure than non-fluorinated one, because the torsional angle at the minimum energy state of fluorinated terthiophene is 0° while the angle of non-fluorinated one is 17°, as shown in Figure 3.12. The high planarity of fluorinated polymer might come from increase of conjugation,[152] and the planar structure of conjugated backbone can improve intermolecular interaction of polymers with extended conjugation.[47]

The fluorinated terthiophene has higher dipole moment (1.73 D) than non-fluorinated terthiophene (1.37 D) (Figure 3.13), and thus fluorinated PDAT is expected to exhibit more closed packed structure because high dipole moment enhances molecular ordering.

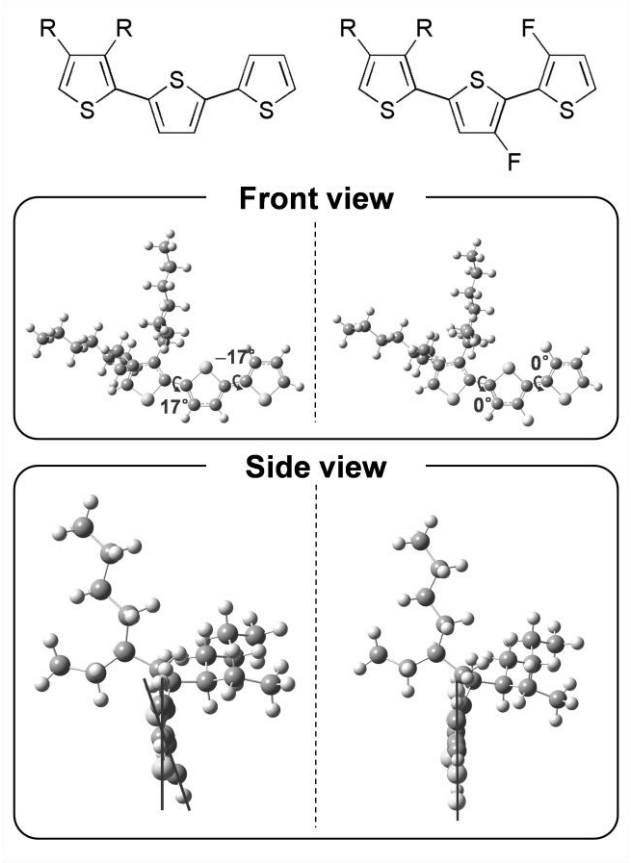

Figure 3.12. Torsion angle at the minimum energy state of non-fluorinated and fluorinated terthiophene (R = 2-ethylhexyl) calculated using DFT with a basis set of B3LYP/6-31G(d,p).

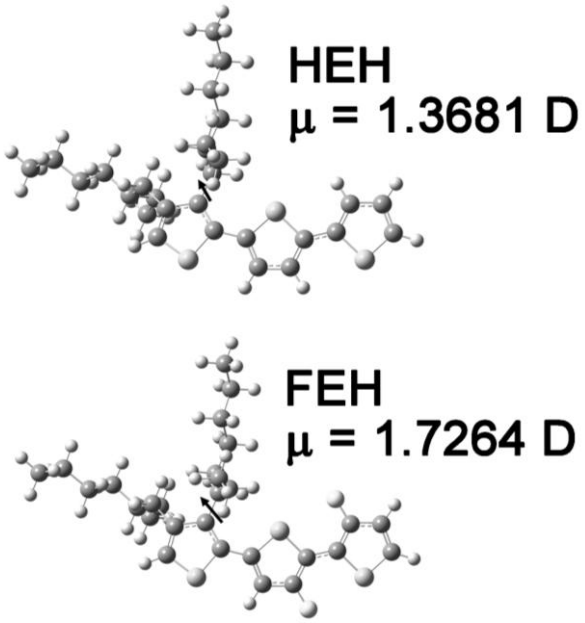

Figure 3.13. Dipole moments of non-fluorinated and fluorinated terthiophene (R = 2-ethylhexyl) calculated using DFT with a basis set of B3LYP/6-31G(d,p).

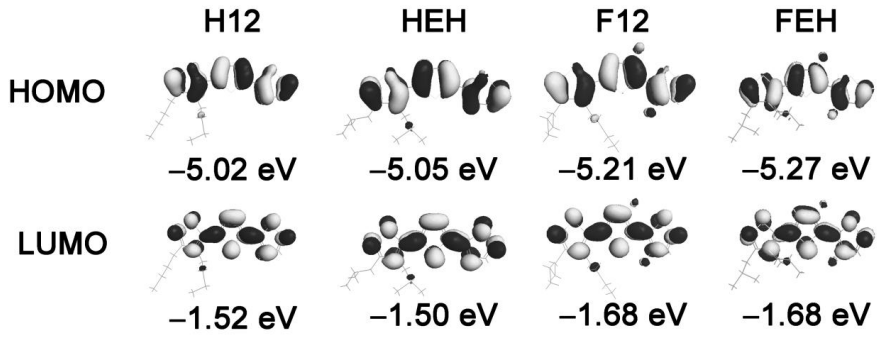

Figure 3.14. Calculated HOMO and LUMO of terthiophenes at the B3LYP/6-31G(d,p) level.

3.1.4 Photovoltaic properties

The photovoltaic properties were measured with the standard device configuration of ITO/PEDOT:PSS/polymer:$PC_{71}BM$/Ca/Al (Figure 3.15a) and listed in Table 3.2. Since deeper HOMO energy level of donor polymer affords higher V_{OC}, the V_{OC}s of fluorinated polymers are higher than those of the corresponding non-fluorinated polymers. Particularly, FEH shows a remarkably high V_{OC} over 0.87 V. As a result, the FEH-based device exhibits a promising PCE of 5.2% at the optimized film thickness of 140 nm, which is 3.5 times larger than HEH-based device. Considering that the devices fabricated from the most commonly used polythiophene derivative in OPVs, P3HT, exhibit a V_{OC} of around 0.6 V,[155] the high V_{OC} of FEH-based device indicates that the photovoltaic properties of conjugated polymers can be effectively controlled by fluorine substitution.

The EQEs of solar cell devices were measured under monochromatic light (Figure 3.15b). Since the polymers have limited optical absorption with a bandgap of 1.95 eV, the EQEs over 650 nm arise from $PC_{71}BM$.[156] FEH exhibits EQE over 60% yielding in higher J_{SC}, while polymers with dodecyl side chain (H12 and F12) show EQEs below 40% in the wavelength range of 400−650 nm.

When hole mobilities are estimated from dark *J*–*V* curve by using the SCLC model, as shown in Figure 3.16, the SCLC hole mobility of FEH/$PC_{71}BM$ device is one order magnitude higher than those of the others (Table 3.2), indicating that FEH/$PC_{71}BM$ blend provides more effective

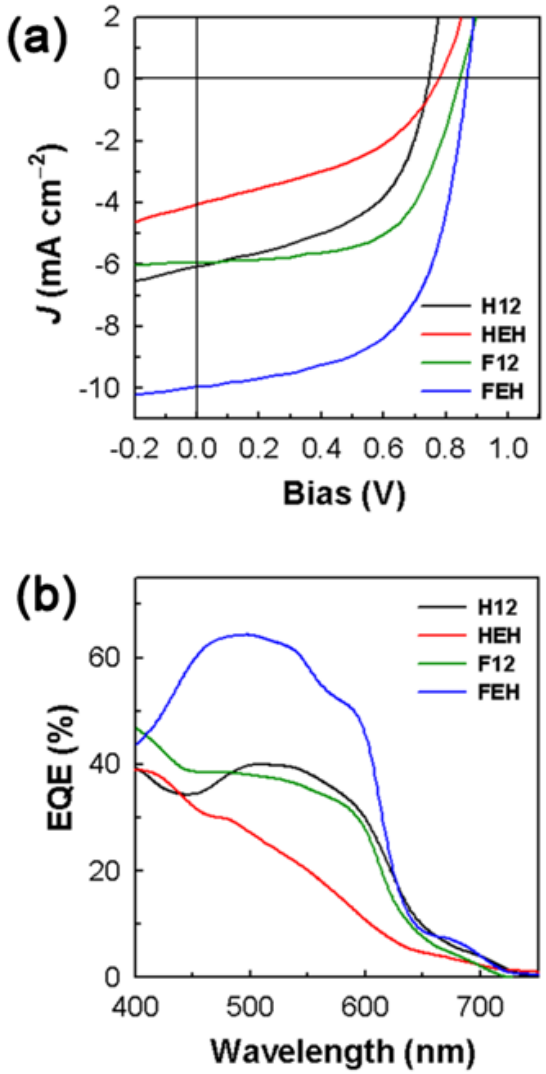

Figure 3.15. (a) *J*−*V* curves and (b) EQE spectra of PDAT/$PC_{71}BM$ solar cells.

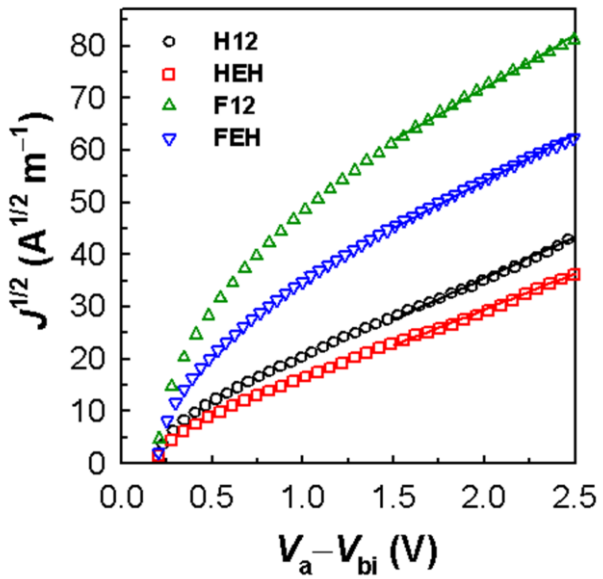

Figure 3.16. Dark *J*−*V* characteristics of PDAT/$PC_{71}BM$ blends with hole-only device, where the solid lines represent the best linear fit of the data points.

Table 3.2. Photovoltaic properties of devices with PDATs under standard AM 1.5G illumination.

PDAT	Polymer:$PC_{71}BM$ (w/w)	Thickness (nm)	μ_h SCLC ($cm^2/V\,s$)	V_{OC} (V)	J_{SC} (mA/cm^2)	FF (%)	PCE_{max} ($_{aver}$) (%)
H12	1:0.8	75	3.5×10^{-5}	0.77	6.09	53	2.49 (2.24)
HEH	1:0.8	70	2.2×10^{-5}	0.80	4.04	43	1.39 (1.18)
F12	1:1	80	6.3×10^{-5}	0.84	5.93	61	3.04 (2.86)
FEH	1:0.8	90		0.88	8.79	63	4.87 (4.64)
FEH	1:0.8	140	3.0×10^{-4}	0.87	9.82	61	5.20 (4.94)

charge pathway in out-of-plane direction.

3.1.5 Molecular orientation

The preferential orientation of polymers was investigated by GIWAXS. All pristine polymer films show only (*h*00) reflections in the out-of-plane (q_z) direction, as shown in Figure 3.18, indicating that most of polymer chains take edge-on orientation on the substrate. The (100) peaks of H12, HEH, F12 and FEH are observed at q_z = 0.24, 0.34, 0.31 and 0.44 $Å^{-1}$, respectively, corresponding to the interchain distance of 26.2, 18.5, 20.3 and 14.3 Å. The polymers with shorter side chain (ethylhexyl) exhibit shorter interchain distance than those with longer side chain (dodecyl). It has also been observed that the interchain distances of fluorinated polymers are shorter than those of the corresponding non-fluorinated polymers, indicating that fluorinated polymers are more closely packed in ordered crystalline domain.

Another important feature is that F12 and FEH clearly show the (010) reflection at q_{xy} = 1.7 $Å^{-1}$ corresponding to the π–π stacking distance of 3.7 Å, as shown in Figure 3.18b, while non-fluorinated polymers do not exhibit discernibly the (010) reflection as also observed in previous report.[149,150] This leads us to conclude that fluorination significantly enhances polymer chain packing in the π–π direction.

It has also been observed that the FEH/$PC_{71}BM$ blend exhibits weak (010) diffraction peak in the out-of-plane direction along with stronger (100) diffraction in the in-plane direction of GIWAXS as compared with the other

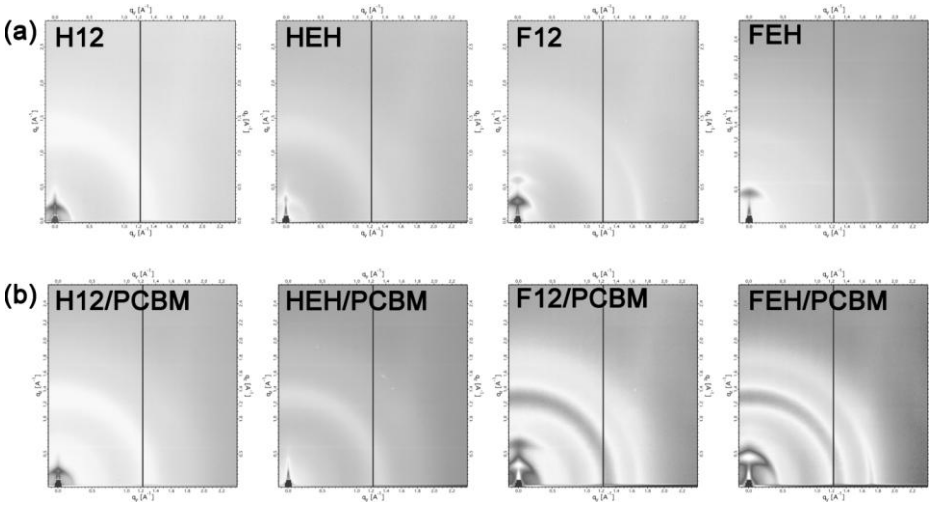

Figure 3.17. GIWAXS pattern images of (a) PDATs and (b) PDAT/$PC_{71}BM$ blend films.

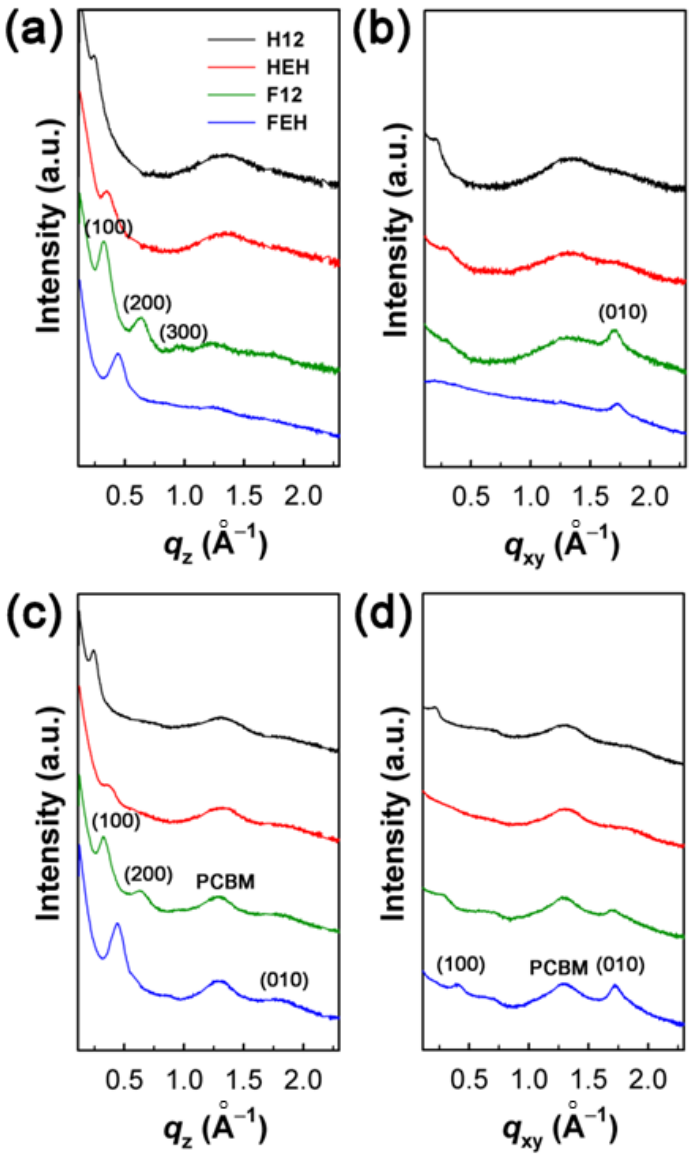

Figure 3.18. (a) q_z and (b) q_{xy} scans of GIWAXS from thin films of PDATs; (c) q_z and (d) q_{xy} scans of GIWAXS from blend films of PDAT/$PC_{71}BM$.

blends, as shown in Figure 3.18d, indicating a part of FEH crystals take the face-on orientation after blending with $PC_{71}BM$, which may contribute to effective charge transport. It should be noted here that the (100) *d*-spacings of all polymer/$PC_{71}BM$ blends are the same as those of corresponding pristine polymers, implying that $PC_{71}BM$ molecules do not intercalate in between side chains of polymers.[157]

3.1.5 Morphologies of active layers

Morphologies of active layers were observed by TEM, as shown in Figure 3.19. The active layer of H12/$PC_{71}BM$ shows a large phase separation between polymer and PCBM while that of HEH/$PC_{71}BM$ exhibits a homogenously mixed morphology. The large domain sizes of H12/PCBM over 100 nm are not effective for charge generation because of limited exciton diffusion length (~10 nm) in OPVs.[158] However, the active layer of fluorinated polymer/$PC_{71}BM$ shows well-developed fibril structure, which indicates improved polymer ordering by fluorination and is beneficial for charge transport. Particularly, FEH with bulky side chain exhibits finer fibrils than F12 with linear side chain, as shown in Figure 3.19c and 3.19d, leading to higher J_{SC} due to larger interface area between polymer and PCBM domains.

The transmission R-SoXS were measured at the carbon K absorption edge to determine the average domain size of polymer/PCBM blend. The R-SoXS scattering profiles of four blends at the photon energy of 248.2 eV,

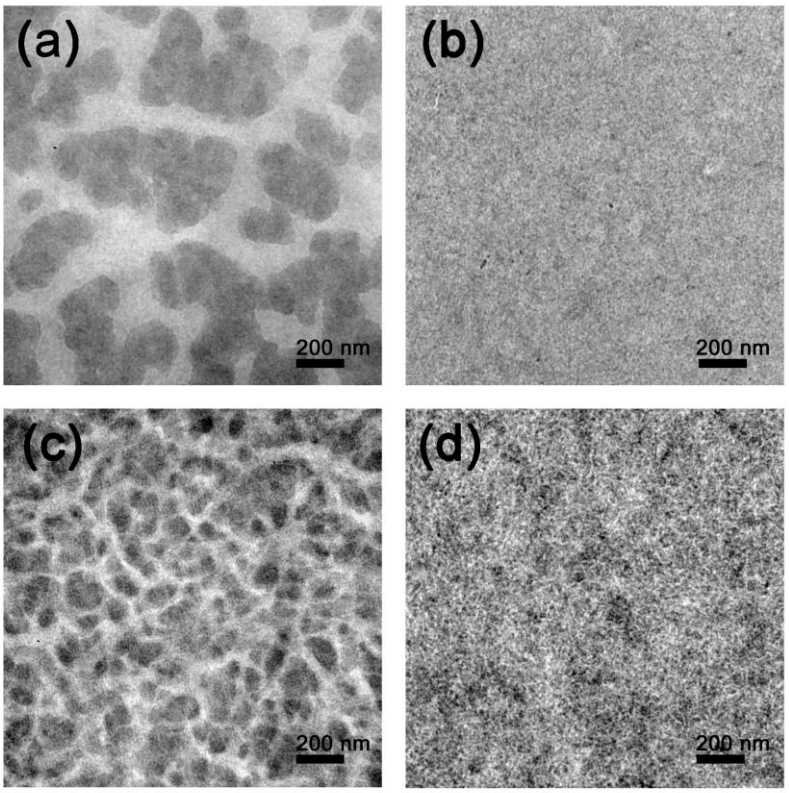

Figure 3.19. TEM images of PDAT/$PC_{71}BM$ blend films: (a) H12, (b) HEH, (c) F12, and (d) FEH.

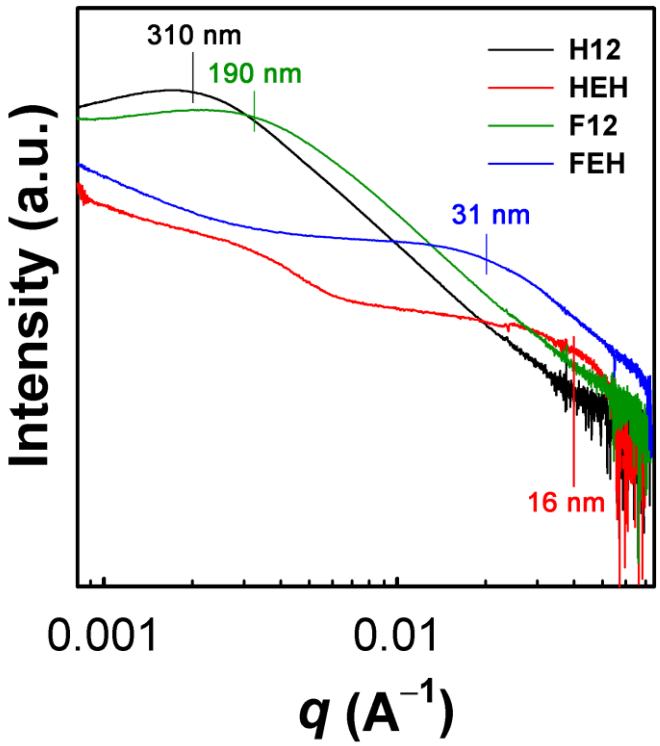

Figure 3.20. R-SoXS profiles of PDAT/$PC_{71}BM$ blend films.

where the contrast between $PC_{71}BM$ and PDATs is the maximum, are shown in Figure 3.20. The domain sizes of H12, HEH, F12 and FEH as determined from the peak of the profile are 310, 16, 190, 31 nm, respectively, which are very consistent with the sizes estimated from TEM images in Figure 3.19. It is also realized that polymers with bulky side chain have smaller domain sizes than those with linear side chains. In short, fluorination increases planarity of chains and thus enhances chain packing which contributes to the increase of J_{SC}, and also lowers the HOMO energy level which increases the V_{OC} as compared to non-fluorinated one.

3.1.7 Summary

We designed and synthesized polythiophene derivatives difluoro-bithiophene. Fluorination on polymer backbone changes its electronic structure, leading to deeper HOMO energy level and enhances molecular packing of the polymers as evidenced by strong vibronic shoulder in UV−Vis absorption spectrum and π−π stacking pattern in GIWAXS. When bulky side chain (ethylhexyl) are introduced as a solubilizing group, fluorinated polythiophenes develop finer fibril structure and exhibit a promising PCE of 5.12% with a V_{OC} of 0.87 V and a J_{SC} of 9.82 mA/cm^2. Our results suggest that the photophysical properties and device performances of conjugated polymers can be easily tuned by substitution of fluorine atom on polymer chain.

3.2 Effect of fluorination in D–A type polymer based on diketopyrrolopyrrole for high performance solar cells

3.2.1 Synthesis and characterization

In past decade, D–A type copolymers have been considered to be most promising candidate for developing low-bandgap polymers because internal charge transfer between D and A unit can reduce the bandgap of polymers and the electronic properties of polymers can be manipulated by a proper combination of D and A units.[71,91]

Among several moieties for D–A type polymers, DPP have attracted extensive interest as an A unit due to their advantages including strong electron deficiency with amide group, efficient charge transport with well conjugated and highly planar structure, high self–assembly ability, and ease to attach solubilizing side groups. And also various DPP-based D–A type polymers have been reported for PSCs and high PCEs over 6% have been achieved with DPP-based polymers.[159] However, compared with other D–A type polymers such as TPD-based, BT-based and Ii-based polymers, DPP-based polymers have exhibited relatively low V_{OC} below 0.75 V, which is a limiting factor for high efficiency PSCs.[160]

Recently, Janssen group reported DPP-based polymers substituted by fluorine atoms for lowering HOMO energy levels of polymers. The incorporation of fluorinated biphenyl units into DPP-based polymer provided deep HOMO energy level of −5.48 eV and a PCE of 4.1% with a high V_{OC} of

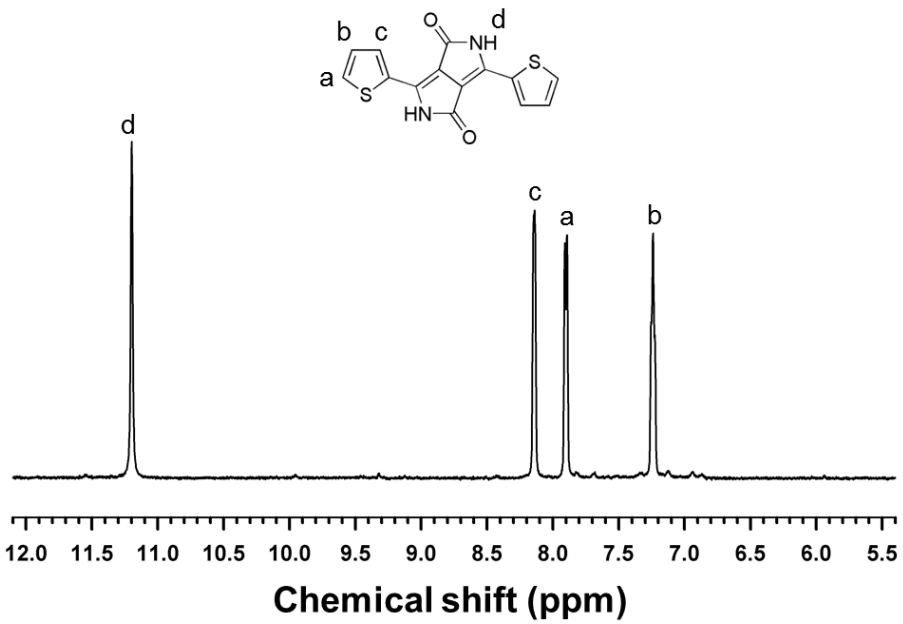

Figure 3.21. ^{1}H NMR spectrum of compound **10** in Scheme 2.2.

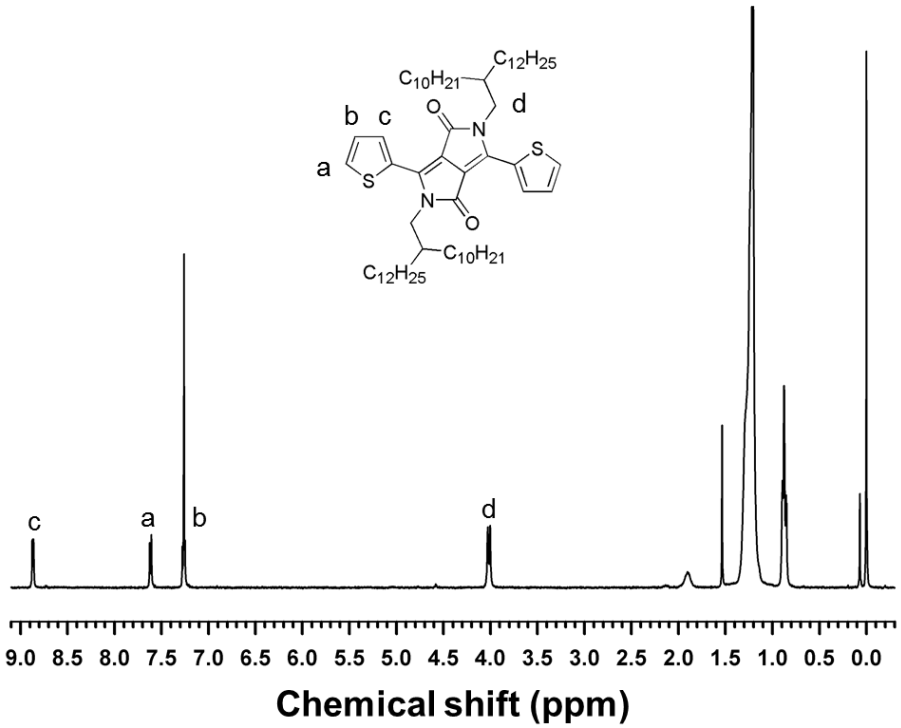

Figure 3.22. ^{1}H NMR spectrum of compound **11** in Scheme 2.2.

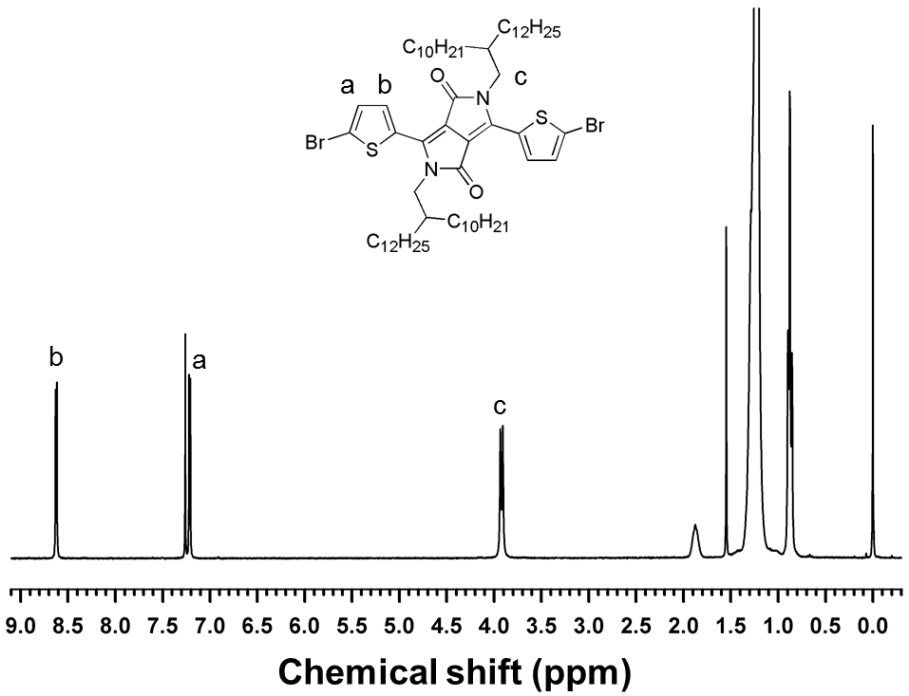

Figure 3.23. ^{1}H NMR spectrum of compound **12** in Scheme 2.2.

0.93 V.[161]

In this work, we prepared a fluorinated D–A type polymer copolymerized by DPP as an A unit and difluoro-bithiophene as a D unit in order to obtain DPP-based polymer with deep HOMO energy level and clarify the effect of fluorine atom substitution on the properties of D–A type polymers.

A non-fluorinated polymer (denoted as PDPP-0F) and a fluorinated D–A type polymers (denoted as PDPP-2F) were synthesized via the Stille coupling reaction in toluene with $Pd_2(dba)_3$/P(o-toyl)$_3$ as a catalyst, as shown in Scheme 2.2. When the number average molecular weights and PDI of polymers were measured by GPC, as listed in Table 3.3, it reveals that all polymers have sufficient molecular weight (>100 kg/mol) not as to significantly affect their photovoltaic performances. Long and branched alkyl chains (2-decyltetradecyl) were introduced to enhance the solubility of polymers in organic solvents and the synthesized polymers are highly soluble in common organic solvents such as chloroform, chlorobenzene and dichlorobenzene.

3.2.2 Optical and electrochemical properties

The UV–Vis absorption spectra of polymers in chloroform solution and film state are shown in Figure 3.24. An identical onset of absorption spectrum is observed at 880 nm for both polymers, corresponding to a bandgap of 1.41 eV. Moreover, both polymers show almost same absorption spectra in whole range of wavelengths, indicating fluorination do not significantly affect

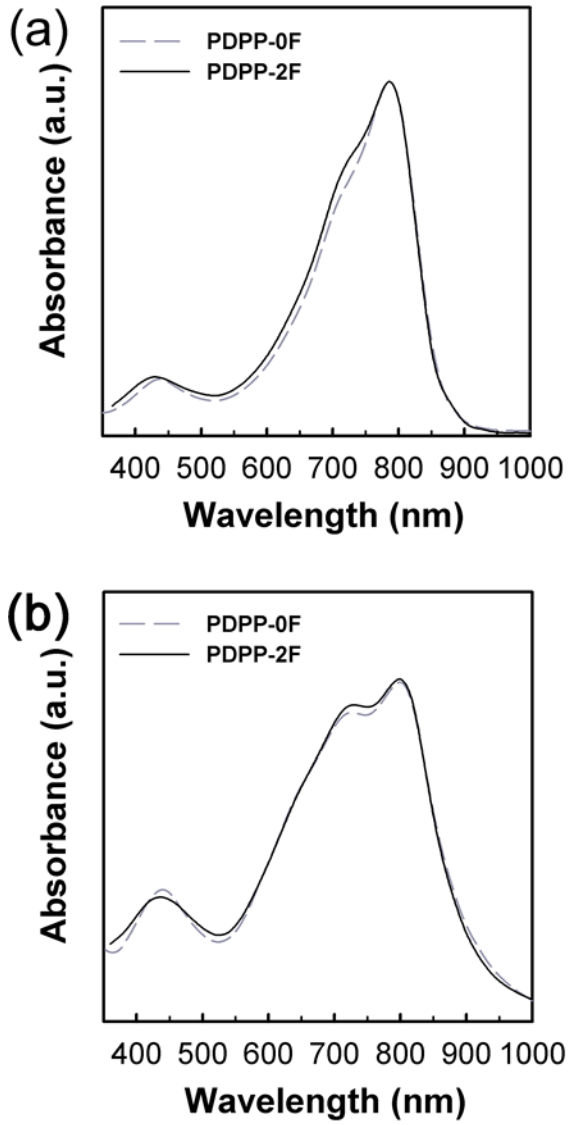

Figure 3.24. UV−Vis absorption spectra of DPP-based polymers in (a) $CHCl_3$ solution and (b) film state.

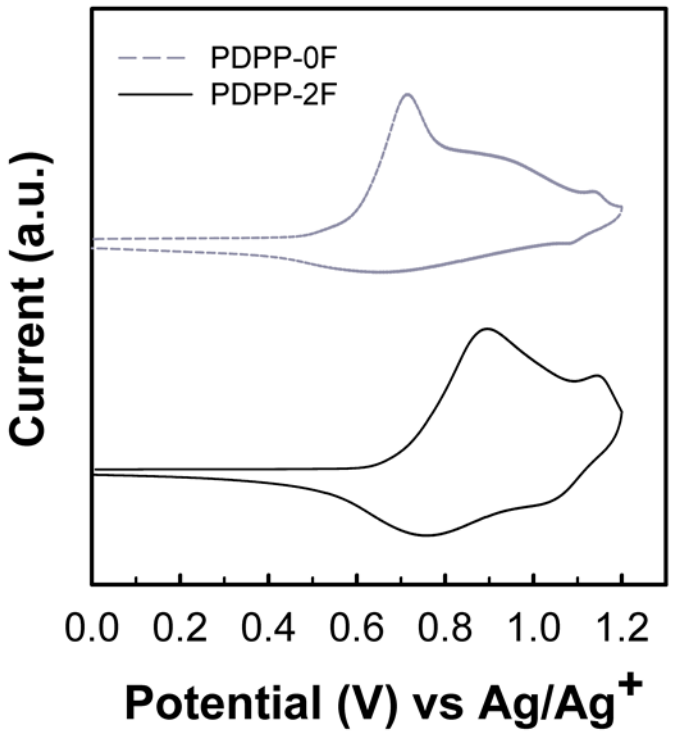

Figure 3.25. Cyclic voltammograms of DPP-based polymers.

Table 3.3. Characteristics of DPP-based polymers.

Polymer	M_n[a] (kg/mol)	PDI	$E_{g,opt}$[b] (eV)	HOMO (eV)	LUMO[c] (eV)
PDPP-0F	110	1.31	1.41	–5.16	–3.75
PDPP-2F	140	1.34	1.41	–5.27	–3.86

[a] Measured from $CHCl_3$ GPC.

[b] Determined from the onset of UV−Vis absorption spectra.

[c] $E_{g,opt}$ + HOMO.

optical properties of DPP-based polymer. The red shift by ~10 nm in film state compared to the absorption maximum of chloroform solution indicates an increased π–π stacking of polymer backbone in solid film.

When electrochemical properties are measured by cyclic voltammetry, as shown in Figure 3.25, the HOMO energy levels of PDPP-2F were around –5.27 eV while those of PDPP-0F are around –5.16 eV, as listed in Table 3.3. Since V_{OC} is proportional to the difference the HOMO energy level of donor polymer and the LUMO energy level of acceptor, higher V_{OC} are expected in the devices fabricated from PDPP-2F.

3.2.3 Computational simulation

To further understand the effect of fluorination on properties of D–A type polymers, torsional angles and orbital distribution were calculated using the DFT (Figure 3.26), and the calculated data are summarized in Table 3.4. Nearly planar structures of both polymers imply that introduction of fluorine atoms, which are the smallest electro-withdrawing group (van der Waals radius, r = 1.35 Å), cannot significantly induce steric hindrance on the conjugated backbone of polymer. Furthermore, the orbital distributions of HOMO and LUMO in both polymers are almost same, indicating that fluorination do not have noticeable effects on orbital distributions in D–A alternating polymers.

Recently, it has been reported that a large dipole change from ground to excited state ($\Delta\mu_{ge}$) facilitates exciton dissociation and generation of charge-

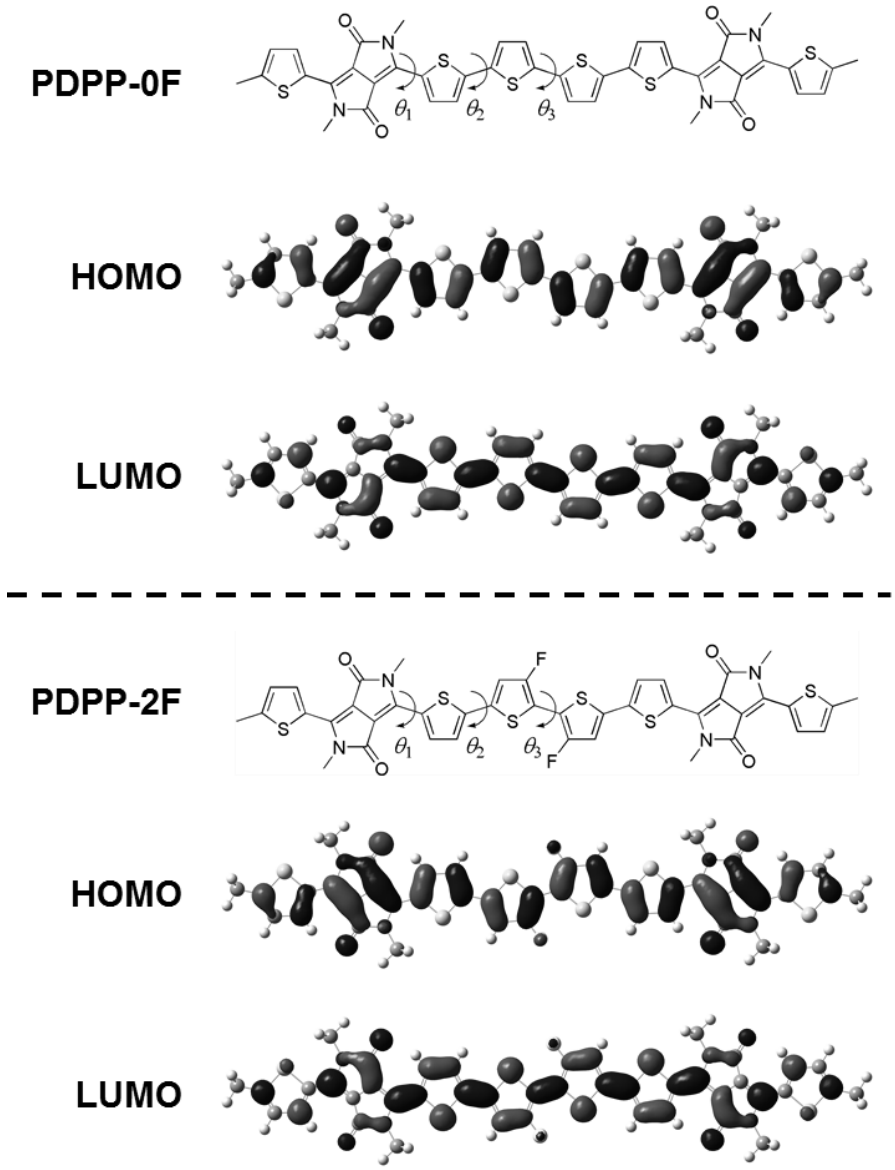

Figure 3.26. Chemical structure of repeating units for simulation, and HOMO and LUMO orbital distributions as calculated at the B3LYP/6-31G(d,p) level.

Table 3.4. Torsion angles and energy levels of DPP-based repeating units calculated by DFT.

Polymer	θ_1 (Deg)	θ_2 (Deg)	θ_3 (Deg)	HOMO (eV)	LUMO (eV)
PDPP-0F	0.02	–0.22	–0.53	–4.70	–2.82
PDPP-2F	0	–0.01	–0.01	–4.74	–2.88

Table 3.5. Dipole moments of DPP-based repeating units calculated by time-dependent DFT.

Polymer	μ_g (D)	μ_{ex} (D)	$\Delta\mu_{ge}$ [a] (D)
PDPP-0F	1.26	1.05	1.18
PDPP-2F	0.26	2.90	1.85

[a] $\Delta\mu_{ge} = [(\mu_{gx} - \mu_{ex})^2 + (\mu_{gy} - \mu_{ey})^2 + (\mu_{gz} - \mu_{ez})^2]^{1/2}$

separated state.[162,163] When dipole moments were calculated for repeating units of the DPP-based polymers, as listed in Table 3.5, fluorinated polymer, PDPP-2F (1.85 D) have a lager $\Delta\mu_{ge}$ than, non-fluorinated polymer, PDPP-0F (1.18 D) and higher J_{SC} values in the PSC devices fabricated with fluorinated polymers are expected.

3.2.4 Photovoltaic properties

The PSCs were fabricated with the conventional device configuration of glass/ITO/PEDOT:PSS/polymer:$PC_{71}BM$/Ca/Al. *J–V* characteristics under AM 1.5G illumination are shown in Figure 3.27a and relevant photovoltaic properties are summarized in Table 3.6. When the blend ratio of polymer to $PC_{71}BM$ was varied, the optimized ratio was 1:1.5 and $CHCl_3$:DCB (4:1, v/v) was used as a casting solvent to optimize the morphologies of active layers. Although fluorinated polymer has higher $\Delta\mu_{ge}$ than non-fluorinated polymer, PDPP-0F exhibits higher J_{SC} values than PDPP-2F. However, after fluorination, the V_{OC} of DPP-based polymer is highly improved due to deeper HOMO energy level induced by electro-withdrawing fluorine atoms. Consequently, PDPP-2F exhibits a higher PCE of 6.39% with a V_{OC} of 0.77 V, a J_{SC} of 14.3 mA/cm^2 and a FF of 0.58 than PDPP-0F, indicating that introduction of fluorination on backbone of D–A type polymer is a promising method for achieving high performance PSC.

When EQEs of solar cell devices were measured under monochromatic light, as shown in Figure 3.27b, both DPP-based polymers exhibit similar

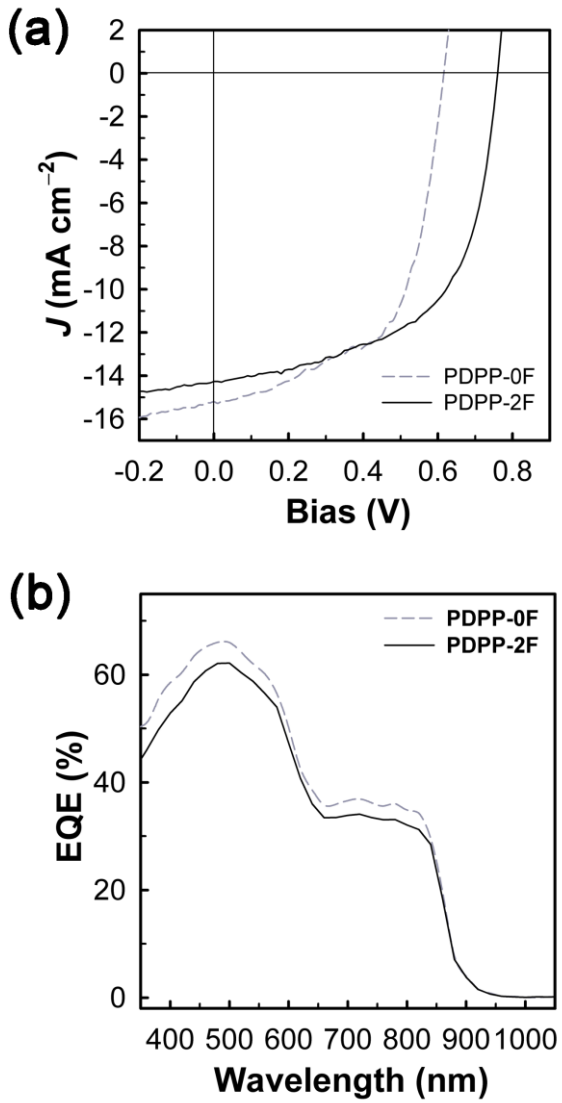

Figure 3.27. (a) *J*−*V* curves and (b) EQE spectra of DPP-based polymer/$PC_{71}BM$ solar cells.

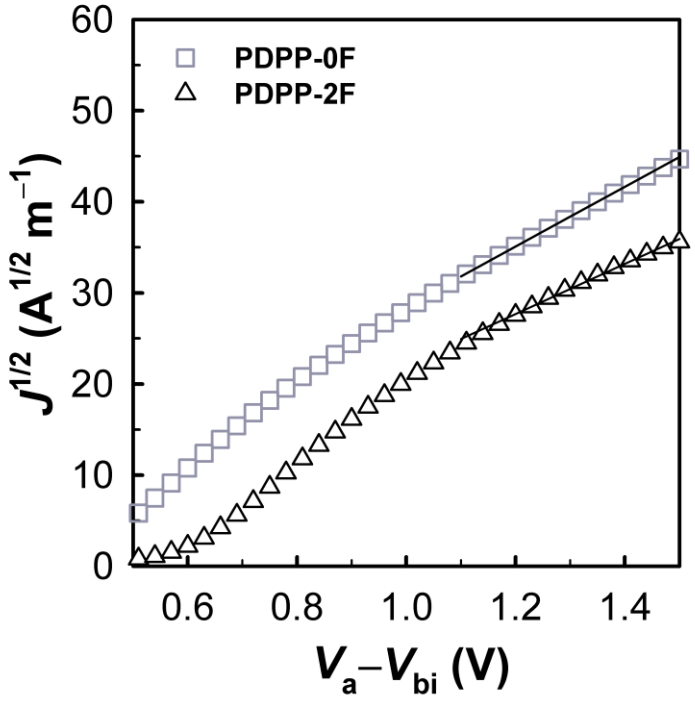

Figure 3.28. Dark *J*−*V* characteristics of DPP-based polymer/$PC_{71}BM$ blends with hole-only device, where the solid lines represent the best linear fit of the data points.

Table 3.6. Photovoltaic properties of devices under standard AM 1.5G illumination.

Polymer	Thickness (nm)	V_{OC} (V)	J_{SC} (mA/cm^2)	FF (%)	PCE (%)
PDPP-0F	200	0.62	15.2	58	5.47
PDPP-2F	160	0.77	14.3	58	6.39

EQEs in the whole range of wavelengths due to similar optical properties of both polymers. However, PDPP-0F shows slightly higher EQE values, consistent with higher J_{SC} of the device with PDPP-0F than the device with PDPP-2F.

When hole mobilities were measured from dark *J*–*V* curve of hole-only device by using the SCLC model, as shown in Figure 3.28, high hole mobilities are observed in both PDPP-0F/$PC_{71}BM$ (1.03×10^{-3} $cm^2/V\cdot s$) and PDPP-2F/$PC_{71}BM$ (2.41×10^{-3} $cm^2/V\cdot s$) blend films, which contribute to efficient charge transport in the polymer of active layers.

3.2.5 Molecular ordering

The molecular ordering of PDPP-0F and PDPP-2F was studied by X-ray diffraction (XRD) (Figure 3.29). Both polymers exhibit an intense (100) peak with discernible (200) and (300) reflection peaks, indicating high crystallinity of both DPP-based polymers. The interchain distance of fluorinated polymer is larger than the non-fluorinated polymer because the (100) peaks of PDPP-0F and PDPP-2F are observed at q = 0.29 and 0.28 $Å^{-1}$, corresponding to the interchain distance of 21.8 and 22.8 Å, respectively.

3.2.6 Morphologies of active layers

Morphologies of active layers were observed by TEM, as shown in Figure 3.30. The active layers of both polymers show well-developed interconnected

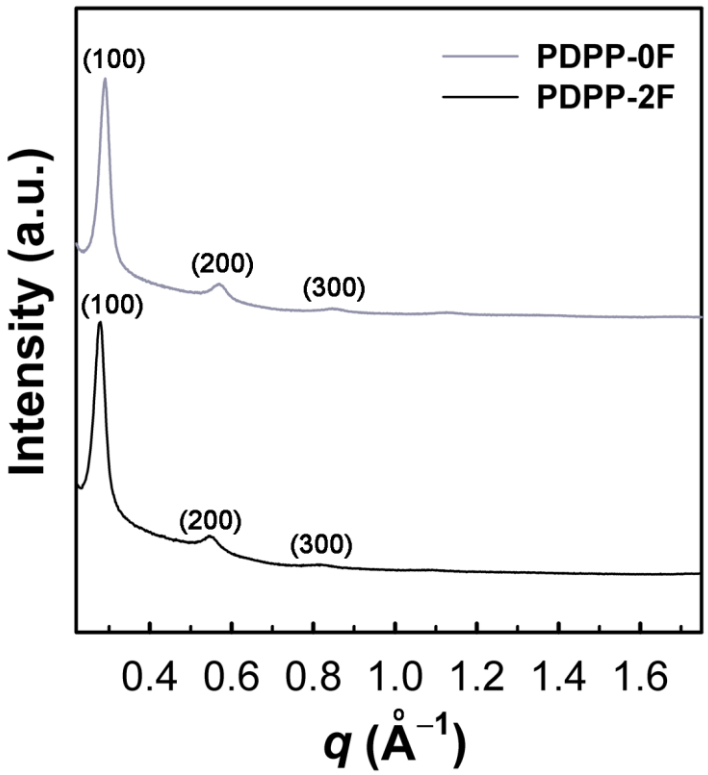

Figure 3.29. XRD patterns of PDPP-0F and PDPP-2F films.

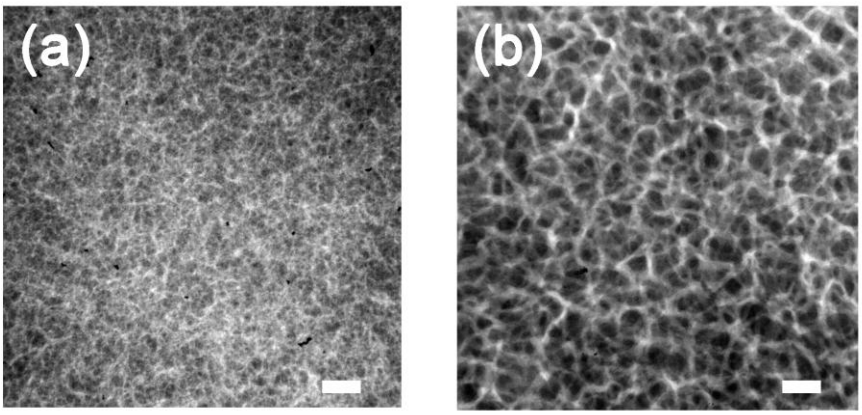

Figure 3.30. TEM images of DPP-based polymer/$PC_{71}BM$ blend films: (a) PDPP-0F and (d) PDPP-2F. The scale bar denotes 200 nm.

network with nanoscale fibril structure, which is beneficial for charge carriers generation and charge transport. Recently, Weiwei et al.[164,165] have demonstrated that wider fibrils of DPP-based polymer in active layer of PSC result in lower EQEs. Since fluorination on the backbone enhances aggregation of polymers and facilitates phase separation between polymer and PCBM, the fibril size of PDPP-2F is larger than that of PDPP-0F, resulting in lower EQE values of the device with PDPP-2F than the device with PDPP-0F.

3.2.7 Summary

We synthesize fluorinated D–A type polymer consisting of DPP and difluoro-bithiophene. Introduction of fluorine atoms on conjugated backbone leads to deeper HOMO energy level of polymer without significant change of optical properties. Although the fluorinated DPP-based polymer exhibits lower J_{SC}, PDPP-2F exhibits higher PCE of 6.39% than PDPP-0F (PCE = 5.47%) due to large improvement of V_{OC}. Therefore, the introduction of fluorination on backbone of D–A type polymer is a promising strategy for achieving high performance PSC.

3.3 Comparison of two D–A type polymers with each being fluorinated on D and A unit for high performance solar cells

3.3.1 Synthesis and characterization

BT has widely been used as an A unit in D–A type polymers for organic electronics including PSC and organic field-effect transistor. Although BT has low solubility and relatively high-lying LUMO energy level, BT-based polymers have been considered promising candidates for high performance PSCs owing to many efforts to improve electro-optical properties of BT-based polymer by modifying their chemical structures. Recently, as one of the modification methods for BT-based polymers, introduction of fluorine atoms on polymer backbone have been proposed and fluorinated BT-based polymers have achieved PCEs above 7%.[136-138] However, the effect of fluorination on D unit in BT-based D–A polymer on photovoltaic properties has scarcely been studied, while most of studies have focused on the fluorination on A unit in the copolymers.

In this work, we synthesized two kinds of D–A polymers with each being fluorinated on A and D unit, where quaterthiophene and BT are used as D and A unit, respectively, in order to investigate the effect of fluorination position on photophysical properties of polymers and their device performances of PSCs.

A non-fluorinated D–A polymer (denoted as HH) and two different

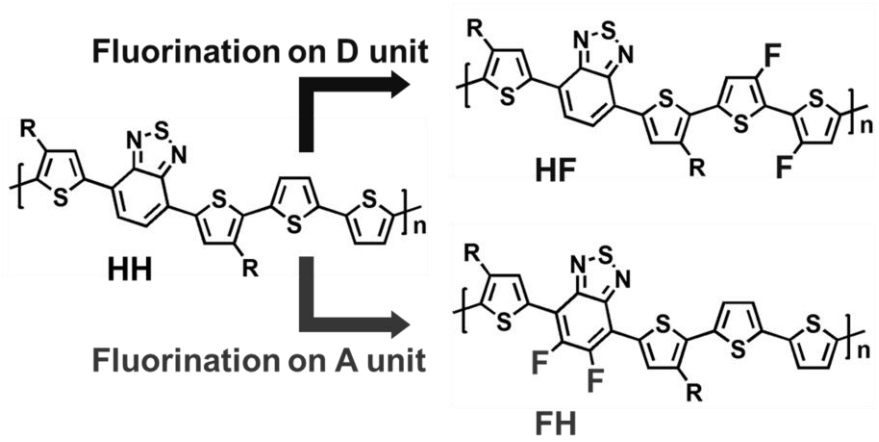

Scheme 3.1. Structure of fluorinated and non-fluorinated BT-based polymers.

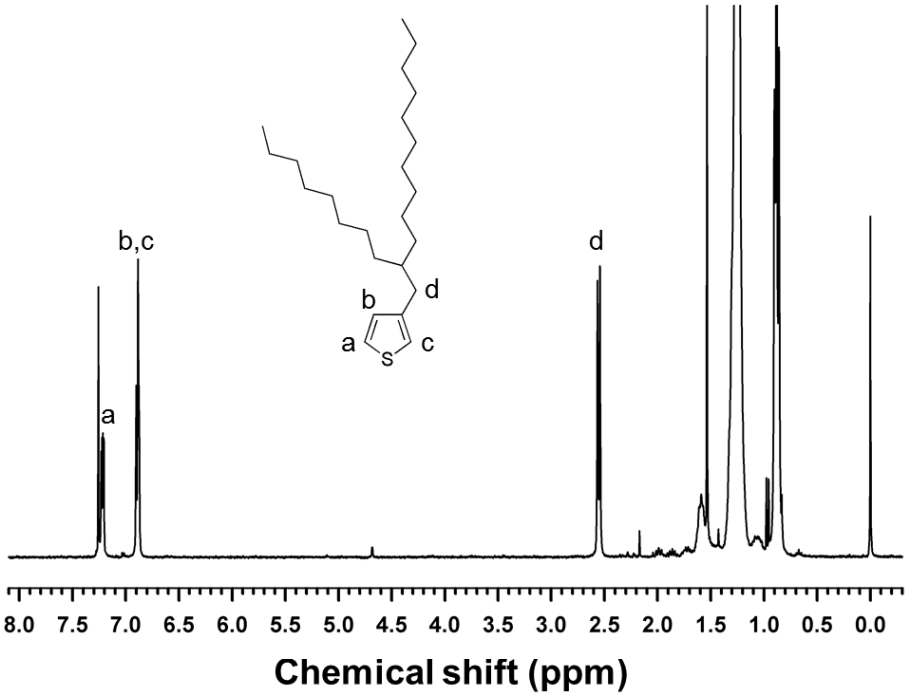

Figure 3.31. ^{1}H NMR spectrum of compound **13** in Scheme 2.3.

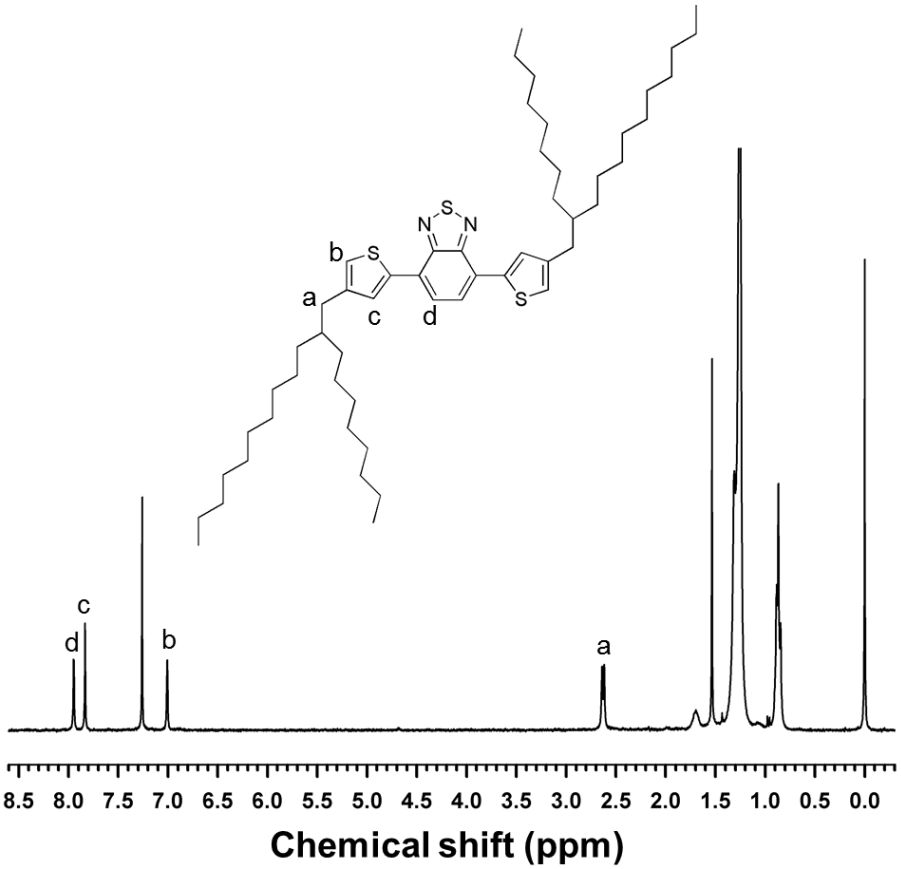

Figure 3.32. ^{1}H NMR spectrum of compound **15** in Scheme 2.3.

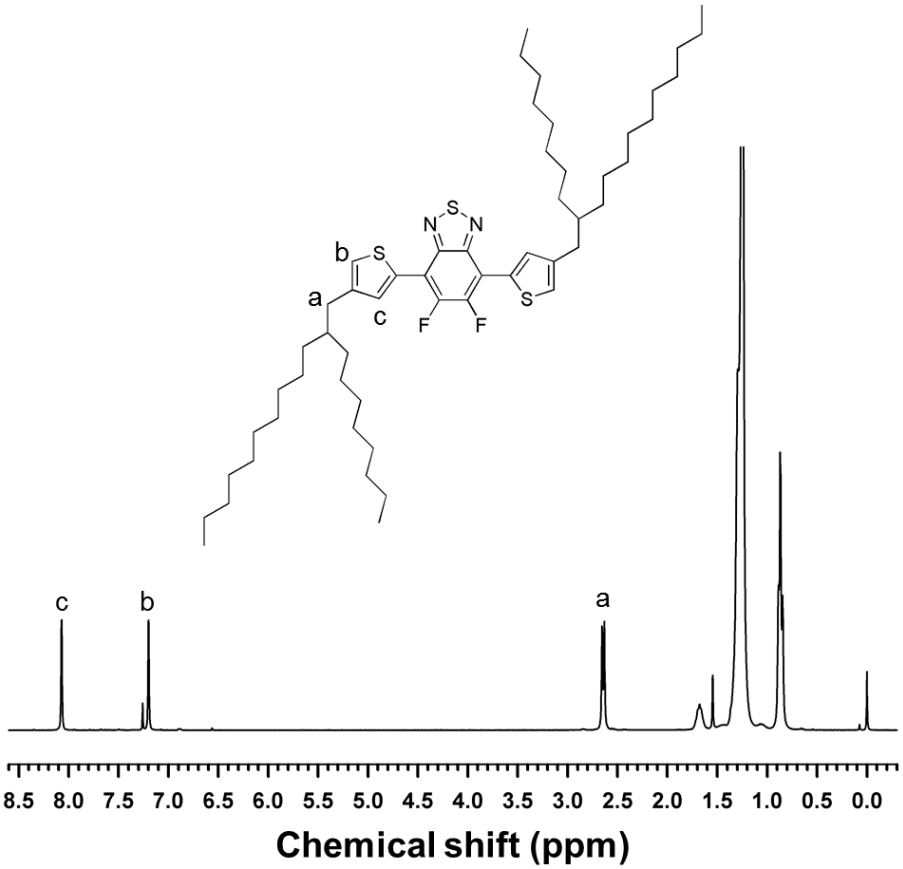

Figure 3.33. ^{1}H NMR spectrum of compound **16** in Scheme 2.3.

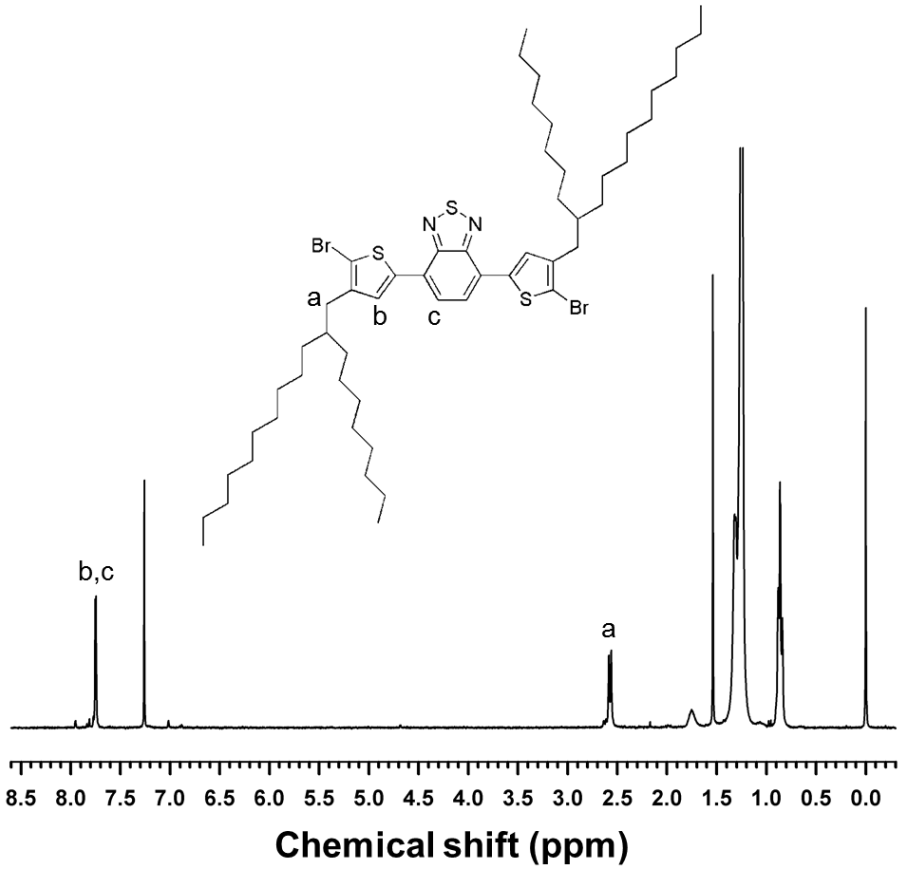

Figure 3.34. ^{1}H NMR spectrum of compound 1**7** in Scheme 2.3.

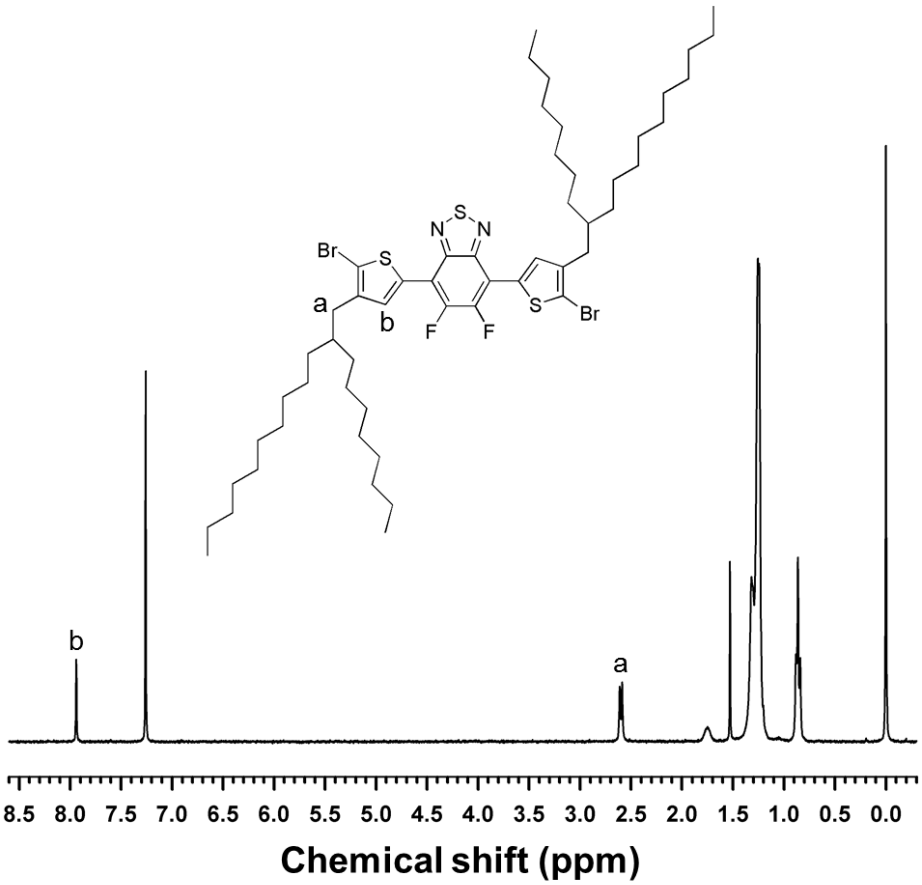

Figure 3.35. ^{1}H NMR spectrum of compound **18** in Scheme 2.1.

fluorinated D–A polymers (denoted as HF and FH for the copolymer with fluorinated D unit and the copolymer with fluorinated A unit, respectively) were synthesized via the Stille coupling reaction in toluene/DMF with $Pd(PPh_3)_4$ as a catalyst, as shown in Scheme 2.3. When the number average molecular weights and PDI of polymers were measured by high temperature GPC, as listed in Table 3.7, it reveals that all polymers have sufficient molecular weight (>40 kg/mol) not as to significantly affect their photovoltaic performances. Synthesized polymers are highly soluble in common organic solvents such as chloroform, chlorobenzene and dichlorobenzene at room temperature.

All polymers are thermally stable up to 400 ^{o}C (see Figure 3.36). When the melting and crystallization temperatures are measured by a differential scanning calorimetry, the melting and crystallization temperatures of fluorinated polymers (HF and FH) are higher than non-fluorinated one (HH) (see Figure 3.37).

3.3.2 Optical and electrochemical properties

When UV–Vis absorption spectra of the D–A polymers in chloroform solution and film state are compared, as shown in Figure 3.38, an identical onset of absorption spectrum is observed at 785 nm for all polymers, corresponding to a bandgap of 1.58 eV. While the absorption spectrum of HH in film state is red-shifted as compared to that in solution, the absorption spectra of HF and FH in solution are similar to those of film state, respectively,

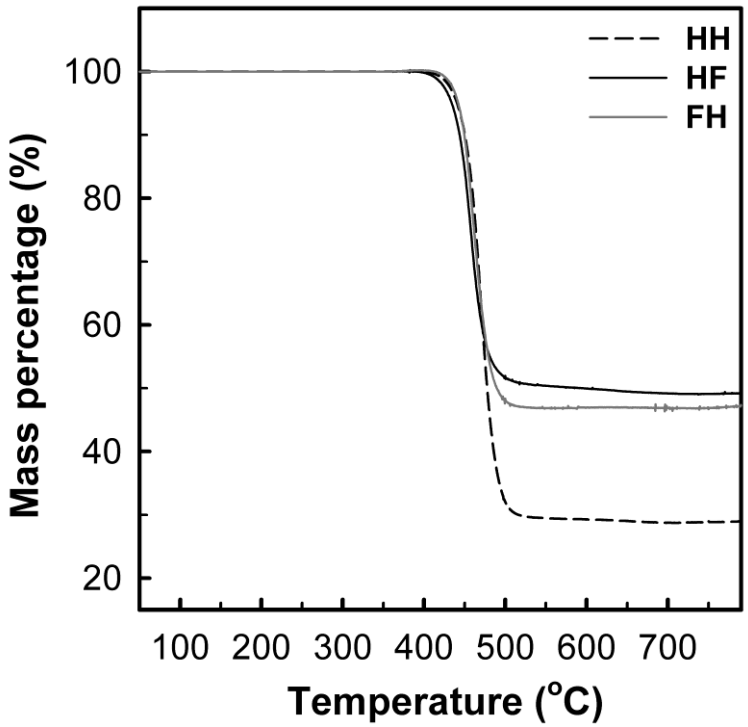

Figure 3.36. TGA curves of HH, HF and FH polymers.

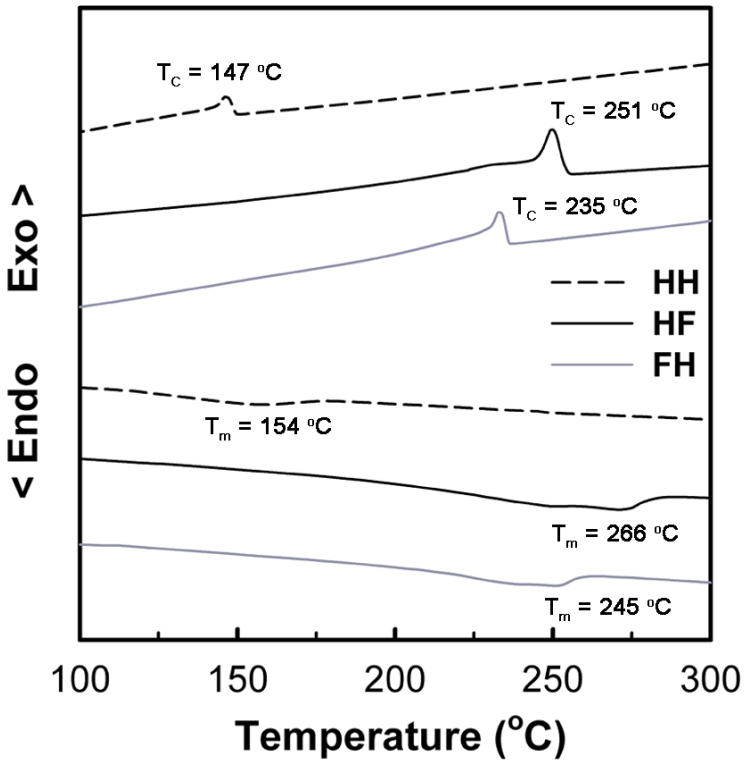

Figure 3.37. DSC thermograms of HH, HF and FH polymers.

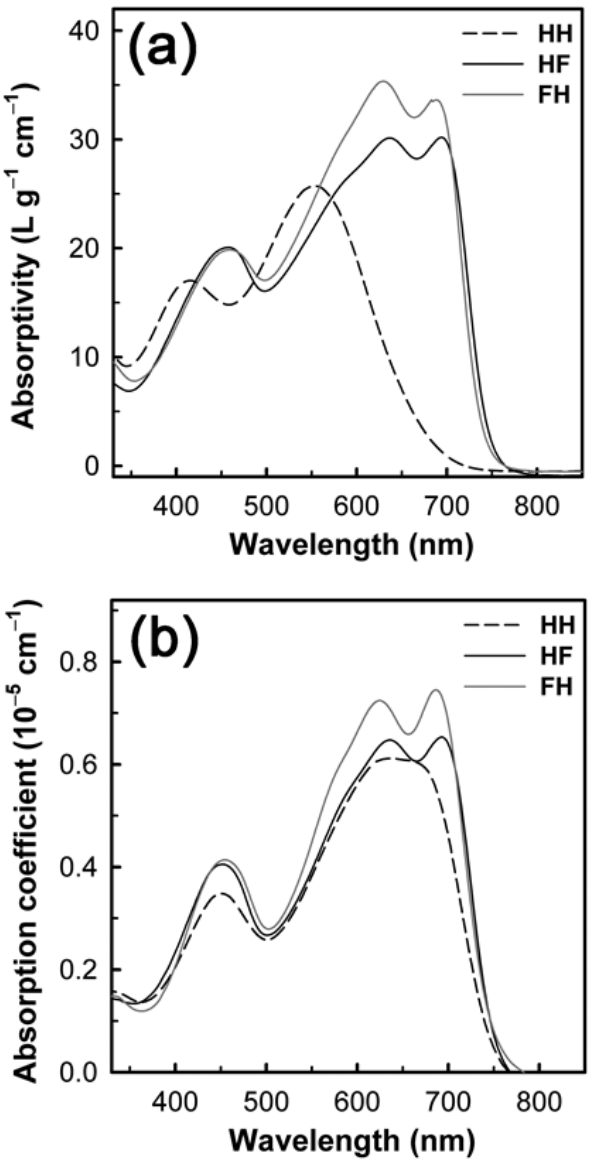

Figure 3.38. (a) UV−Vis absorption spectra of HH, HF and FH polymers in (a) $CHCl_3$ solution and (b) film state.

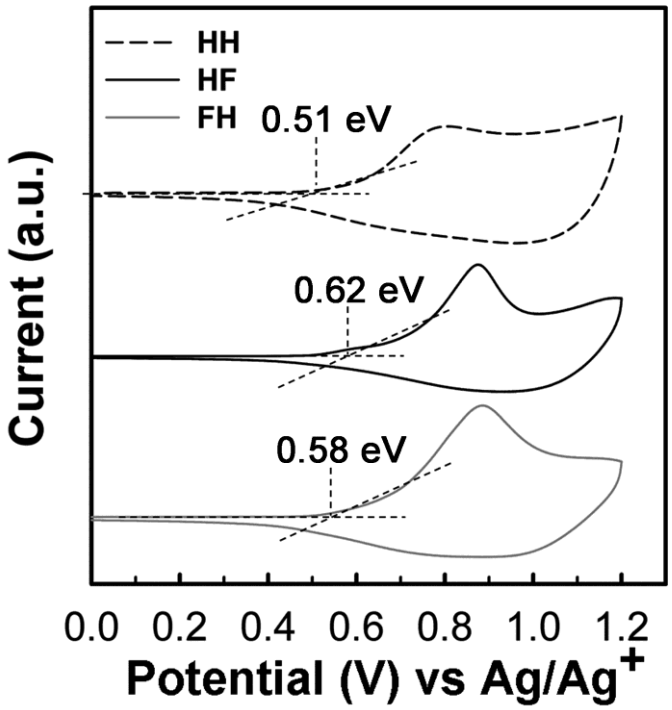

Figure 3.39. Cyclic voltammograms of HH, HF and FH polymers.

Table 3.7. Characteristics of HH, HF and FH polymers.

Polymer	M_n[a] (kg/mol)	PDI	$E_{g,opt}$[b] (eV)	HOMO (eV)	LUMO[c] (eV)
HH	42	1.45	1.58	–5.31	–3.73
HF	58	1.92	1.58	–5.42	–3.84
FH	54	1.69	1.58	–5.38	–3.80

[a] Measured from 1,2,4-trichlorobenzene GPC at 135 ℃.

[b] Determined from the onset of UV−Vis absorption spectra.

[c] $E_{g,opt}$ + HOMO.

indicating that fluorinated polymers already aggregate in solution due to strong intermolecular interaction. Furthermore, the two fluorinated polymers (HF and FH) exhibit stronger vibronic shoulder around 690 nm and higher absorptivity than HH, because the substitution of fluorine atom enhances interaction between polymer chains. Hence, well-developed crystallites of the fluorinated polymers due to strong interchain interaction are expected to afford higher photocurrents.

When electrochemical properties of polymer films are measured by cyclic voltammetry, as shown in Figure 3.39, HH, HF and FH have the HOMO energy levels of −5.31, −5.42 and −5.38 eV, respectively, indicating that the fluorine atom substitution can effectively lower the HOMO energy level of polymer, particularly more effective when the D unit is fluorinated. Therefore, the device fabricated from HF is expected to exhibit the highest V_{OC}, because V_{OC} is proportional to the difference between the HOMO energy level of donor polymer and the LUMO energy level of fullerene acceptor.

3.3.3 Computational simulation

The torsion angle and orbital distribution of fluorinated polymers simulated by the DFT are shown in Figure 3.40, and the calculated data are summarized in Table 3.8. Since fluorine atom has small size (van der Waals radius, r = 1.35 Å) and thus may not significantly induce steric hindrance, all polymers exhibit nearly planar structure, leading to improved intermolecular interaction between polymer chains with extended π-conjugation.

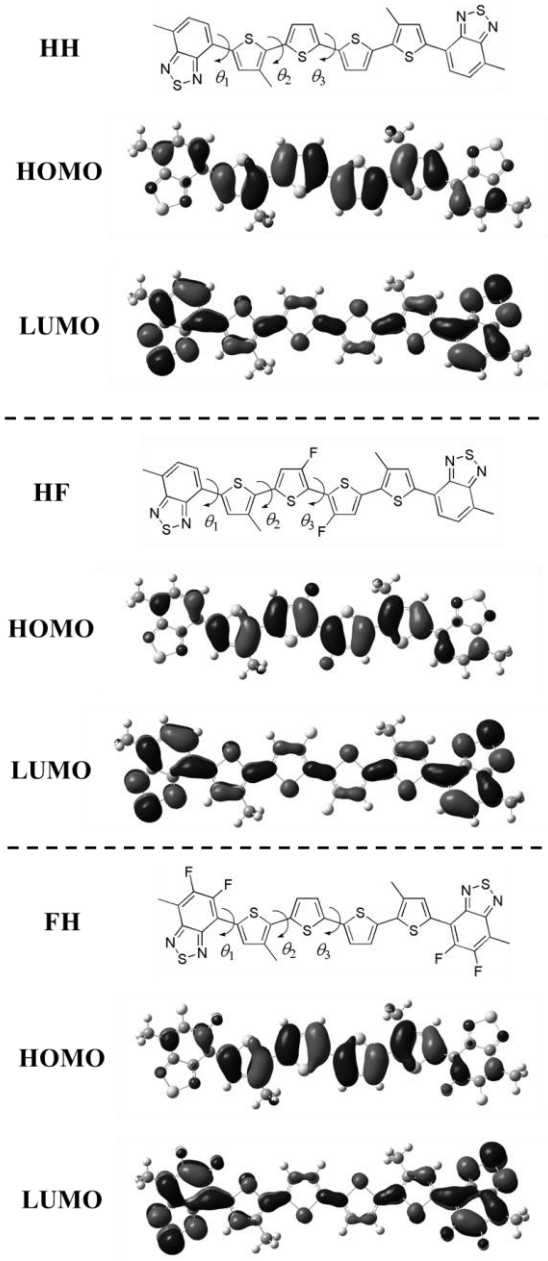

Figure 3.40. Chemical structure of repeating units for simulation, and HOMO and LUMO orbital distributions as calculated at the B3LYP/6-31G(d,p) level.

Table 3.8. Torsion angles and energy levels of BT-based repeating units calculated by DFT.

Polymer	θ_1 (Deg)	θ_2 (Deg)	θ_3 (Deg)	HOMO (eV)	LUMO (eV)
HH	3.93	–12.4	–0.86	–4.79	–2.57
HF	2.08	–8.99	0.48	–4.85	–2.63
FH	0.21	14.88	–2.70	–4.88	–2.68

Table 3.9. Dipole moments of BT-based repeating units calculated by time-dependent DFT.

Polymer	μ_g (D)	μ_{ex} (D)	$\Delta\mu_{ge}$ [a] (D)
HH	3.26	22.5	19.7
HF	2.97	22.5	24.3
FH	2.82	23.5	26.3

[a] $\Delta\mu_{ge} = [(\mu_{gx} - \mu_{ex})^2 + (\mu_{gy} - \mu_{ey})^2 + (\mu_{gz} - \mu_{ez})^2]^{1/2}$

The HOMO and LUMO energy levels of both fluorinated polymers are well localized on the D and A unit, respectively, and also exhibit similar orbital distribution and energy levels, indicating that intramolecular charge transfer takes place upon excitation regardless of the fluorination position in D–A type polymers.

It has recently been demonstrated that a large dipole change from ground to excited state ($\Delta\mu_{ge}$) facilitates exciton dissociation and generation of charge-separated state.[162,163] When dipole moments were calculated for repeating units of the three polymers, as listed in Table 3.9, FH (26.3 D) and HF (24.3 D) have a lager $\Delta\mu_{ge}$ than HH (19.7 D), predicting that the solar cell devices with fluorinated polymers exhibit higher J_{SC} values.

3.3.4 Photovoltaic properties

The polymer solar cells were fabricated with the conventional device configuration of glass/ITO/PEDOT:PSS/polymer:$PC_{71}BM$/Ca/Al. *J*–*V* characteristics under AM 1.5G illumination are shown in Figure 3.41a and relevant photovoltaic properties are summarized in Table 3.10. When the blend ratio of polymer to $PC_{71}BM$ was varied, the optimized ratio was 1:1. It is expected that both fluorinated polymers (HF and FH) exhibit larger J_{SC} and higher FF than non-fluorinated one (HH) due to higher absorption coefficient, enhanced interchain interaction and higher $\Delta\mu_{ge}$ of fluorinated polymers while HF exhibits higher V_{OC}s than the other two polymers becuase of the deepest HOMO energy level. Consequently, HF and FH exhibit high PCEs of 7.10%

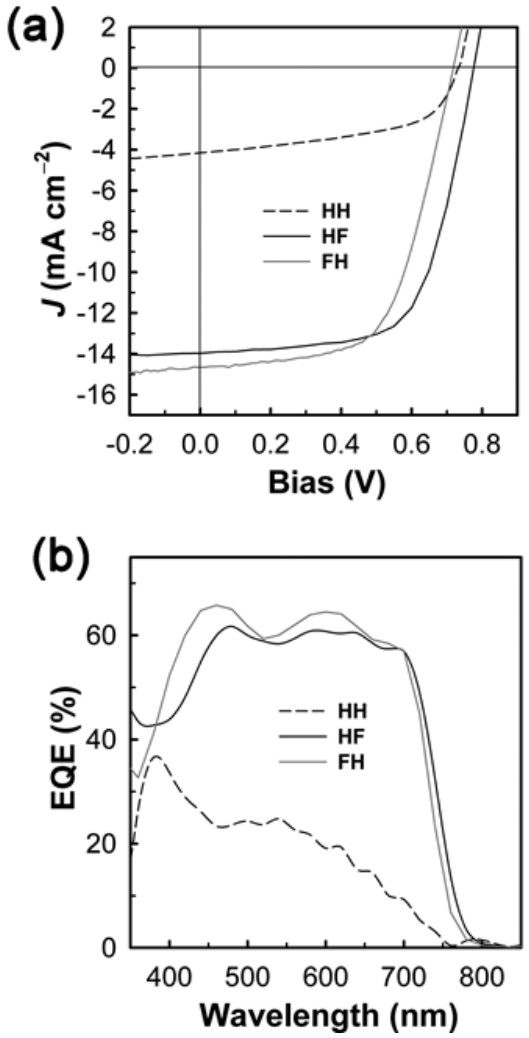

Figure 3.41. (a) *J*–*V* curves and (b) EQE spectra of polymer/$PC_{71}BM$ solar cells.

Table 3.10. Photovoltaic properties of devices with HH, HF and FH under standard AM 1.5G illumination.

Polymer	Thickness (nm)	V_{OC} (V)	J_{SC} (mA/cm^2)	FF (%)	PCE_{max} ($_{aver}$) (%)
HH	90	0.73	4.15	54	1.64 (1.45)
HF	100	0.78	14.0	65	7.10 (6.70)
FH	90	0.72	14.6	61	6.41 (6.15)

Table 3.11. Photovoltaic properties of devices using polymer:$PC_{71}BM$ blend (1:1 wt%) with additive under standard AM 1.5G illumination.

Polymer	additive[a]	amount (vol%)	V_{OC} (V)	J_{SC} (mA/cm^2)	FF (%)	PCE (%)
HH	DIO	1	0.67	4.06	48	1.34
	DIO	3	0.67	1.97	49	0.65
	CN	1	0.65	4.88	39	1.23
	CN	3	0.50	1.05	20	0.10
HF	DIO	1	0.74	13.5	64	6.44
	DIO	3	0.68	13.0	53	4.72
	CN	1	0.75	13.9	63	6.59
	CN	3	0.64	8.98	59	3.39
FH	DIO	1	0.71	12.9	69	6.17
	DIO	3	0.69	9.86	57	3.90
	CN	1	0.72	13.3	56	5.33
	CN	3	0.68	9.22	63	3.93

[a] DIO: 1,8-diiodooctane, CN: 1-chloronaphthalene.

and 6.41%, respectively, while HH exhibits a low PCE of 1.64%, indicating that the fluorination on D unit in D–A polymer is a competitive strategy for developing high performance polymer solar cells as compared to the fluorination on A unit. It should be noted here that addition of additives does not enhance the photovoltaic performance (see Table 3.11).

When EQEs of devices were measured under monochromatic light, as shown in Figure 3.41b, both fluorinated polymers exhibit higher EQEs (about 60%) than that of HH in the range of 450–720 nm, consistent with higher J_{SC} of solar cells with fluorinated polymers than the solar cell with non-fluorinated one.

Intensity-dependent photocurrent (J_{ph}) were measured between 0.4 and 2.5 sun and the relative J_{ph} at V = 0 V are plotted against light intensity (P_{light}) in Figure 3.42a. The relationship between J_{ph} and P_{light} can be represented by a power law equation: $J_{ph} \propto (P_{light})^{\alpha}$, where α is recombination parameter.[166,167] Since α=1 corresponds to the absence of photocurrent loss due to bimolecular recombination, higher α values for HF (0.97) and FH (0.96) than the value for HH (0.93) indicate that bimolecular recombination is more suppressed in active layers with fluorinated polymers than the active layer with non-fluorinated polymer while the fluorinated position does not affect the recombination.

When hole mobilities were measured from dark J–V curve of hole-only device by using the SCLC model, as shown in Figure 3.42b, HF/$PC_{71}BM$ (1.26×10^{-3} $cm^2/V\cdot s$) and FH/$PC_{71}BM$ (1.16×10^{-3} $cm^2/V\cdot s$) exhibit higher mobilities than HH/$PC_{71}BM$ (5.24×10^{-4} $cm^2/V\cdot s$), implying that the charge

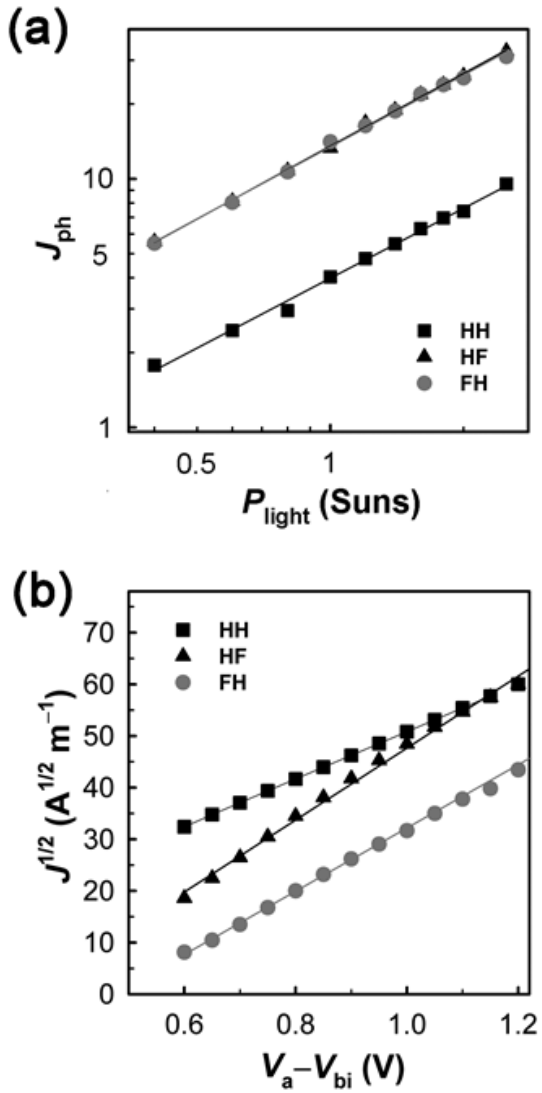

Figure 3.42. (a) a plot of relative J_{ph} vs. light intensity as measured at V = 0 V; (b) dark J–V characteristics of polymer/$PC_{71}BM$ blends with hole-only device, where the solid lines represent the best linear fit of the data points.

pathway are well formed in the active layers of fluorinated polymers.

3.3.5 Molecular orientation

The crystal structure and its orientation of fluorinated polymers were investigated by GIWAXS. All blend films of polymer and $PC_{71}BM$ show only (*h*00) reflections in the out-of-plane (q_z) direction, as shown in Figure 3.44, indicating that polymers have preferentially edge-on orientation on the substrate. Since the (100) peaks of HH, HF and FH are observed at q_z = 0.36, 0.33 and 0.33 $Å^{-1}$, corresponding to the interchain distance of 17.5, 19.0 and 19.0 Å, respectively, the inter-chain distances of fluorinated polymers are larger than the non-fluorinated one. Another feature to be noted from GIWAXS is that the two fluorinated polymers exhibit the (010) reflection at q_{xy} = 1.7 $Å^{-1}$ corresponding to the π–π stacking distance of 3.70 Å, while HH does not show discernibly the (010) peak, indicating that fluorinated polymer chains are better packed in π–π direction.

3.3.6 Morphologies of active layers

The morphologies of polymer/$PC_{71}BM$ blend films as observed by TEM reveal that both the blend films of HF:$PC_{71}BM$ and FH:$PC_{71}BM$ exhibit well-developed interconnected network with nanoscale fibril structure, as shown in Figure 3.45. In a previous report, D–A polymers with fluorinated D unit showed poor miscibility with PCBM and thus large phase separation between

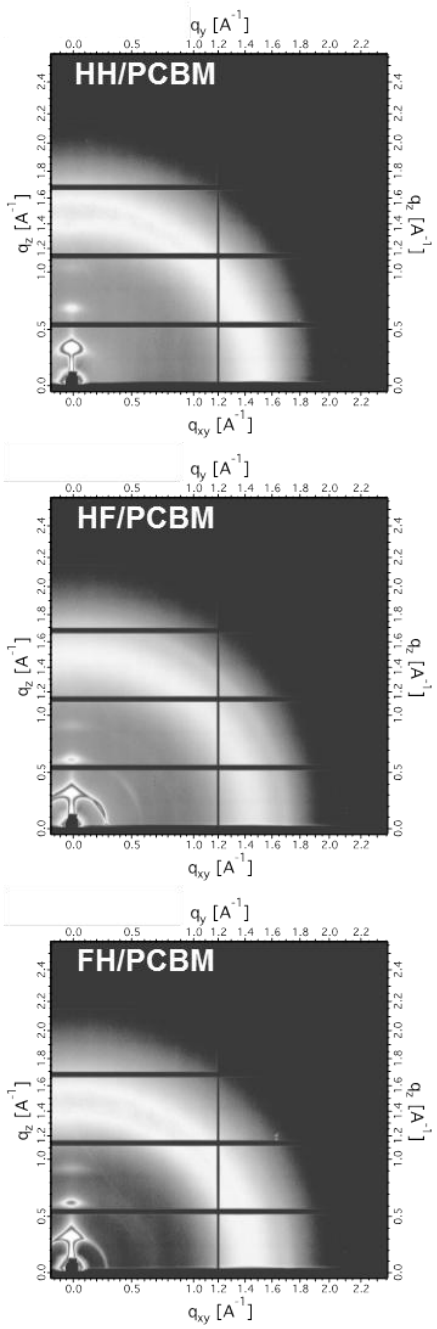

Figure 3.43. GIWAXS pattern images of polymer/$PC_{71}BM$ blend films.

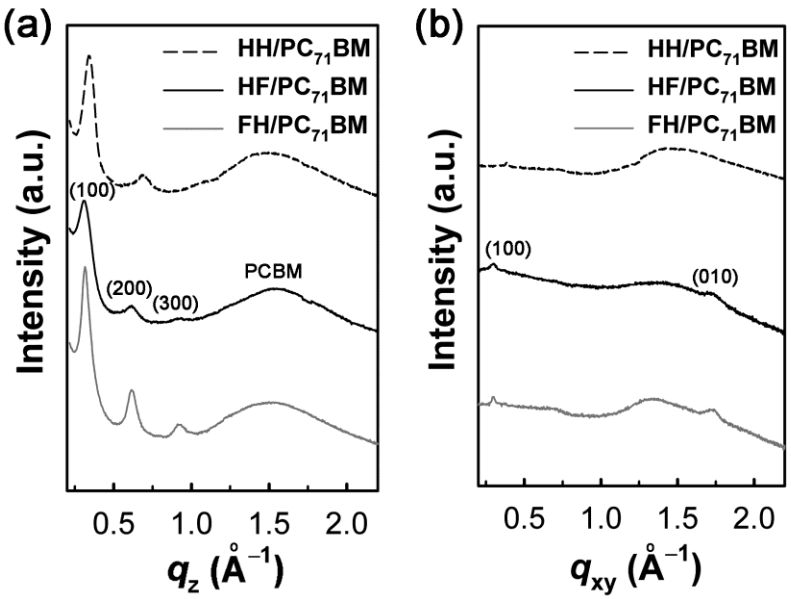

Figure 3.44. (a) q_z and (b) q_{xy} scans of GIWAXS from blend films of polymer/$PC_{71}BM$.

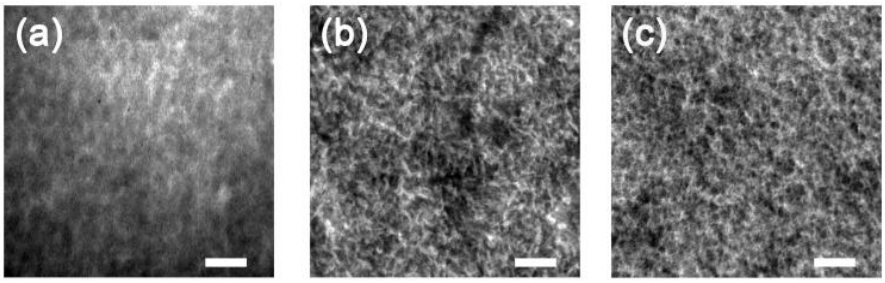

Figure 3.45. TEM images of (a) HH/$PC_{71}BM$, (b)HF/$PC_{71}BM$, and (c) FH/$PC_{71}BM$ blend films. The scale bar denotes 200 nm.

polymer and PCBM, which is not beneficial for generation of charge carriers.[152] But, this is contradictory to our system, because HF with fluorinated D unit in our system shows well-developed interconnected network structure with nanoscale phase separation.

3.3.7 Summary

We designed and synthesized two types of fluorinated D–A polymers with each being fluorinated on D and A unit, where QT and BT used as D and A units, respectively. Compared to non-fluorinated polymer, both fluorinated polymers have deeper HOMO energy levels without change of optical bandgap and exhibit stronger vibronic shoulder in optical spectrum. The HF polymer with fluorinated D unit exhibits higher PCE of 7.10% than FH with fluorinated A unit (PCE = 6.41%). Since the HF polymer exhibits low bimolecular recombination, high hole mobility and well-developed fibril network, it is conclusive that the fluorination on D unit in D–A polymer could be a promising method for achieving high performance polymer solar cells.

3.4 Influence of the degree of fluorination on D–A type polymers for organic solar cells

3.4.1 Synthesis and characterization

Over the years, understanding about the relationship between chemical structure and optoelectrical properties of polymers significantly contribute to developing high performance PSCs and high PCEs of PSCs have been achieved by modifying the chemical structures of conjugated polymers such as atomic substitution, fusion of aromatic rings, optimization of length and position of alkyl chains, and end-group modification.

Among several modification strategies, the introduction of fluorine atoms on conjugated backbone in polymer has attracted much attention for the past few years due to unique advantages including small size of fluorine atom (van der Waals radius, r = 1.35 Å), energy level lowering without sacrifice of bandgap and improvement of molecular ordering by induced dipole along C–F bond.[136-138,148] However, although fluorination on conjugated polymers has many benefits, fluorination can also lead to harmful effects on polymer such as low solubility in organic solvent, unsuitable energy levels for charge transfer and large aggregation of polymers in active layer.[151-153] For highly efficient PSC with fluorinated conjugated polymer, the degree of fluorination should be controlled cautiously to optimize morphology of active layer and energy levels of polymer.

In this work, we synthesized three kinds of fluorinated D–A polymers,

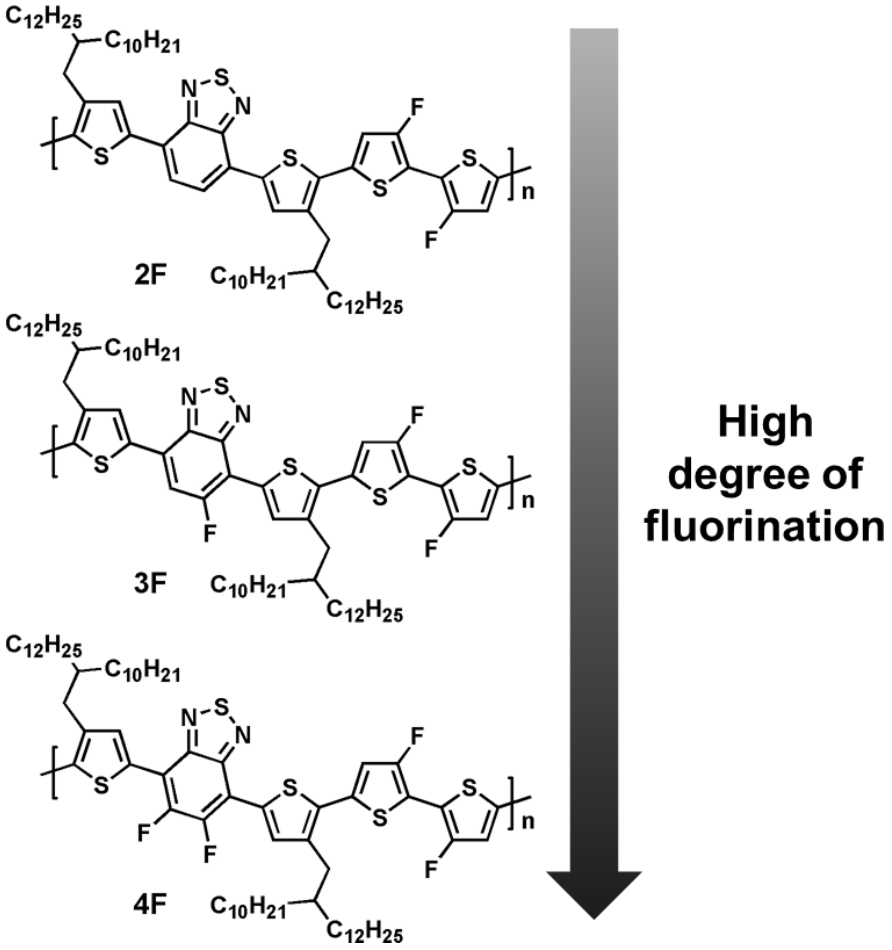

Scheme 3.2. Structure of D–A polymers with different degree of fluorination.

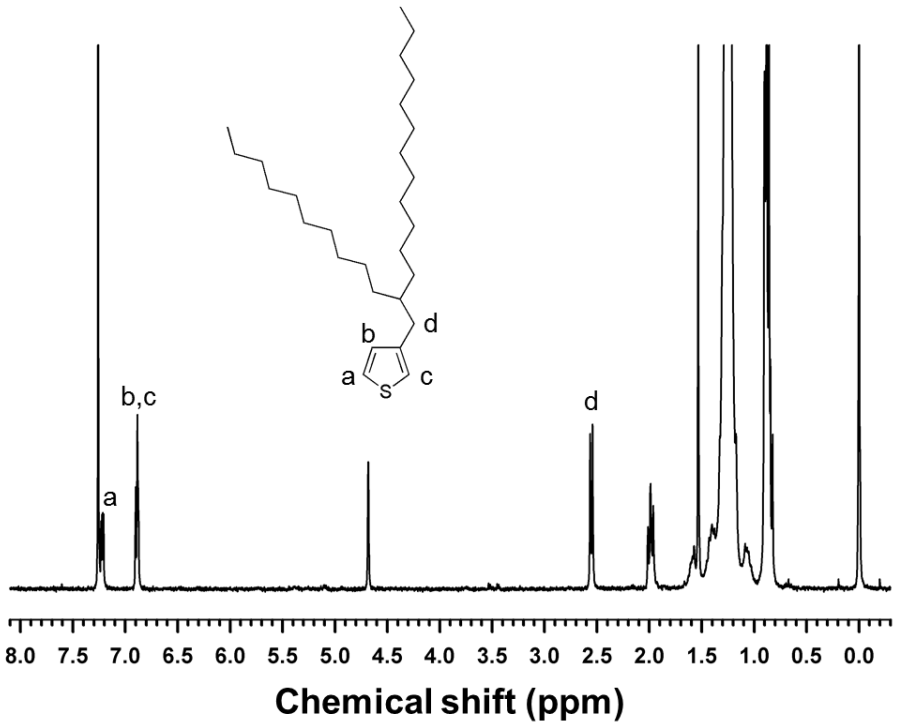

Figure 3.46. ^{1}H NMR spectrum of compound **19** in Scheme 2.4.

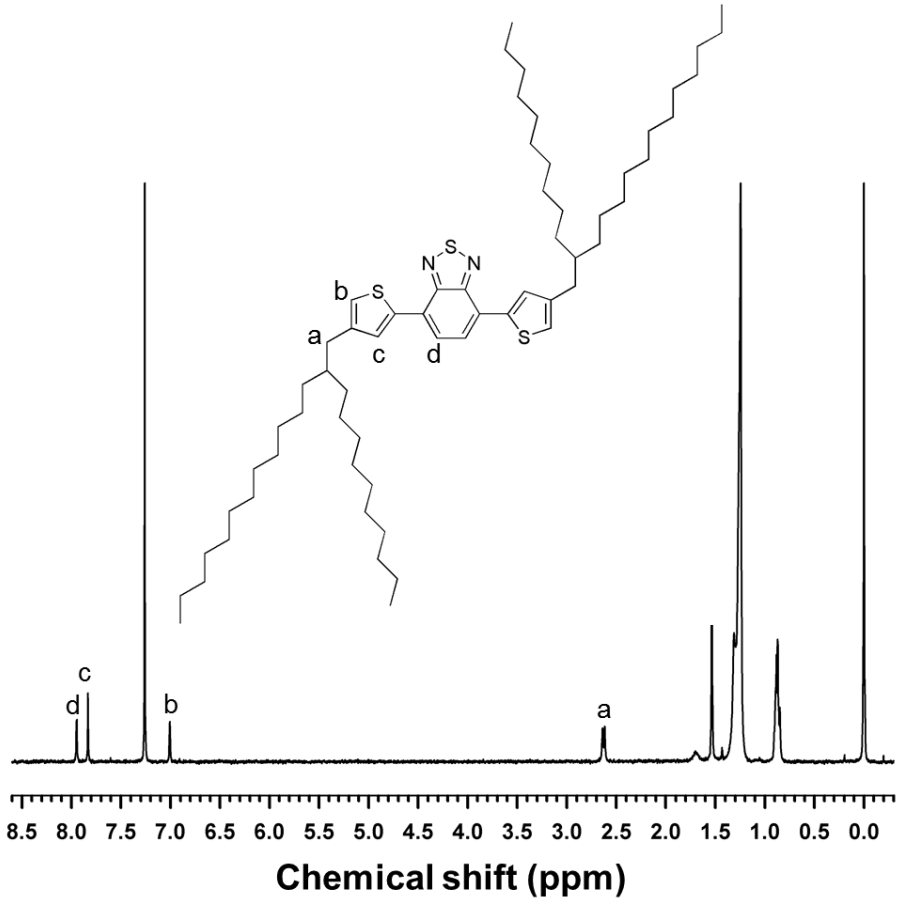

Figure 3.47. ^{1}H NMR spectrum of compound **21** in Scheme 2.4.

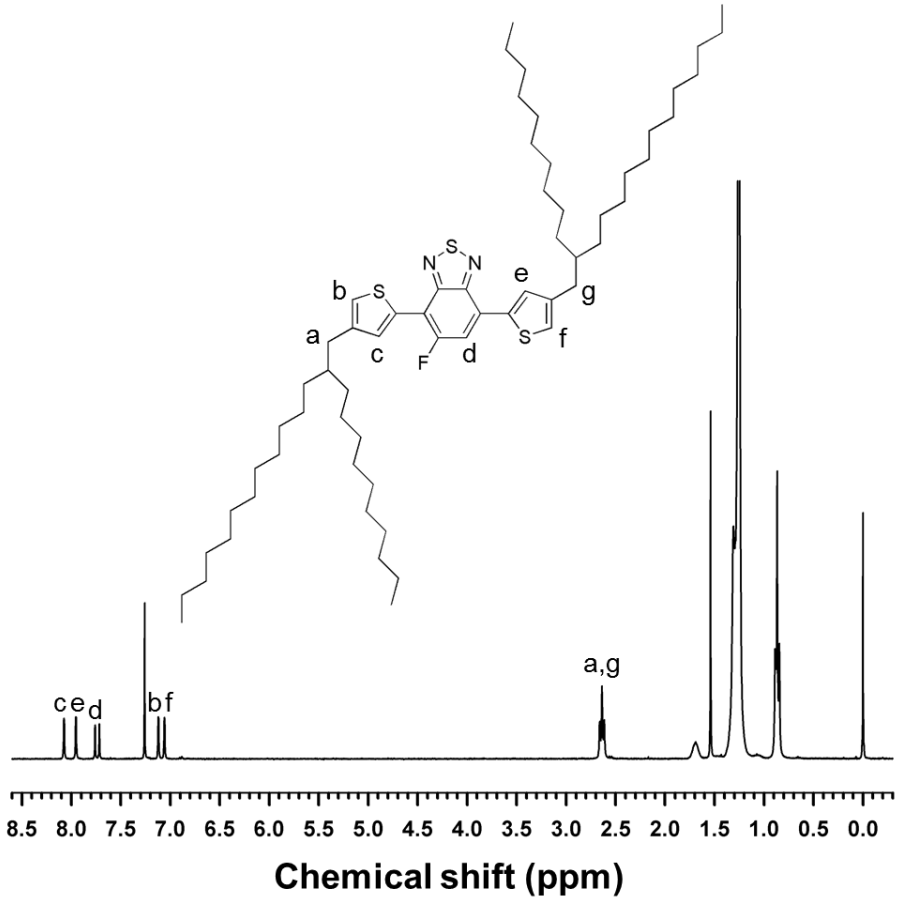

Figure 3.48. ^{1}H NMR spectrum of compound **22** in Scheme 2.4.

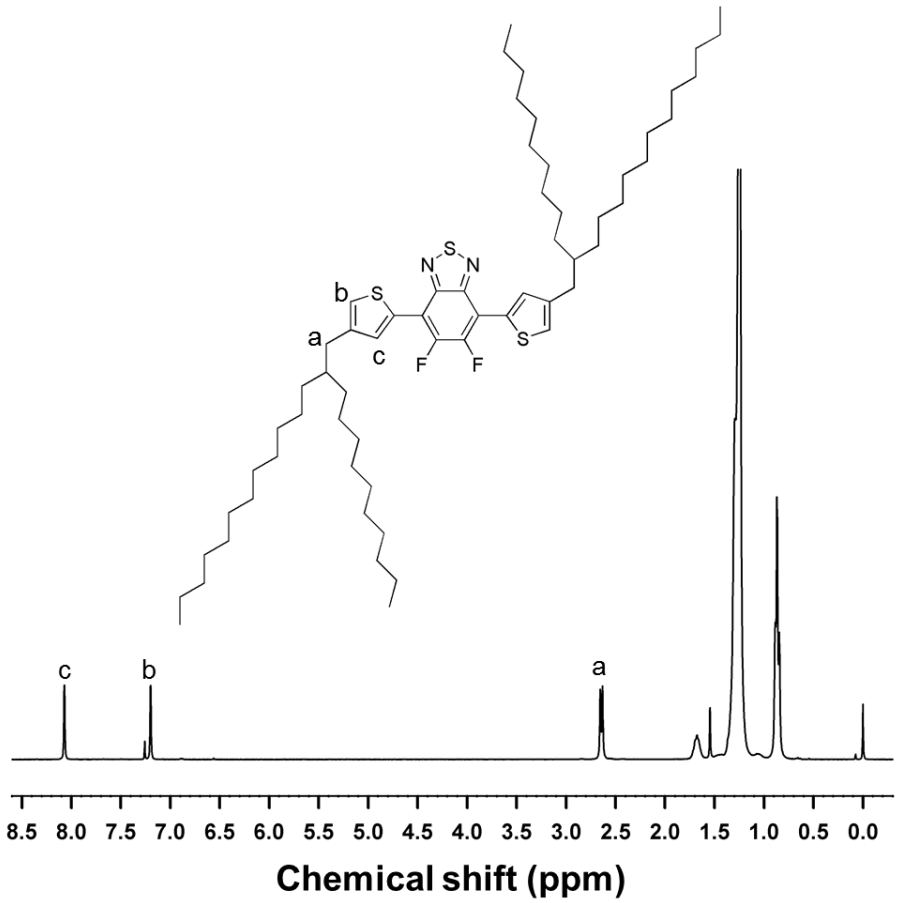

Figure 3.49. [1]H NMR spectrum of compound **23** in Scheme 2.4.

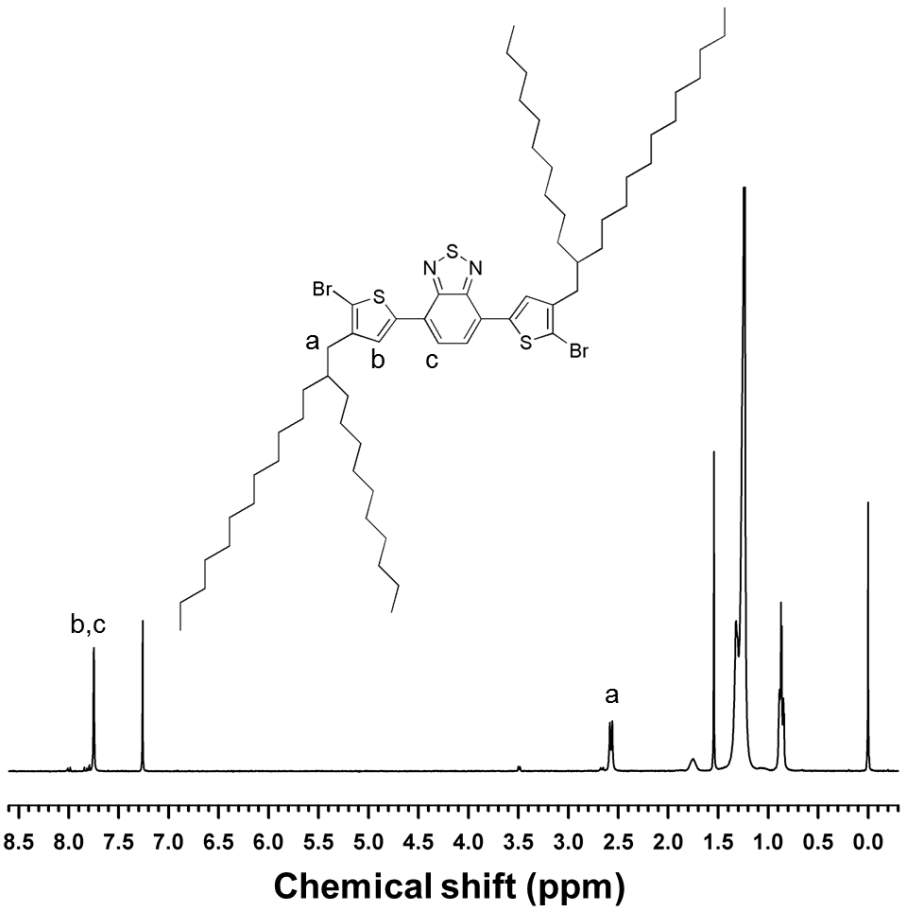

Figure 3.50. [1]H NMR spectrum of compound **24** in Scheme 2.4.

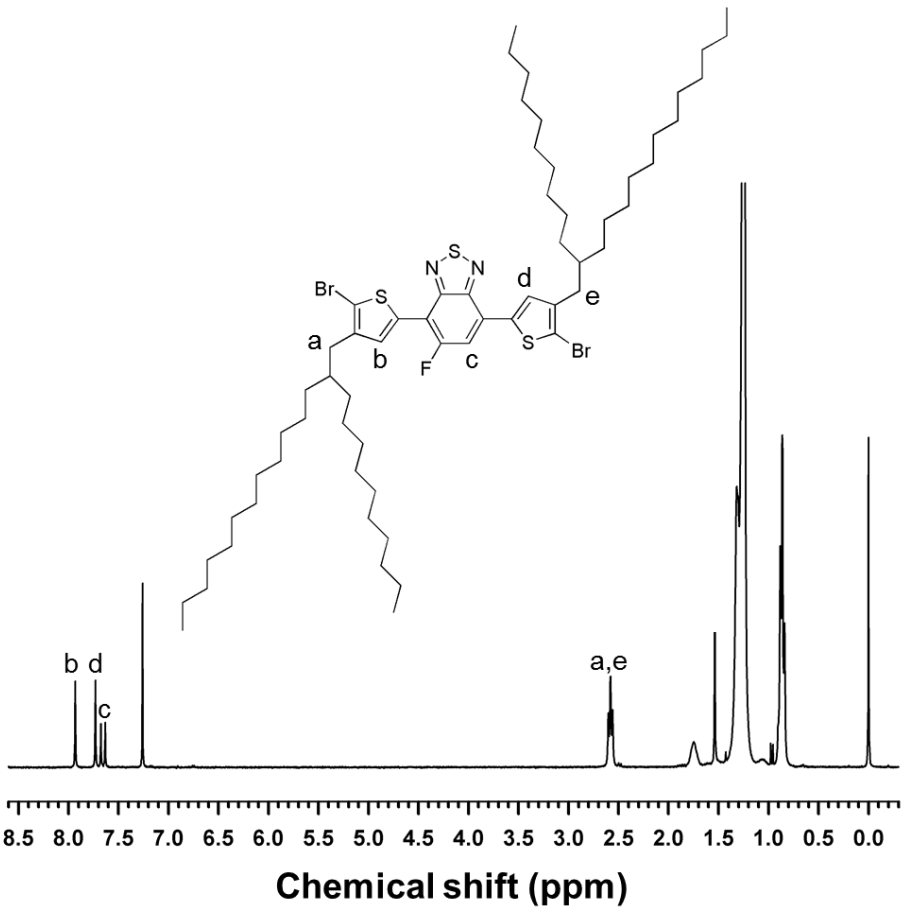

Figure 3.51. ^{1}H NMR spectrum of compound **25** in Scheme 2.4.

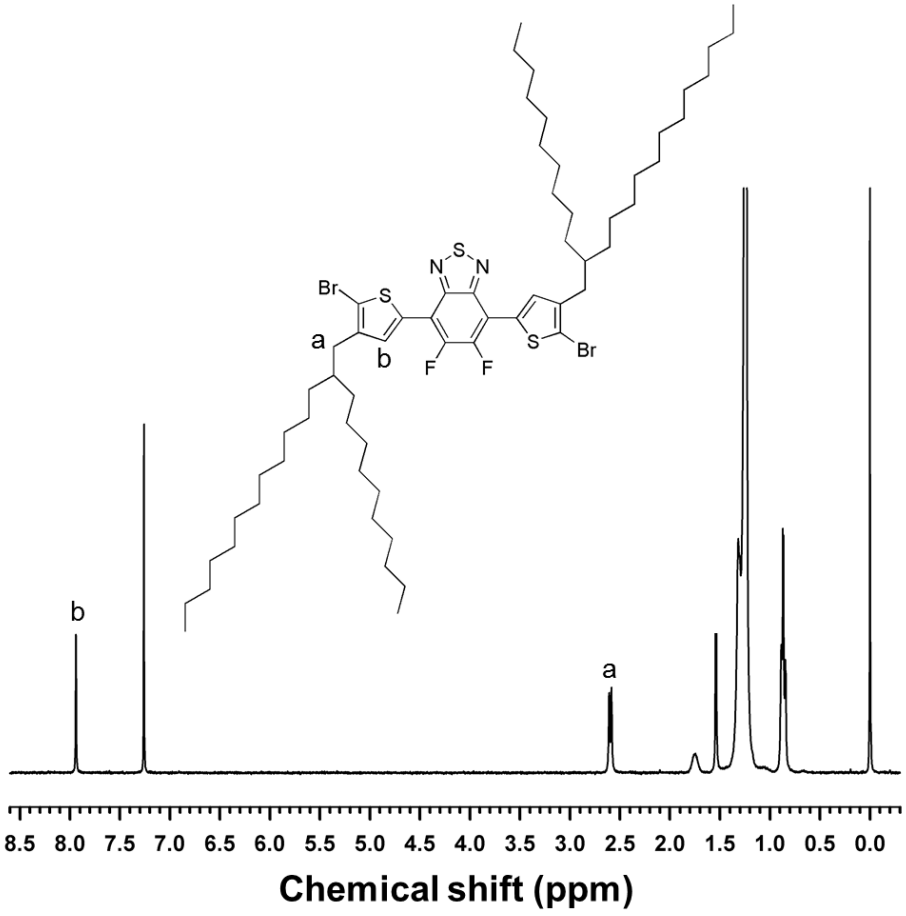

Figure 3.52. ^{1}H NMR spectrum of compound **26** in Scheme 2.4.

where quaterthiophene and BT are used as D and A unit, respectively, and the degree of fluorination is controlled by using BT unit substituted by different number of fluorine atoms, as shown in Scheme 3.2.

Three fluorinated polymers, denoted as 2F, 3F and 4F, were synthesized via microwave-assisted Stille coupling reaction in toluene/DMF with $Pd(PPh_3)_4$ as a catalyst, as shown in Scheme 2.4. The molecular weights of polymers were measured by GPC and listed in Table 3.12. The number average molecular weights of 2F, 3F and 4F are 30, 33 and 40 kg/mol with PDI of 1.31, 2.07 and 1.76, respectively, and all polymers have sufficient molecular weight not as to significantly affect their photovoltaic properties. Long and branched alkyl chains (2-decyltetradecyl) were introduced on conjugated backbone to improve the solubility of fluorinated polymers in organic solvents.

3.4.2 Optical and electrochemical properties

The UV–Vis absorption spectra of polymers in chloroform solution and film state are shown in Figure 3.53. All polymers showed two absorption peaks, a common feature of D−A polymers, where the absorption peak at shorter wavelength is attributed to π–π^* transition of the backbone while the absorption peak at longer wavelength corresponds to the intramolecular charge transfer from D to A units in the alternating copolymer.[104] When optical bandgaps of polymers are determined from the onset of UV–Vis absorption spectra in film state, the bandgaps of 2F and 3F are nearly identical (1.59 eV), but 4F has slightly wider bandgap of 1.57 eV. Interestingly, 3F and

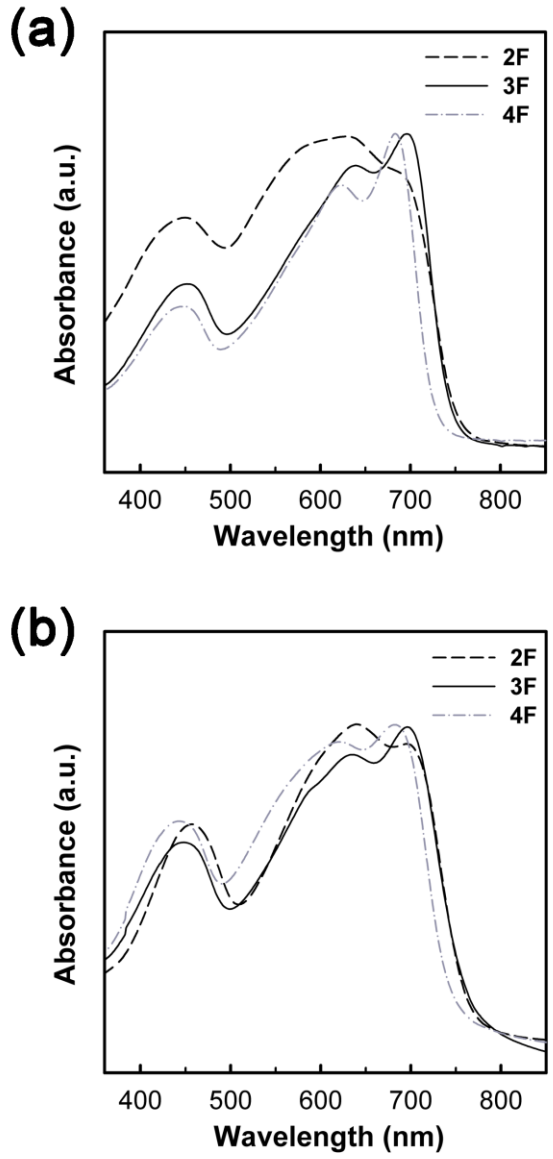

Figure 3.53. (a) UV−Vis absorption spectra of 2F, 3F and 4F polymers in (a) $CHCl_3$ solution and (b) film state.

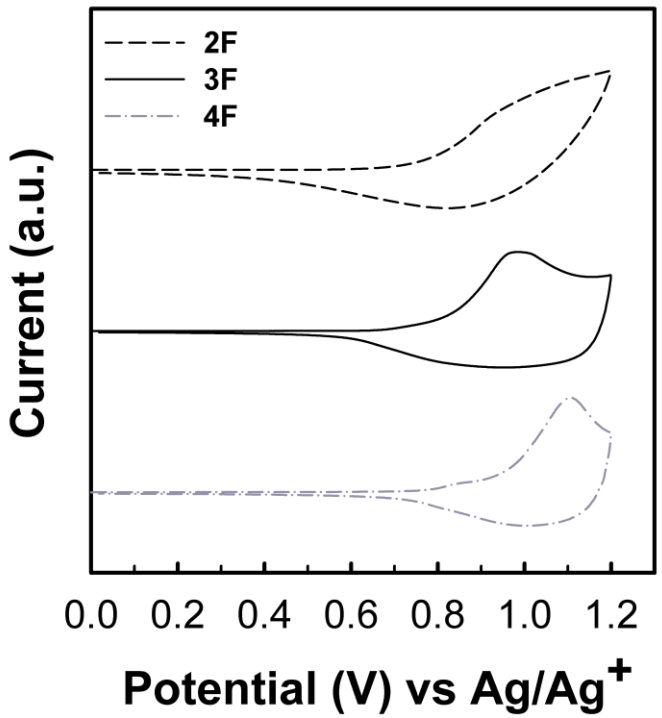

Figure 3.54. Cyclic voltammograms of 2F, 3F and 4F polymers.

Table 3.12. Characteristics of 2F, 3F and 4F polymers.

Polymer	M_n[a] (kg/mol)	PDI	$E_{g,opt}$[b] (eV)	HOMO (eV)	LUMO[c] (eV)
2F	30	1.31	1.57	–5.33	–3.76
3F	33	2.07	1.57	–5.37	–3.80
4F	40	1.76	1.59	–5.46	–3.87

[a] Measured from $CHCl_3$ GPC.

[b] Determined from the onset of UV−Vis absorption spectra.

[c] $E_{g,opt}$ + HOMO.

4F polymers show stronger vibronic shoulder at around 705 nm than 2F polymers, indicating that the introduction of fluorine atoms enhances interchain interaction between polymers.

Electrochemical properties of polymer films are measured by cyclic voltammetry, as shown in Figure 3.54, and are summarized in Table 3.12. Since strong electron-withdrawing ability of fluorine atoms lowers energy levels of polymers, 3F (–5.37 eV) and 4F (–5.46 eV) polymers have deeper HOMO energy levels than 2F (–5.33 eV). When the LUMO energy levels of polymers were estimated by adding the optical bandgap to the HOMO energy level, 2F, 3F and 4F polymers have LUMO energy levels of –3.76, –3.80 and –3.87 eV, respectively, which provides sufficient LUMO level offset between polymers and PCBM (–4.3 eV) for effective exciton dissociation at the interface between donor and acceptor.[154]

3.4.3 Computational simulation

The torsion angle and orbital distribution of fluorinated polymers simulated by the DFT are shown in Figure 3.55, and the calculated data are summarized in Table 3.8. All fluorinated polymers exhibit nearly planar structure because the small size of fluorine atom does not significantly induce steric hindrance, and these planar structures of conjugated backbone can improve intermolecular interaction between polymers with extended π–conjugation. The HOMO and LUMO in all fluorinated polymers are well localized on the D and A unit, respectively, indicating that intramolecular charge transfer from

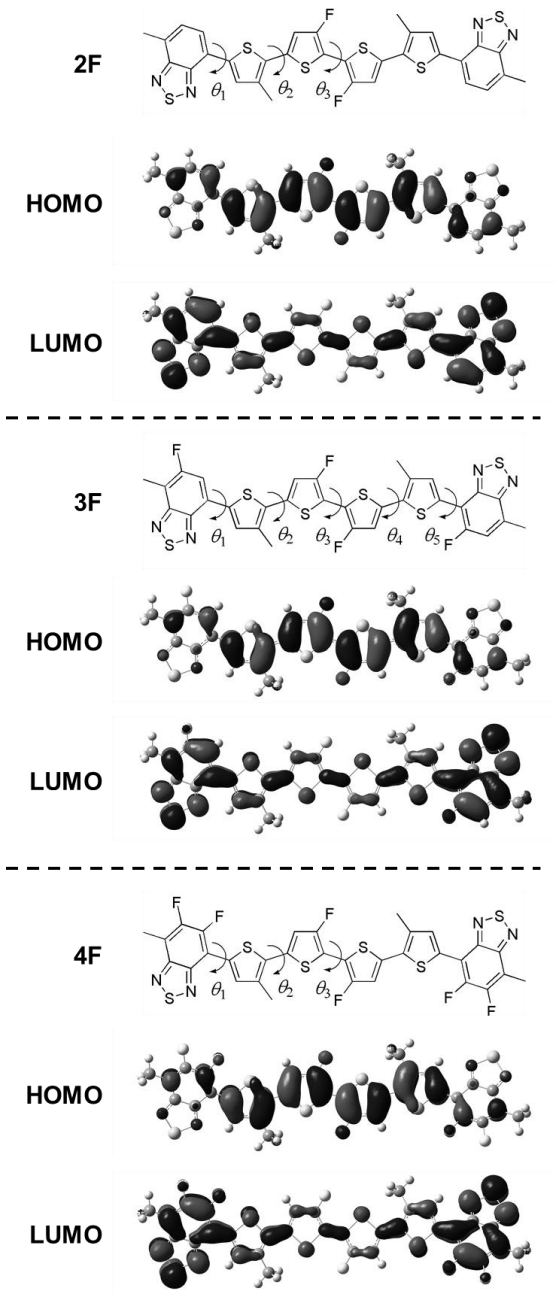

Figure 3.55. Chemical structure of repeating units for simulation, and HOMO and LUMO orbital distributions as calculated at the B3LYP/6-31G(d,p) level.

Table 3.13. Torsion angles and energy levels of 2F-, 3F- and 4F-repeating units calculated by DFT.

Polymer	θ_1 (Deg)	θ_2 (Deg)	θ_3 (Deg)	θ_4 (Deg)	θ_5 (Deg)	HOMO (eV)	LUMO (eV)
2F	2.08	–8.99	0.48			–4.85	–2.63
3F	1.36	–8.81	–0.41	7.79	–0.17	–4.89	–2.71
4F	0.21	11.01	0.46			–4.94	–2.75

D to A unit takes place regardless of the degree of fluorination. The HOMO and LUMO of polymers have deeper energy levels as the amounts of fluorine atoms on conjugated backbone are increased.

3.4.4 Photovoltaic properties

The polymer solar cells were fabricated with the conventional device configuration of glass/ITO/PEDOT:PSS/polymer:$PC_{71}BM$/Ca/Al. *J–V* characteristics under AM 1.5G illumination are shown in Figure 3.56 and relevant photovoltaic properties are summarized in Table 3.14. When the blend ratio of polymer to $PC_{71}BM$ was varied, the optimized ratio was 1:1.5. 2 vol% of 1-chloronaphthalene (CN) was used as an additive for optimization of morphologies of active layer and improving performances of PSCs.[168] Since V_{OC} of PSCs is proportional to the difference the HOMO energy level of donor polymer and the LUMO energy level of fullerene acceptor, as the number of fluorine atoms in backbone increases the V_{OC} of the polymers increase from 0.77 to 0.80 and 0.82 V for 2F, 3F and 4F, respectively. Among fluorinated polymers, 3F exhibited significantly higher J_{SC} values than the other polymers and after device optimization with CN additive, the J_{SC} of 3F reached 15.0 mA/cm^2. As a result, the solar cell device of 3F processed from a mixed solvent of DCB and 2 vol% CN exhibits a promising PCE of 7.92% with a high J_{SC} of 15.0 mA/cm^2, V_{OC} of 0.80 V and FF of 66%.

When EQEs of devices were measured under monochromatic light, as shown in Figure 3.57a, 3F polymer exhibits higher EQEs than 2F and 4F

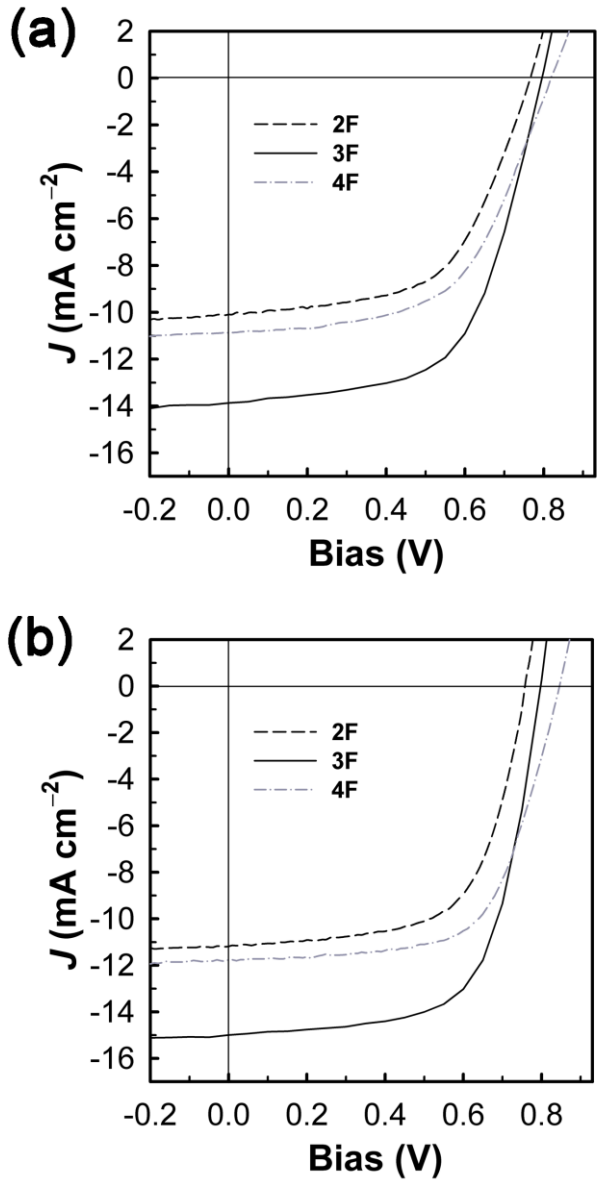

Figure 3.56. *J–V* curves of polymer/$PC_{71}BM$ (1:1.5 w/w) solar cells prepared from (a) DCB and (b) DCB containing 2 vol% of CN.

Table 3.14. Photovoltaic properties of devices with 2F, 3F and 4F under standard AM 1.5G illumination.

Polymer	Thickness (nm)	V_{OC} (V)	J_{SC} (mA/cm^2)	FF (%)	PCE (%)
2F	110	0.77	10.1	57	4.43
2F[a]	110	0.76	11.5	64	5.59
3F	120	0.80	13.9	60	6.67
3F[a]	120	0.80	15.0	66	7.92
4F	120	0.82	10.9	56	5.01
4F[a]	120	0.84	11.8	63	6.24

[a] Processed from DCB containing 2 vol% of CN.

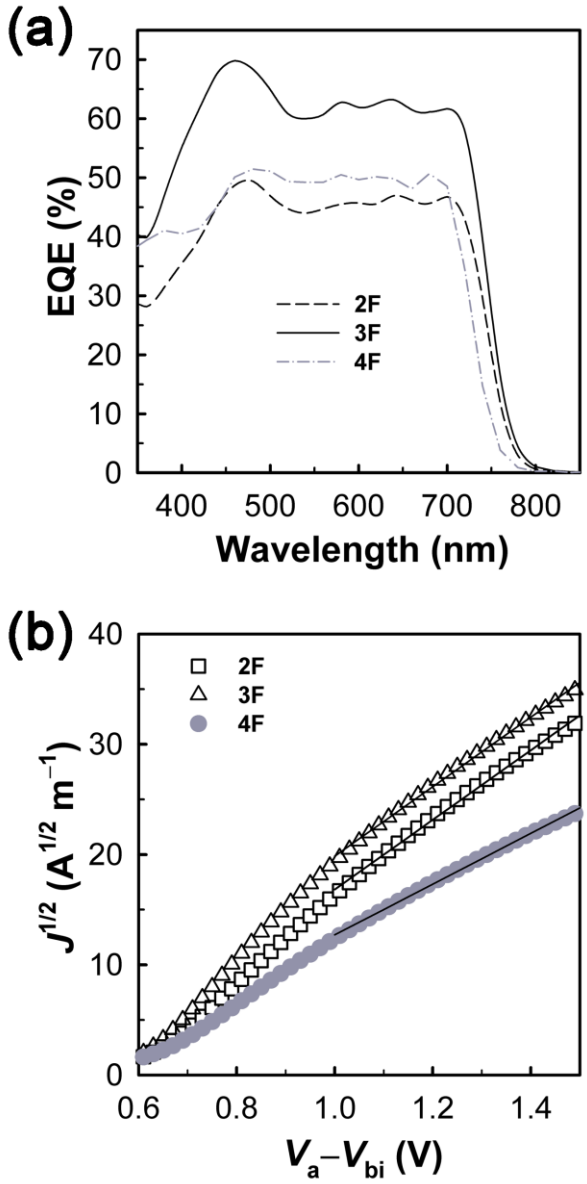

Figure 3.57. (a) EQE spectra of polymer/$PC_{71}BM$ solar cells and (b) dark *J*–*V* characteristics of polymer/$PC_{71}BM$ blends with hole-only device, where the solid lines represent the best linear fit of the data points.

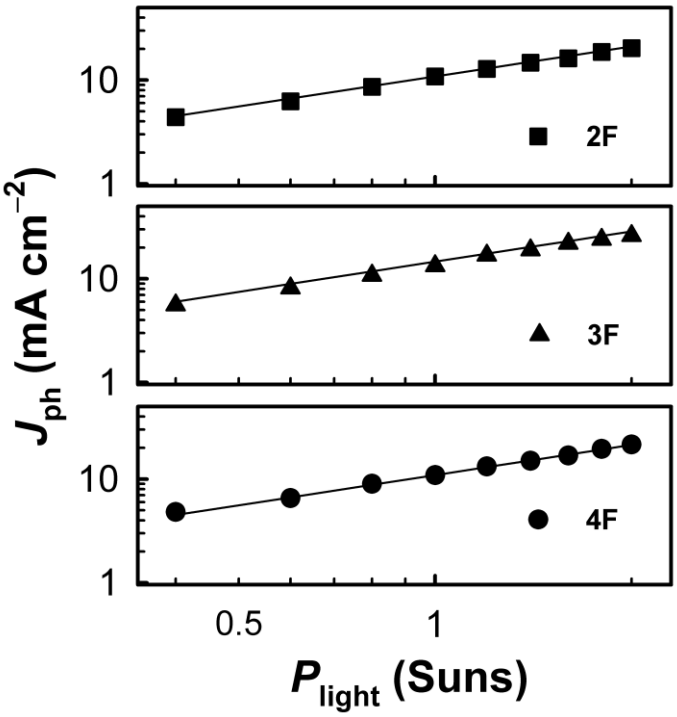

Figure 3.58. A plot of J_{ph} vs. light intensity as measured at V = 0 V in 2F-, 3F- and 4F- based solar cells.

polymers in the whole range of wavelengths, consistent with higher J_{SC} of solar cells with 3F.

Hole mobilities were measured from dark *J*–*V* curve of hole-only device by using the SCLC model, as shown in Figure 3.28. The 3F/$PC_{71}BM$ (5.74×10^{-4} $cm^2/V\cdot s$) exhibits higher hole mobility than 2F/$PC_{71}BM$ (4.41×10^{-4} $cm^2/V\cdot s$) and 4F/$PC_{71}BM$ (2.75×10^{-4} $cm^2/V\cdot s$), implying that the charge pathway are well developed in the active layers of solar cells fabricated with 3F polymers.

Intensity-dependent photocurrent (J_{ph}) were measured between 0.4 and 2.5 sun and the J_{ph} at V = 0 V are plotted against light intensity (P_{light}) in Figure 3.58. The relationship between J_{ph} and P_{light} can be represented by a power law equation: $J_{ph} \propto (P_{light})^{\alpha}$, where α is recombination parameter and α=1 corresponds to the absence of photocurrent loss due to bimolecular recombination.[166,167] Since higher α value represents lower bimolecular recombination, higher α value for 3F (0.98) than the values for 2F (0.97) and 4F (0.95) indicates that bimolecular recombination is more suppressed in active layers with 3F polymers and it may be related to high SCLC hole mobility of 3F polymer.

3.4.5 Molecular ordering

When the molecular ordering of fluorinated polymers was studied by X-ray diffraction (XRD), as shown in Figure 3.59, all polymers exhibit an intense (100) peak with discernible (200) and (300) reflection peaks. The interchain distances of fluorinated polymers are identical because the (100) peaks of all

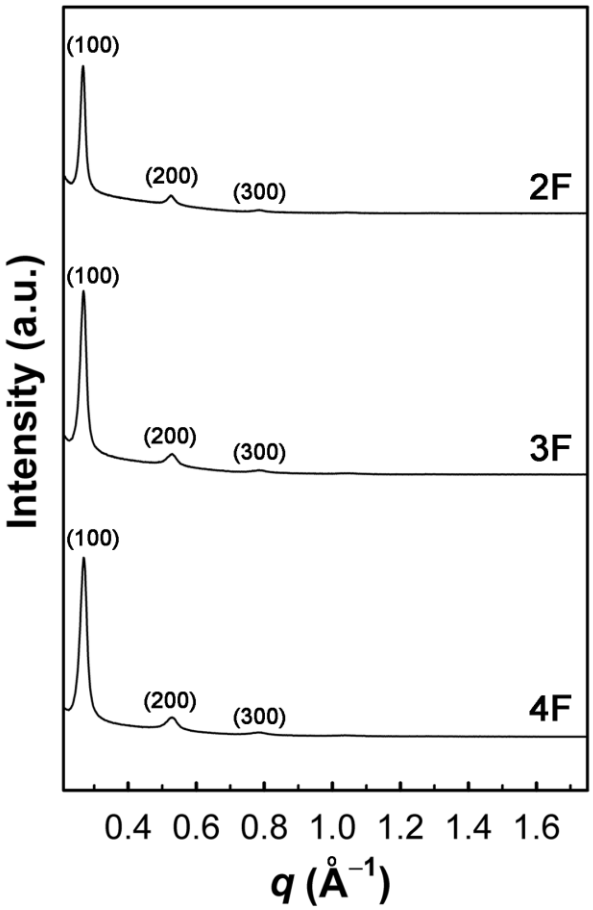

Figure 3.59. XRD patterns of 2F, 3F and 4F films.

polymers are observed at q = 0.27 Å^{-1}, corresponding to the interchain distance of 23.6 Å.

3.4.6 Morphologies of active layers

Morphologies of active layers in 2F-, 3F- and 4F-based PSCs were observed by TEM, as shown in Figure 3.60. Recently, Weiwei et al.[164,165] have demonstrated that the fiber width is correlated with the solubility of the polymers and narrower fibers can be obtained by decreasing the solubility of polymers. Liu et al.[170] have also shown that size of phase separation in polymer/PCBM blend film decreases with increasing fluorine content on conjugated backbone of polymer. Although interconnected network with nanoscale fibril structure are well-developed in the blend films of all polymers, 3F and 4F polymers show narrower fibril size, which is beneficial for exciton dissociation and charge generation, than 2F polymer because introducing more fluorine atoms on conjugated backbone leads to enhanced aggregation and reduced solubility of polymers.

Photoinduced charge transfer from polymer to PCBM can be observed by Photoluminescence (PL).[171] As shown in Figure 3.61, PLs of 3F and 4F polymers are almost quenched after blending with $PC_{71}BM$ (>95% PL quenching efficiency), while 2F/$PC_{71}BM$ shows a relatively low PL quenching efficiency of 84%. Since PL is more effectively quenched in polymer/PCBM blend films with smaller domain size of polymer, this lower PL quenching efficiency of 2F indicates that 2F has larger domain size of

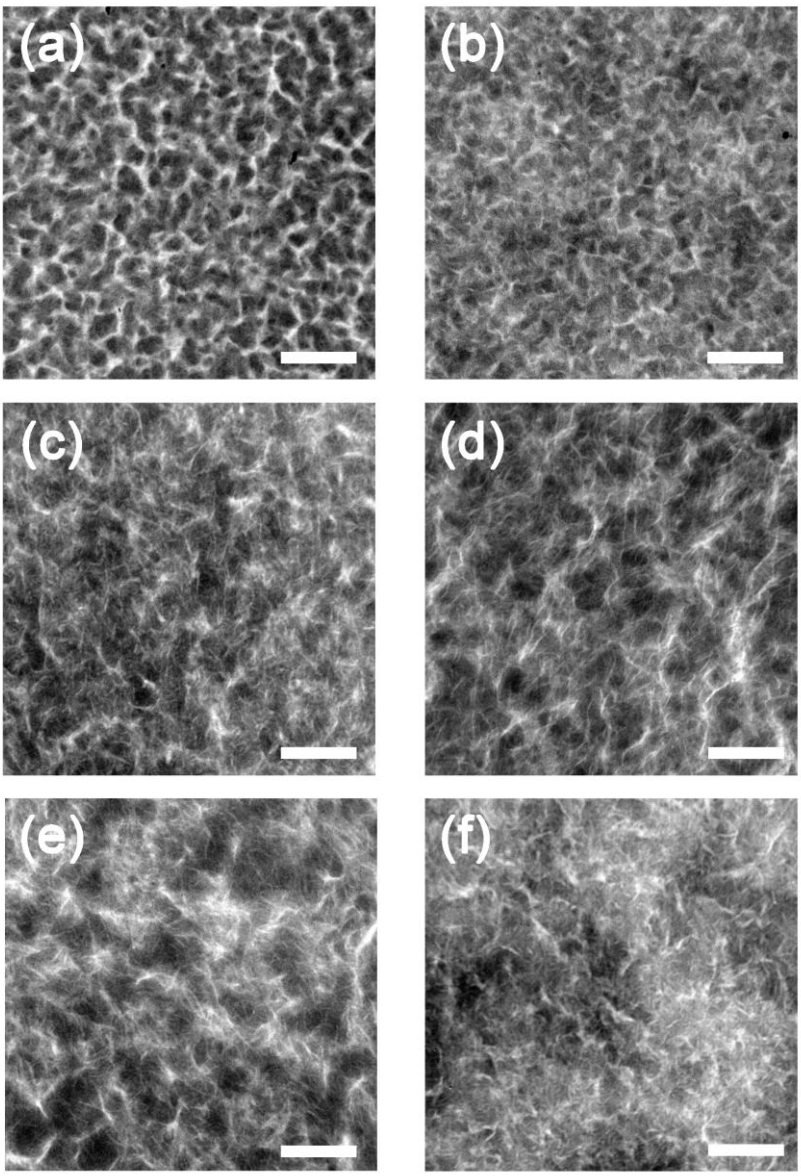

Figure 3.60. TEM images of (a, b) 2F/$PC_{71}BM$, (c, d) 3F/$PC_{71}BM$, and (e, f) 4F/$PC_{71}BM$ blend films processed (a, c, e) without and (b, d, f) with CN additive. The scale bar denotes 500 nm.

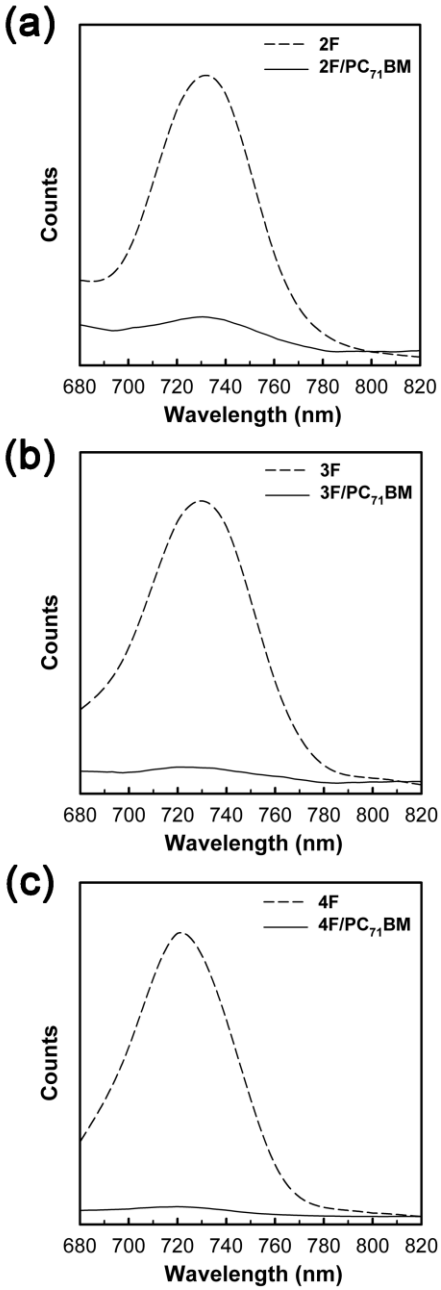

Figure 3.61. Photoluminescence spectra (excitation wavelength: 650 nm) measured from polymer and blend films of (a) 2F, (b) 3F and (c) 4F.

polymer than 3F and 4F in blend films with PCBM and it is consistent with wider fibril size of 2F polymer in TEM images of blend film (Figure 3.60).

3.4.7 Summary

We synthesized three kinds of fluorinated D–A polymers, where quaterthiophene and BT are used as D and A unit, respectively, and the degree of fluorination is controlled by using BT unit substituted by different number of fluorine atoms. 3F with mono-fluorinated BT and 4F with di-fluorinated BT have deeper HOMO energy levels, stronger vibronic shoulder in UV-Vis absorption spectra, and narrower size of fibril in blend film with PCBM than 2F with non-fluorinated BT. Among fluorinated polymers, 3F exhibits the highest PCE of 7.92% with low bimolecular recombination, high hole mobility and well-developed interconnected network with nanoscale fibril. Therefore, it can be concluded that the optoelectrical and photovoltaic properties of conjugated polymer are influenced by the degree of fluorination and the amount of fluorine substituent on conjugated backbone should be controlled cautiously.

Chapter 4. Conclusions

In this work, we synthesized difluoro-bithiophene as a new fluorinated building block in conjugated polymers for PSCs and various fluorinated copolymers based on difluoro-bithiophene are successfully designed and synthesized.

First, fluorinated poly(3,4-dialkylterthiophenes) (PDATs) composed of difluoro-bithiophene and 3,4-dialkylterthiophene were synthesized in order to clarify the effect of fluorination on the properties of polymers and its device performance of PSCs. Fluorination on polymer backbone changes its electronic structure, leading to deeper HOMO energy level and enhances molecular packing of the polymers as evidenced by strong vibronic shoulder in UV−Vis absorption spectrum and π−π stacking pattern in GIWAXS. When bulky side chain (ethylhexyl) are introduced as a solubilizing group, fluorinated polythiophenes develop finer fibril structure and exhibit a promising PCE of 5.12% with a V_{OC} of 0.87 V and a J_{SC} of 9.82 mA/cm^2. This work clearly demonstrated that the photophysical properties and device performances of conjugated polymers can be easily tuned by substitution of fluorine atom on polymer chain.

Secondly, for investigating the effect of fluorine atom substitution on the optoelectrical and photovoltaic properties of D–A type polymer, we prepared a fluorinated D–A type polymer copolymerized by diketopyrrolo[3,4-*c*]-pyrrole (DPP) as an A unit and difluoro-bithiophene as a D unit. D–A type polymers have been considered the most promising molecular structure for

high performance PSCs, because energy levels of the copolymers can be effectively tuned with a proper combination of D and A units. After introduction of fluorine atoms on conjugated backbone of DPP-based polymer, deeper HOMO energy level of polymer is observed without significant change of optical properties. However, enhanced aggregation behavior by introducing fluorine atoms increases the fibril size of fluorinated polymer, leading lower J_{SC} values in devices by reducing the efficiencies of exciton dissociation and charge generation. Although the fluorinated DPP-based polymer lower J_{SC}, PDPP-2F exhibits higher PCE of 6.39% than PDPP-0F (PCE = 5.47%) due to large improvement of V_{OC}. Therefore, it can be demonstrated that the introduction of fluorination on backbone of D–A type polymer is a promising strategy for achieving high performance PSC.

Thirdly, two kinds of D–A polymers with each being fluorinated on A and D unit, where quaterthiophene and BT are used as D and A unit, respectively, are synthesized to compare photovoltaic properties between two D–A polymers substituted by fluorine at different positions. Compared to non-fluorinated polymer, both fluorinated polymers have deeper HOMO energy levels without change of optical bandgap and exhibit stronger vibronic shoulder in optical spectrum. The HF polymer with fluorinated D unit exhibits high PCE of 7.10%, which is higher than FH with fluorinated A unit (PCE = 6.41%), with low bimolecular recombination, high hole mobility and well-developed fibril network. From this study, it can be also demonstrated that the fluorination on D unit in D–A polymer could be a promising method for achieving high performance polymer solar cells.

Finally, three kinds of fluorinated D–A polymers, where quaterthiophene and BT are used as D and A unit, respectively, are synthesized and the degree of fluorination is controlled by using BT unit substituted by different number of fluorine atoms. 3F with mono-fluorinated BT and 4F with di-fluorinated BT have deeper HOMO energy levels, stronger vibronic shoulder in UV-Vis absorption spectra, and narrower size of fibril in blend film with PCBM than 2F with non-fluorinated BT. Among fluorinated polymers, 3F exhibits the highest PCE of 7.92% with low bimolecular recombination, high hole mobility and well-developed interconnected network with nanoscale fibril. This work clearly showed that the optoelectrical and photovoltaic properties of conjugated polymer are influenced by the degree of fluorination and the amount of fluorine substituent on backbone should be controlled cautiously.

In conclusion, optoelectrical and photovoltaic properties of conjugated polymer are significantly influenced by introduction of fluorine atoms. Especially, fluorination on conjugated backbone changes the electronic structures of polymers, and thus affords lower-lying energy levels of polymer without change of bandgap, resulting in higher V_{OC} of PSCs fabricated with fluorinated polymer. Furthermore, strong interaction involving C–F bond highly improves morphology of active layers and charge mobility of polymer due to enhanced intermolecular interaction between polymers, which contribute to the increases of J_{SC} and FF in solar devices. Therefore, introduction of fluorine atom could be a promising method for achieving high performance polymer solar cells.

Bibliography

(1) Kazmerski, L. *Renew. Sust. Energ. Rev.* **1997**, *1*, 71.

(2) Alsema E. *Renew. Sust. Energ. Rev.* **1998**, *2*, 387.

(3) Spanggaard, H.; Krebs, F. C. *Sol. Energy Mater. Sol. Cells* **2004**, *83*, 125.

(4) Maennig, B.; Drechsel, J.; Gebeyehu, D.; Simon, P.; Kozlowski, F.; Werner, A.; Li, F.; Grundmann, S.; Sonntag, S.; Koch, M.; Leo, K.; Pfeiffer, M.; Hoppe, H.; Meissner, D.; Sariciftci, N. S.; Riedel, I.; Dyakonov, V.; Parisi. J. *Appl. Phys. A* **2004**, *79*, 1.

(5) Chapin, D. M.; Fuller, C. S.; Pearson, G. L. *J. Appl. Phys.* **1954**, *25*, 676.

(6) Bergman, R. B. *Appl. Phys. A* **1999**, *69*, 187.

(7) Green, M. A. *Prog. Photovolt: Res. Appl.* **2009**, *17*, 183.

(8) Green, M. A.; Emery, K.; Hishikawa, Y.; Warta, W.; Dunlop, E. D. *Prog. Photovolt: Res. Appl.* **2012**, *20*, 12.

(9) Chamberlain, G. A. *Sol. Cells* **1983**, *8*, 47.

(10) Yu, G.; Gao, J.; Hummelen, J. C.; Wudl, F.; Heeger, A. J. *Science* **1995**, *270*, 1789.

(11) Halls, J. J. M.; Walsh, C. A.; Greenham, N. C.; Marsegli, E. A.; Friend, R. H.; Moratti, S. C.; Holmes, A. B. *Nature* **1995**, *376*, 498.

(12) Brabec, C. J. *Sol. Energy Mater. Sol. Cells* **2004**, *83*, 273.

(13) Winder, C.; Sariciftci, N. S. *J. Mater. Chem.* **2004**, *14*, 1077.

(14) Kim, J. Y.; Lee, K. H.; Coates, N. E.; Moses, D.; Nguyen, T. Q.; Dante, M.; Heeger, A. J. *Science* **2007**, *317*, 222.

(15) Cheng, Y.-J.; Yang, S.-H, Hsu, C.-S. *Chem. Rev*. **2009**, *109*, 5868.

(16) Helgesen, M.; Søndergaard, R.; Krebs, F. C. *J. Mater. Chem* **2010**, *20*, 36.

(17) Beaujuge, P. M.; Fréchet, J. M. J. *J. Am. Chem. Soc.* **2011**, *133*, 20009.

(18) Peumans, P.; Forrest, S. R. *Chem. Phys. Lett.* **2004**, *398*, 27.

(19) Veenstra, S. C.; Loos, J.; Kroon, J. M. *Prog. Photovolt: Res. Appl.* **2007**. *15*, 727.

(20) Chu, T. Y.; Lu, J. P.; Beaupre, S.; Zhang, Y. G.; Pouliot, J. R.; Wakim, S.; Zhou, J. Y.; Leclerc, M.; Li, Z.; Ding, J. F.; Tao, Y. *J. Am. Chem. Soc.* **2011**, *133*, 4250.

(21) Chen, H. Y.; Hou, J. H.; Zhang, S. Q.; Liang, Y. Y.; Yang, G. W.; Yang, Y.; Yu, L. P.; Wu, Y.; Li, G. *Nat. Photonics* **2009**, *3*, 649.

(22) Cao, J.; Liao, Q.; Du, X.; Chen, J.; Xiao, Z.; Zuo, Q.; Ding, L. *Energy Environ. Sci.* **2013**, *6*, 3224.

(23) Wang, N.; Chen, Z.; Wei, W.; Jiang, Z. H. *J. Am. Chem. Soc*. **2013**, *135*, 17060.

(24) Jheng, J. F.; Lai, Y. Y.; Wu, J. S.; Chao, Y. H.; Wang, C. L.; Hsu, C. S. *Adv. Mater*. **2013**, *25*, 2445.

(25) Chen, Z. H.; Cai, P.; Chen, J. W.; Liu, X. C.; Zhang, L. J.; Lan, L. F.; Peng, J. B.; Ma, Y. G.; Cao, Y. *Adv. Mater*. **2014**, *26*, 2586.

(26) Dou, L.; Chen, C.-C.; Yoshimura, K.; Ohya, K.; Chang, W.-H.; Gao, J.; Liu, Y.; Richard, E.; Yang, Y. *Macromolecules* **2013**, *46*, 3384.

(27) You, J. B.; Dou, L. T.; Yoshimura, K. Kato, T.; Ohya, K.; Moriarty, T.; Emery, K.; Chen, C. C.; Gao, J.; Li, G.; Yang, Y.; *Nat. Commun.* **2013**, *4*, 1446.

(28) Hendriks, K. H.; Heintges, G. H. L.; Gevaerts, V. S.; Wienk, M.; Janssen, R. A. J. *Angew. Chem. Int. Ed.* **2013**, *52*, 8341.

(29) Ho, C.-C.; Chen, C.-A.; Chang, C.-Y.; Darling, S. B.; Su, W.-F.; *J. Mater. Chem. A* **2014**, *2*, 8026.

(30) Deng, Y.; Liu, J.; Wang, J.; Liu, L.; Li, W.; Tian, H.; Zhang, X.; Xie, Z.; Geng, Y.; Wang, F. *Adv. Mater*. **2014**, *26*, 471.

(31) Brabec, C. J.; Sariciftci, N. S.; Hummelen, J. C. *Adv. Func. Mater.* **2001**, *11*, 15.

(32) Pope, M.; Swenberg, C. E. *Electronic processes in organic crystals* **1982**, Clarendon Press, Oxford.

(33) Nalwa, H. S. Handbook of organic conductive molecules and polymers **1997**, Wiley, New York.

(34) Skotheim, T. A.; Reynolds, J. R. *Handbook of conjugated polymers* **1998**, Taylor & Francis group, Abingdon.

(35) Hartnagel, H. L.; Dawar, A. L.; Jain, A. K.; Jagadish, C. *Semiconducting transparent thin films* **1995**, Institute of Physics, Bristol.

(36) Tang, C. W.; Van Slyke, S. A. *Appl. Phys. Lett.* **1987**, *51*, 913.

(37) Carter, S. A.; Angelopoulos, M.; Karg, S.; Brock, B. J.; Scott, J. C. *Appl. Phys. Lett.* **1997**, *70*, 2067.

(38) Cao, Y.; Yu, G.; Zhang, C.; Menon, R.; Heeger, A. J. *Synth. Met.* **1997**, *87*, 171.

(39) Brown, T. M.; Kim, J. S.; Friend, R. H.; Cacialli, F.; Daik, R.; Feast, W. J. *Appl. Phys. Lett.* **1999**, *75*, 1679.

(40) Khodabakhsh, S.; Sanderson, B. M.; Nelson, J.; Jones, T. S. *Adv. Funct. Mater.* **2006**, *16*, 95.

(41) Brabec, C. J.; Shaheen, S. E.; Winder, C.; Sariiftci, N. S.; Denk, P. *Appl. Phys. Lett.* **2002**, *80*, 1288.

(42) Kim, J. Y.; Kim, S. H.; Lee, H.-H.; Lee, K.; Ma, W.; Gong, X.; Heeger, A. J.; *Adv. Mater.* **2006**, *18*, 572.

(43) Ma, H.; Yip, H.-L.; Huang, F.; Jen, A. K.-Y. *Adv. Funct. Mater.* **2010**, *20*, 1371.

(44) Oh, S.-H.; Na, S.-I.; Jo, J.; Lim, B.; Vak, D.; Kim, D.-Y. *Adv. Funct. Mater.* **2010**, *20*, 1977.

(45) He, Z.; Zhong, C.; Huang, X.; Wong, W.-Y.; Wu, H.; Chen, L.; Su, S.; Cao, Y. *Adv. Mater.* **2011**, *23*, 4636.

(46) Rostalski, J.; Meissner, D. *Sol. Energy Mater. Sol. Cells* **2000**, *61*, 87.

(47) Facchetti, A. *Chem. Mater.* **2011**, *23*, 733.

(48) Jong, D.; Friedlein, M. P.; Osikowicz, R. W.; Salaneck, W. R.; Fahlman, M. *Mol. Cryst. Liq. Cryst.* **2006**, *455*, 193.

(49) Hoppe, H.; Sariciftci, N. S. *J. Mater. Chem.* **2006**, *16*, 45.

(50) Shaheen, S.; Brabec, C. J.; Sariciftci, N. S.; Padinger, F.; Fromherz, T.; Hummelen, J. C. *Appl. Phys. Lett.* **2001**, *78*, 841.

(51) Zheng, L.; Zhou, Q.; Deng, X.; Yuan, M.; Yu, G.; Cao, Y. *J. Phys. Chem. B* **2004**, *108*, 11921.

(52) Wang, L.; Liu, Y.; Jiang, X.; Qin, D.; Cao, Y. *J. Phys. Chem. C* **2007**, *111*, 9538.

(53) Turner, J. A. *Science* **1999**, *285*, 687.

(54) Hoffert, M. I.; Caldeira, K.; Benford, G.; Criswell, D. R.; Green, C.; Herzog, H.; Jain, A. K.; Kheshgi, H. S.; Lackner, K. S.; Lewis, J. S.; Lightfoot, H. D.; Manheimer, W.; Mankins, J. C.; Mauel, M. E.; Perkins, L. J.; Schlesinger, M. E.; Volk T.; Wigley, T. M. L. *Science* **2002**, *298*, 981.

(55) Sirringhaus, H.; Brown, P. J.; Friend, R. H.; Nielsen, M. M.; Bechgaard, K.; Langeveld-Voss, B. M. W.; Spiering, A. J. H.; Janssen, R. A. J.; Meijer, E. W.; Herwig P.; de Leeuw, D. M. *Nature* **1999**, *401*, 685.

(56) Goffri, S.; Muller, C.; Stingelin-Stutzmann, N.; Breiby, D. W.; Radano, C. P.; Andreasen, J. W.; Thompson, R.; Janssen, R. A. J.; Nielsen, M. M.; Smith, P.; Sirringhaus, H. *Nat. Mater.* **2006**, *5*, 950.

(57) Jung, J. W.; Jo, W. H. *Adv. Funct. Mater.* **2010**, *20*, 2355.

(58) Lee, J. U.; Jung, J. W.; Emrick, T.; Russell, T. P.; Jo, W. H. *J. Mater. Chem.* **2010**, *20*, 3287.

(59) Johnson, R. D.; Meijer, G; Bethune, D. S *J. Am. Chem. Soc.* **1990**, *112*, 8983.

(60) Johnson, R. D.; Bethune, D. S.; Yannoni, C. S. *Acc. Chem. Res.* **1992**, *25*, 169.

(61) Yu, G.; Gao, J.; Hummelen, J. C.; Wudl F.; Heeger, A. J. *Science* **1995**, *270*, 1789.

(62) He, Y. J.; Chen, H. Y.; Hou, J. H.; Li, Y. F. *J. Am. Chem. Soc.* **2010**, *132*, 5532.

(63) He, Y. J.; Zhao, G. J.; Peng, B.; Li, Y. F. *Adv. Funct. Mater.* **2010**, *20*, 3383.

(64) Lenes, M.; Wetzelaer, G. J. A. H.; Kooist, F. B.; Veenstra, S. J.; Hummelen, J. C.; Blom, P. W. M. *Adv. Mater.* **2008**, *20*, 2116.

(65) Lenes, M.; Shelton, S. W.; Sieval, A. B.; Kronholm, D. F.; Hummelen, J. C.; Blom, P. W. M. *Adv. Funct. Mater.* **2009**, *19*, 3002.

(66) Qi, B.; Wang, J.; *J. Mater. Chem.* **2012**, *22*, 24315.

(67) Gendron, D.; Leclerc, M. *Energy Environ. Sci.* **2011**, *4*, 1225.

(68) Boudreault, P. T.; Najari, A.; Leclerc, M. *Chem. Mater.* **2011**, *23*, 456.

(69) Bundgarrd, E.; Krebs, F. C. *Sol. Energy Mater. Sol. Cells* **2007**, *91*, 954.

(70) Günes, S.; Neugebauer, H.; Sariciftci, N. S. *Chem. Rev.* **2007**, *107*, 1324.

(71) Chochos, C. L.; Choulis, S. A. *Prog. Polym. Sci.* **2011**, *36*, 1326.

(72) Zhou, H.; Yang, L.; You, W. *Macromolecules* **2012**, *45*, 607.

(73) Chen, J.; Cao, Y. *Acc. Chem. Res.* **2009**, *42*, 1709.

(74) Uy, R. L.; Price, S. C.; You, W. *Macromol. Rapid Commun.* **2012**, *33*, 1162.

(75) Li, G.; Zhu, R.; Yang, Y. *Nat. Photonics* **2012**, *6*, 153.

(76) Li, Y. *Acc. Chem. Res.* **2012**, *45*, 723.

(77) Faist, M. A.; Kirchartz, T.; Gong, W.; Ashraf, R. S.; McCulloch, I.; de Mello, J. C.; Ekins-Daukes, N. J.; Bradley, D. D. C.; Nelson, J. *J. Am. Chem. Soc.* **2012**, *134*, 685.

(78) Maurano, A.; Hamilton, R.; Shuttle, C. G.; Ballantyne, A. M.; Nelson, J.; O'Regan, B.; Zhang, W. M.; McCulloch, I.; Azimi, H.; Morana, M.; Brabec, C. J.; Durrant, J. R. *Adv. Mater.* **2010**, *22*, 4987.

(79) Perez, M. D.; Borek, C.; Forrest, S. R.; Thompson, M. E. *J. Am. Chem. Soc.* **2009**, *131*, 9281.

(80) Shoaee, S.; Clarke, T. M.; Huang, C.; Barlow, S.; Marder, S. R.; Heeney, M.; McCulloch, I.; Durrant, J. R. *J. Am. Chem. Soc.* **2010**, *132*, 12919.

(81) Peuman, P.; Forrest, S. R.; *Chem. Phys. Lett.* **2004**, *398*, 27.

(82) Lee, Y.; Jo, W. H. *J. Phys. Chem. C* **2012**, *116*, 8379.

(83) Veldman, D.; Meskers, S. C. J.; Janssen, R. A. J. *Adv. Funct. Mater.* **2009**, *19*, 1939.

(84) Dennler, G.; Scharber, M. C.; Brabec, C. J. *Adv. Mater.* **2009**, *21*, 1323.

(85) Jen, K.-Y.; Maxfield, M. R.; Shacklette, L. W.; Elsenbaumer, R. L. J. *Chem. Soc., Chem. Commun.* **1987**, *28*, 309.

(86) Roncali, J.; Thobie-Gautier, C. *Adv. Mater.* **1994**, *6*, 846.

(87) Cheng, Y.-J.; Chen, C.-H.; Lin, Y.-S.; Chang, C.-Y.; Hsu, C.-S. *Chem. Mater.* **2011**, *23*, 5068.

(88) Zheng, Q.; Jung, B. J.; Sun, J.; Katz, H. E. *J. Am. Chem. Soc.* **2010**, *132*, 5394.

(89) Coppo, P.; Turner, M. L. *J. Mater. Chem.* **2005**, *15*, 1123.

(90) Zhang, M.; Guo, X.; Ma, Wei.; Ade, H.; Hou, J. *Adv. Mater.* **2014**, *26*, 5880.

(91) Zhang, Z.-G.; Wang, J. *J. Mater. Chem.* **2012**, *22*, 4178.

(92) Ong, K.-H.; Lim, S.-L.; Tan, H.-S.; Wong, H.-K.; Li, J.; Ma, Z.; Moh, L. C. H.; Lim, S.-H.; de Mello, J. C.; Chen, Z.-K. *Adv. Mater.* **2011**, *23*, 1409.

(93) Wang, Y.; Xin, X.; Lu, Y.; Xiao, T.; Xu, X.; Zhao, N.; Hu, X.; Ong, B. S.; Ng, S. C. *Macromolecules* **2013**, *46*, 9587.

(94) Jung, J. W.; Liu, F.; Russell, T. P.; Jo, W. H. *Energy Environ. Sci.* **2012**, *5*, 6857.

(95) Bijleveld, J. C.; Gevaerts, V. S.; Nuzzo, D. D.; Turbiez, M.; Mathijssen, S. G. J.; de Leeuw, D. M.; Wienk, M. M.; Janssen, R. A. J. *Adv. Mater.* **2010**, *22*, E242.

(96) Sonor, P.; Singh, S. P.; Li, Y.; Ooi, Z.-E.; Ha, T.-J.; Wong, I.; Soh, M. S.; Dodabalapur, A. *Energy Environ. Sci.* **2011**, *4*, 2288.

(97) Li, Z.; Ding, J.; Song, N.; Du, X.; Zhou, J.; Lu, J.; Tao, Y. *Chem. Mater.* **2011**, *23*, 1977.

(98) Li, Z.; Ding, J.; Song, N.; Lu, J.; Tao, Y. *J. Am. Chem. Soc.* **2010**, *132*, 13160.

(99) Liu, C.; Cai, W.; Guan, X.; Duan, C.; Xue, Q.; Ying, L.; Huang, F.; Cao, Y. *Polym. Chem.* **2013**, *4*, 3949.

(100) Huo, L.; Hou, J. *Polym. Chem.* **2011**, *2*, 2453.

(101) Ye, L.; Zhang, S.; Huo, L.; Zhang, M.; Hou, J. *Acc. Chem. Res.* **2014**, *47*, 1595.

(102) Liang, Y.; Feng, D.; Wu, Y.; Tsai, S.-T.; Li, G.; Ray, C.; Yu, L. P. *J. Am. Chem. Soc.* **2009**, *131*, 7792.

(103) Jo, J. W.; Kim, S. S.; Jo, W. H. *Org. Electron.* **2012**, *13*, 1322.

(104) Lee, Y.; Nam, Y. M.; Jo, W. H. *J. Mater. Chem.* **2011**, *21*, 8583.

(105) Watters, D.C.; Yi, H.; Pearson, A. J.; Kingsley, J.; Iraqi, A.; Lidzey, D. *Macromol. Rapid Commun.* **2013**, *34*, 1157.

(106) Blouin, N.; Michaud, A.; Gendron, D.; Wakim, S.; Blair, E.; Neagu-Plesu, R.; Belletete, M.; Durocher, G.; Tao, Y.; Leclerc, M. *J. Am. Chem. Soc.* **2008**, *130*, 732.

(107) Qin, R.; Li, W.; Li, C.; Du, C.; Veit, C.; Schleiermacher, H.-F.; Andersson, M.; Bo, Z.; Liu, Z.; Ingana□s, O.; Wuerfel, U.; Zhang, F. *J. Am. Chem. Soc.* **2009**, *131*, 14612.

(108) Chen, Y.-C.; Yu, C.-Y.; Fan, Y.-L., Hung, L.-I.; Chen, C.-P.; Ting, C. *Chem. Commun.* **2010**, *46*, 6503.

(109) Yu, C.-Y.; Chen, C.-P.; Chan, S.-H.; Hwang, G.-W.; Ting, C. *Chem. Mater.* **2011**, *23*, 733.

(110) Zhang, M. J.; Guo, X.; Wang, X. C.; Wang, H. Q.; Li, Y. F. *Chem. Mater*. **2011**, *23*, 4264.

(111) Zhang, M. J.; Gu, Y.; Guo, X.; Liu, F.; Zhang, S. Q.; Huo, L. J.; Russell, T. P.; Hou, J. H. *Adv. Mater*. **2013**, *25*, 4944.

(112) Lee, W.; Choi, H.; Hwang, S.; Kim, J. Y.; Woo, H. Y. *Chem. Eur. J*. **2012**, *18*, 2551.

(113) Wienk M. M.; Turbiez, M.; Gilot, J.; Janssen, R. A. J. *Adv. Mater.* **2008**, *20*, 2556.

(114) Li, W.; Hendriks, K. H.; Roelofs, W. S. C.; Kim, Y.; Wienk, M. M.; Janssen, R. A. J. *Adv. Mater.* **2013**, *25*, 3182.

(115) Woo, C. H.; Beaujuge, P. M.; Holcombe, T. W.; Lee O. P.; Frechet, J. M. J. *J. Am. Chem. Soc.* **2010**, *132*, 15547.

(116) Bijleveld, J. C.; Karsten, B. P.; Mathijssen, S. G. J.; Wienk, M. M.; Leeuw, D. M.; Janssen, R. A. J. *J. Mater. Chem.* **2011**, *21*, 1600.

(117) Wang, E. G.; Hou, L. T.; Wang, Z. Q.; Hellstrom, S. F.; Zhang, F. L.; Inganas, O.; Andersson, M. R. *Adv. Mater.* **2010**, *22*, 5240.

(118) Zou, Y.; Najari, A.; Berrouard, P.; Beaupré, S.; Réda Aïch, B.; Tao, Y.; Leclerc, M. *J. Am. Chem. Soc*. **2010**, *132*, 5330.

(119) Su, M.-S.; Kuo, C.-Y.; Yuan, M.-C.; Jeng, U. S.; Su, C.-J.; Wei, K.-H. *Adv. Mater*. **2011**, *23*, 3315.

(120) Beaupré, S.; Najari, A.; Leclerc, M.; *Synthetic Met*., **2013**, *182*, 9.

(121) Jung, E. H.; Jo, W. H. *Energy Environ. Sci*. **2014**, *7*, 650.

(122) Ma, Z.; Sun, W.; Himmelberger, S.; Vandewal, K.; Tang, Z.; Bergqvist, J.; Salleo, A.; Andreasen, J. W.; Inganäs, O.; Andersson,

M. R.; Muller, C.; Zhang, F.; Wang, E.; *Energy Environ. Sci*. **2014**, *7*, 361.

(123) Olivier, Y.; Niedzialek, D.; Lemaur, V.; Pisula, W.; Müllen, K.; Koldemir, U.; Reynolds, J. R.; Lazzaroni, R.; Cornil, J.; Beljonne, D. *Adv. Mater.*, 2014, **26**, 2119.

(124) Liang, Y.; Xu, Z.; Xia, J.; Tsai, S.-T.; Wu, Y.; Li, G.; Ray, C.; Yu, L. *Adv. Mater*. **2010**, *22*, E135.

(125) Son, H. J.; Lu, L.; Chen, W.; Xu, T.; Zheng, T.; Carsten, B.; Strzalka, J.; Darling, S. B.; Chen, L. X.; Yu, L. *Adv. Mater*. **2013**, *25*, 838.

(126) Zhang, M.; Guo, X.; Zhang, S.; Hou, J. *Adv. Mater*. **2014**, *26*, 1118.

(127) Hou, J.; Chen, H.-Y.; Zhang, S.; Li, G.; Yang, Y. *J. Am. Chem. Soc.* **2008**, *130*, 16144.

(128) Chen, H. Y.; Hou, J. H.; Hayden, A. E.; Yang, H.; Houk, K. N.; Yang, Y. *Adv. Mater*. **2010**, *22*, 371.

(129) Amb, C. M.; Chen, S.; Graham, K. R.; Subbiah, J.; Small, C. E.; So, F.; Reynolds, J. R. *J. Am. Chem. Soc.* **2011**, *133*, 10062.

(130) Patra, A.; Bendikov, M. *J. Mater. Chem.* **2010**, *20*, 422.

(131) Zade, S. S.; Zamoshchik, N.; Bendikov, M. *Chem. Eur. J.* **2009**, *15*, 8613.

(132) Earmme, T.; Hang, Y.-J.; Murari, N. M.; Subramaniyan, S.; Jenekhe, S. A. *J. Am. Chem. Soc.* **2013**, *135*, 14960.

(133) Zhou, H. X.; Yang, L. Q.; Price, S. C.; Knight, K. J.; You, W. *Angew. Chem. Int. Edit.*, **2010**, *49*, 7992.

(134) Yau, C. P.; Fei, Z.; Ashraf, R. S.; Shahid, M.; Watkins, S. E.; Pattanasattayavong, P.; Anthopoulos, T. D.; Gregoriou, V. G.; Chochos, C. L.; Heeney, M. *Adv. Funct. Mater.*, **2014**, *24*, 678.

(135) Babudri, F.; Farinola, G. M.; Naso, F.; Ragni, R. *Chem. Commun.* **2007**, 1003.

(136) Zhou, H. X.; Yang, L. Q.; Stuart, A. C.; Price, S. C.; Liu, S. B.; You, W. *Angew. Chem. Int. Ed.* **2011**, *50*, 2995.

(137) Price, S. C.; Stuart, A. C.; Yang, L. Q.; Zhou, H. X.; You, W. *J. Am. Chem. Soc.* **2011**, *133*, 4625.

(138) Chang, C.; Zuo, L.; Yip H.; Li, Y.; Li, C.; Hsu, C.; Cheng, Y.; Chen, H.; Jen, A. K. -Y. *Adv. Funct. Mater.* **2013**, *23*, 5084.

(139) Woo, C. H.; Beaujuge, P. M.; Holcombe, T. W.; Lee, O. P.; Frechet, J. M. J. *J. Am. Chem. Soc.* **2010**, *132*, 15547.

(140) Yang, L. Q.; Zhou, H. X.; You, W. *J. Phys. Chem. C* **2010**, *114*, 16793.

(141) Cabanetos, C.; El Labban, A.; Bartelt, J. A.; Douglas, J. D.; Mateker, W. R.; Frechet, J. M. J.; McGehee, M. D.; Beaujuge, P. M. *J. Am. Chem. Soc.* **2013**, *135*, 4656.

(142) Jung, J. W.; Jo, J. W.; Liu, F.; Russell, T. P.; Jo, W. H. *Chem. Commun.* **2012**, *48*, 6933.

(143) Lu, J. P.; Liang, F. S.; Drolet, N.; Ding, J. F.; Tao, Y.; Movileanu, R. *Chem. Commun.* **2008**, 5315.

(144) Zhou, E. J.; Yamakawa, S.; Zhang, Y.; Tajima, K.; Yang, C. H.; Hashimoto, K. *J. Mater. Chem.* **2009**, *19*, 7730.

(145) Fei, Z. P.; Shahid, M.; Yaacobi-Gross, N.; Rossbauer, S.; Zhong, H. L.; Watkins, S. E.; Anthopoulos, T. D.; Heeney, M. *Chem. Commun.* **2012**, *48*, 11130.

(146) Park, J. K.; Jo, J.; Seo, J. H.; Moon, J. S.; Park, Y. D.; Lee, K.; Heeger, A. J.; Bazan, G. C. *Adv. Mater.* **2011**, *23*, 2430.

(147) Lee, J. U.; Kim, Y. D.; Jo, J. W.; Kim, J. P.; Jo, W. H. *J. Mater. Chem.* **2011**, *21*, 17209.

(148) Okamoto, T.; Nakahara, K.; Saeki, A.; Seki, S.; Oh, J. H.; Akkerman, H. B.; Bao, Z. N.; Matsuo, Y. *Chem. Mater.* **2011**, *23*, 1646.

(149) Ko, S. W.; Verploegen, E.; Hong, S.; Mondal, R.; Hoke, E. T.; Toney, M. F.; McGehee, M. D.; Bao, Z. N. *J. Am. Chem. Soc.* **2011**, *133*, 16722.

(150) Ko, S. W.; Hoke, E. T.; Pandey, L.; Hong, S. H.; Mondal, R.; Risko, C.; Yi, Y. P.; Noriega, R.; McGehee, M. D.; Bredas, J. L.; Salleo, A.; Bao, Z. A. *J. Am. Chem. Soc.* **2012**, *134*, 5222.

(151) Park, J. H.; Jung, E. H.; Jung, J. W.; Jo, W. H. *Adv. Mater.* **2013**, *25*, 2583.

(152) Son, H. J.; Wei, W.; Xu, T.; Liang, Y.; Wu, Y.; Li, G.; Yu, L. *J. Am. Chem. Soc.* **2011**, *133*, 1885.

(153) Jo, J. W.; Jung, J. W.; Wang, H.-W.; Kim, P.; Russell, T. P.; Jo, W. H. *Chem. Mater.* **2011**, *23*, 4264.

(154) Brabec, C. J.; Gowrisanker, S.; Halls, J. J. M.; Laird, D.; Jia, S. J.; Williams, S. P. *Adv. Mater.* **2010**, *22*, 3839.

(155) Li, G.; Shrotriya, V.; Huang, J. S.; Yao, Y.; Moriarty, T.; Emery, K.; Yang, Y. *Nat. Mater.* **2005**, *4*, 864.

(156) Wienk, M. M.; Kroon, J. M.; Verhees, W. J. H.; Knol, J.; Hummelen, J. C.; van Hal, P. A.; Janssen, R. A. J. *Angew. Chem., Int. Ed.* **2003**, *42*, 3371.

(157) Cates, N. C.; Gysel, R.; Beiley, Z.; Miller, C. E.; Toney, M. F.; Heeney, M.; McCulloch, I.; McGehee, M. D. *Nano Lett.* **2009**, *9*, 4153.

(158) Liu, F.; Gu, Y.; Jung, J. W.; Jo, W. H.; Russell, T. P. *J. Polym. Sci. Polym. Phys.* **2012**, *50*, 1018.

(159) Qu, S.; Tian, H. *Chem. Commun.* **2012**, *48*, 3039.

(160) Li, Y.; Sonar, P.; Murphy, L.; Hong, W. *Energy Environ. Sci.* **2013**, *6*, 1684.

(161) Li, W.; Furlan, A.; Roelofs, W. S. C.; Hendriks, K.; Van Pruissen, G. W. P.; Wienk, M. M.; Janssen, R. A. J. *Chem. Commun.* **2014**, *50*, 679.

(162) Carsten, B.; Szarko, J. M.; Son, H. J.; Wang, W.; Lu, L. Y.; He, F.; Rolczynski, B. S.; Lou, S. J.; Chen, L. X.; Yu, L. P. *J. Am. Chem. Soc.* **2011**, *133*, 20468.

(163) Rolczynski, B. S.; Szarko, J. M.; Son, H. J.; Liang, Y. Y.; Yu, L. P.; Chen, L. X. *J. Am. Chem. Soc.* **2012**, *134*, 4142.

(164) Li, W.; Hendriks, K. H.; Furlan, A.; Roelofs, W. S. C.; Wienk, M. M.; Janssen, R. A. J. *J. Am. Chem. Soc.* **2013**, *135*, 18942.

(165) Li, W.; Hendriks, K. H.; Furlan, A.; Roelofs, W. S.; Meskers, S. C.; Wienk, M. M.; Janssen, R. A. J. *Adv. Mater.* **2014**, *26*, 1565.

(166) Cowan, S R.; Roy, A,; Heeger, A. J. *Phys. Rev. B* **2010**, *82*, 245207.

(167) Cowan, S. R.; Wang, J.; Yi, J.; Lee, Y. J.; Olson, D. C.; Hsu, J. W. P. *J. Appl. Phys.* **2013** , *113* , 154504.

(168) Moon, J. S.; Takacs, C. J.; Cho, S.; Coffin, R. C.; Kim, H.; Bazan, G. C.; Heeger, A. J. *Nano Lett*. **2010**, *10*, 4005.

(169) Koster, L. J. A.; Mihailetchi, V. D.; Blom, P. W. M. *Appl. Phys. Lett.* **2005**, *87*, 203502.

(170) Liu, P.; Zhang, K.; Liu, F.; Jin, Y.; Liu, S.; Russell, T. P.; Yip, H.-L.; Huang, F.; Cao, Y. *Chem. Mater*. **2014**, *26*, 3009.

(171) Ma, Z.; Dang, D.; Tang, Z.; Gedefaw, D.; Bergqvist, J.; Zhu, W.; Mammo, W.; Andersson, M. R.; Inganäs, O.; Zhang, F.; Wang, E. *Adv. Energy. Mater.* **2014**, 10.1002/aenm.201301455.

초 록

높은 성능의 고분자 태양전지를 위해서는 공액고분자의 전기적 에너지준위는 넓은 영역의 빛을 흡수하기 위한 낮은 밴드갭, 높은 개방전압을 위한 낮은 HOMO 에너지준위, 고분자 전자주개와 플러렌 전자받개 간의 충분한 LUMO 에너지준위 차를 갖도록 조절되어야 하며, 이를 위한 다양한 화학구조의 개선방법들이 보고되고 있다. 최근 몇 년간 여러 방법 중 불소화가 주목을 받고 있으며 불소화 고분자를 이용한 태양전지들이 7% 이상의 높은 전력변환효율을 기록하고 있다. 하지만 아직까지 불소화가 고분자의 광전기적과 광전지적 특성에 미치는 영향이 분명하게 규명되지 않았으며 제한적 고분자시스템 내에서만 연구가 되어왔다. 따라서 추가적인 연구를 위한 불소화 단량체와 고분자의 개발이 필요하다.

본 연구에서는 불소화가 고분자와 태양전지에 미치는 영향을 명확하게 조사하기 위하여 새로운 불소화 단량체인 difluoro-bithiophene를 합성하였고 이를 이용하여 다양한 구조의 불소화 고분자를 중합하였다.

우선 difluoro-bithiophene과 3,4-dialkylterthiophene 구성된 불소화 poly(3,4-dialkylterthiophenes) (PDATs)를 합성하였다. 불소화는 고분자의 전기적 구조를 변형시켜 HOMO 에너지준위가 낮아지는 결과를 만들었다. 그리고 불소화는 고분자의 적층도 향상시켰으며 이는 UV–Vis 흡수스펙트럼에서의 강한 vibronic shoulder와 GIWAXS 에서의 π–π 적층 패턴을 통해 확인하였다. 곁사슬로 ethylhexyl를

도입하였을 때, 불소화 PDAT는 미세한 피브릴 구조를 보였으며 비불소화 고분자 대비 3.5배 향상된 5.12%의 높은 효율을 보였다.

다음으로 불소화가 D–A 고분자에 미치는 영향을 살펴보기 위하여 difluoro-bithiophene과 diketopyrrolo[3,4-c]-pyrrole (DPP)을 각각 D와 A 유닛으로 하여 고분자를 합성하였다. 불소화 후, DPP 기반의 고분자는 광학적 특성의 변화가 거의 없이 낮은 HOMO 에너지준위를 나타내었나 고분자의 집합성이 증가하여 광활성층 내에서 넓은 사이즈의 피브릴을 보였다. 비록 불소화 DPP 고분자는 낮은 단락전류를 보였으나 큰 개방전압의 향상으로 인해 비불소화 고분자(5.47%)에 비해 높은 효율(6.39%)을 나타내었다.

나아가 불소화의 위치에 따른 D–A 고분자의 특성변화를 살펴보기 위하여, 불소가 D에 도입된 HF와 불소가 A에 도입된 FH 고분자를 합성하였다. 비불소화 고분자에 비해 불소화 고분자들은 밴드갭의 변화 없이 낮은 HOMO을 보였으며 분자간의 향상된 상호작용을 나타내었다. HF 고분자는 잘 발달된 피브릴 네트워크, 적은 이분자 재결합, 높은 정공수송도를 보이며 FH 고분자(6.41%)보다 높은 효율인 7.10%를 기록하였다.

마지막으로 다른 개수의 불소를 갖는 2,1,3-benzothiadiazole (BT)를 이용하여 불소화 정도에 따른 세가지 고분자를 합성하였다. 불소가 하나 치환된 BT로 중합한 3F와 불소가 둘 치환된 BT로 중합한 4F는 비불소화 BT로 중합된 2F에 비해 낮은 HOMO 에너지 준위, UV–Vis 흡수스펙트럼에서의 강한 vibronic shoulder, 좁은 사이즈의 피브릴을 보였다. 불소화 고분자 중 3F는 높은 정공수송도와 적은 이분자 재결합으로 인해 높은 효율인 7.92%를 보였다.

이러한 결과들을 통해, 고분자의 광전기적과 광전지적 특성이 불소 원자에 의해 크게 영향을 받는 다는 점을 알 수 있었으며 고효율 태양전지용 물질로써 불소화 고분자의 높은 가능성을 확인하였다.

주요어: 고분자 태양전지, 벌크 이종접합, 공액고분자, 낮은 밴드갭, 불소화, 유기 전자공학

학 번: 2009-20640

List of papers

1. Jo, J. W.; Jung, J. W.; Lee, J. U.; Jo, W. H. *ACS Nano* **2010**, *4*, 5382.
2. Jung, J. W.; Jo, J. W.; Jo, W. H. *Adv. Mater.* **2011**, *23*, 1782.
3. Lee, J. U.; Kim, Y. D.; Jo, J. W.; Kim, J. P.; Jo, W. H. *J. Mater. Chem.* **2011**, *21*, 17209.
4. Jo, J. W.; Kim, S. S.; Jo, W. H. *Org. Electron.* **2012**, *13*, 1322.
5. Jung, J. W.; Jo, J. W.; Liu, F.; Russell, T. P.; Jo, W. H. *Chem. Comm.* **2012**, *48*, 6933.
6. Park, H. J.; Lee, Y.; Jo, J. W.; Jo, W. H. *Polym. Chem.* **2012**, *3*, 2928.
7. Lee, J. U.; Jung, J. W.; Jo, J. W.; Jo, W. H. *J. Mater. Chem.* **2012**, *22*, 24265.
8. Jo, J. W.; Jung, J. W.; Wang, H.-W.; Kim, P.; Russell, T. P.; Jo, W. H. *Chem. Mater.* **2014**, *26*, 4214.
9. Jo, J. W.; Bae, S.; Liu, F.; Russell, T. P.; Jo, W. H. *Adv. Funct. Mater.* DOI: 10.1002/adfm.201402210.